Canadian Mineralogist
Vol. 31, pp. 471-522 (1993)

A METATURBIDITE-HOSTED LODE GOLD DEPOSIT: THE BEAVER DAM DEPOSIT, NOVA SCOTIA. I. VEIN PARAGENESIS AND MINERAL CHEMISTRY

DANIEL J. KONTAK AND PAUL K. SMITH

Nova Scotia Department of Natural Resources, P.O. Box 698, Halifax, Nova Scotia B3J 2T9

ABSTRACT

A study of vein paragenesis and mineral chemistry has been conducted at the Beaver Dam gold deposit, a metaturbidite-hosted mesothermal gold deposit of *ca.* 370 Ma age located in the Meguma Terrane of southern Nova Scotia. Vein formation is considered to have occurred within a brittle–ductile shear-zone environment with transient fluid pressures. Several vein types are recognized, but the most important volumetrically is a bedding-concordant type characterized by crack–seal and ribbon-textured quartz; lesser amounts of various discordant types also are present. The crack–seal texture is herein considered to represent vestiges of an earlier part of the vein history involving replacement of the wallrock during periods when P(fluid) was less than P(lithostatic). In constrast, most of the white vein quartz formed under conditions of P(fluid) greater or equal to P(lithostatic). Veins are dominated by quartz, but locally they are characterized by abundant (>50–60%) silicate, carbonate and sulfide minerals that were deposited in two distinct stages: stage I is dominated by Ca-rich plagioclase ($\leq An_{65}$) + biotite (mg = 0.50 ± 0.05) + tourmaline (± amphibole ± garnet ± epidote ± apatite ± ilmenite), whereas stage II is dominated by calcite + chlorite (mg = 0.50 ± 0.04) + albite (± scheelite); muscovite overlaps the two stages. Sulfides, including Bi–Te compounds, are spatially related to both stages, but paragenetically, they are more abundant in stage II. Gold (> 90% pure; rare electrum) is spatially associated with both stages, but textures indicate a late-stage paragenesis. The major-element chemistry of vein minerals indicates: (1) variable patterns of zonation from complex to simple in silicates (*i.e.*, disequilibrium conditions), and (2) compositions controlled by the wallrocks. The trace-element chemistry (including *REE*) of vein minerals suggests that the chemistry of the vein-forming fluid changed during mineral precipitation and that derivation of the fluids from the Meguma Group (*i.e.*, the metamorphogenic model) is unlikely. The data are consistent with a genetic model invoking a late-stage metamorphic origin for the deposit, with the fluids being exotic to the Meguma Group.

Keywords: gold deposit, Meguma, mineral chemistry, vein paragenesis, concentrations of rare-earth elements, Beaver Dam deposit, Nova Scotia.

SOMMAIRE

Nous présentons les résultats d'une étude de la paragenèse et de la chimie des minéraux des veines aurifères du gisement mésothermal de Beaver Dam, dans les métaturbidites du socle de Meguma (environ 370 Ma), dans le sud de la Nouvelle-Écosse. Ces veines se seraient formées dans un milieu de zone de cisaillement, sous un régime de déformation cassante à ductile, avec des fluctuations en pression de la phase fluide. Plusieurs sortes de veines sont développées, mais la majorité des veines aurifères sont concordantes au litage des roches hôtes, et caractérisées par une texture de cassure et de cicatrisation du quartz et par la présence de quartz rubanné. Les veines discordantes occupent un volume moins important. La texture de cassure et de cicatrisation représenterait les vestiges d'un assemblage précoce dans les veines impliquant le remplacement de la paroi au cours des périodes quand la pression de la phase fluide était inférieure à la pression lithostatique. Par contre, la grande partie du quartz laiteux se serait formée quand la pression de la phase fluide était supérieure ou égale à la pression lithostatique. Le quartz est prédominant dans ces veines; elles peuvent aussi contenir une proportion importante (>50–60%) de silicates, carbonates et sulfures, déposés en deux stades distincts. Le premier a produit surtout un plagioclase calcique ($\leq An_{65}$) + biotite (mg = 0.50 ± 0.05) + tourmaline ± amphibole ± grenat ± épidote ± apatite ± ilménite). Au deuxième stade, c'est l'assemblage calcite + chlorite (mg = 0.50 ± 0.04) + albite (± scheelite) qui domine. La formation de la muscovite chevauche les deux stades. Les sulfures, y inclus les composés à Bi–Te, sont liés dans l'espace aux deux stades, mais sont plus abondants dans les paragenèses du deuxième stade. L'or, dont la pureté dépasse 900 (or pur: 1000), avec électrum rare, est associé aux deux stades dans l'espace, mais les textures impliquent une déposition tardive. En termes des éléments majeurs, les minéraux des veines indiquent: 1) des schémas de zonation variables, de complexes à simples, dans les silicates (indication de conditions de déséquilibre), et 2) des compositions régies par les roches encaissantes. La répartition des éléments traces, les terres rares par exemple, indique que la composition de la phase fluide responsable de la minéralisation a évolué avec la précipitation des divers minéraux, et que le modèle d'une dérivation à partir des roches du Groupe de Meguma (modèle métamorphogénique) est peu probable. Les données impliquent plutôt une origine métamorphique tardive du gisement, et une source de la phase fluide externe au Groupe de Meguma.

(Traduit par la Rédaction)

Mots-clés: gisement d'or, Meguma, chimie des minéraux, paragenèse des veines, concentration des terres rares, gisement de Beaver Dam, Nouvelle-Écosse.

INTRODUCTION

The Lower Paleozoic Meguma Group of southern Nova Scotia is considered a typical example of metaturbidite-hosted gold mineralization (*e.g.*, Boyle 1979, 1986). Although the historical production of *ca.* 30 million grams (Bates 1986) pales in comparison to deposits of similar age in Australia (Boyle 1979, Cox *et al.* 1991), or much older analogues, such as the Archean Superior Province of the Canadian Shield (Colvine *et al.* 1988), the Meguma deposits are nevertheless worthy of study and provide valuable information with respect to the genesis of this type of deposit (Kontak *et al.* 1990a). As part of a regional study of the Meguma gold deposits (Smith & Kontak 1986), the Beaver Dam deposit has been examined in considerable detail.

Although there have been numerous papers documenting various aspects of the geology of Meguma gold deposits, no comprehensive treatment of a single deposit exists. Most previous studies of gold deposits have in general been confined to specific subjects, *e.g.*, vein structure (Graves 1976, Keppie 1976, Mawer 1985, 1986, 1987, Henderson & Henderson 1986, Williams & Hy 1990) and morphology (Haynes 1986, 1987, Henderson *et al.* 1990), wall-rock chemistry (Crocket *et al.* 1986, Kerswill 1988), isotopes (Kontak & Smith 1989a, Kontak *et al.* 1991a, b, Sangster 1992, Sangster *et al.* 1988), and fluid inclusions (Yanover 1984, Kontak *et al.* 1988, Kontak & Smith 1989b); these studies generally proceeded independently. In contrast, this study presents a fully integrated approach in examination of the area of the Beaver Dam deposit and incorporates the following work: (1) underground mapping and logging of drill core, (2) structural studies on a macro- and microscopic scale, (3) study of the mineral paragenesis and related chemistry, (4) geochemical characterization of all lithologies, (5) isotopic study (O, C, H, S, Sr, ^{40}Ar/^{39}Ar) of all vein types, and (6) examination of fluid inclusions. In this paper, data relating to vein paragenesis and mineral chemistry are presented. These data suggest that the vein-forming fluid is exotic to the Meguma Group, but that local contamination with the Meguma Group is reflected in some of the characteristics of the veins and mineral chemistry.

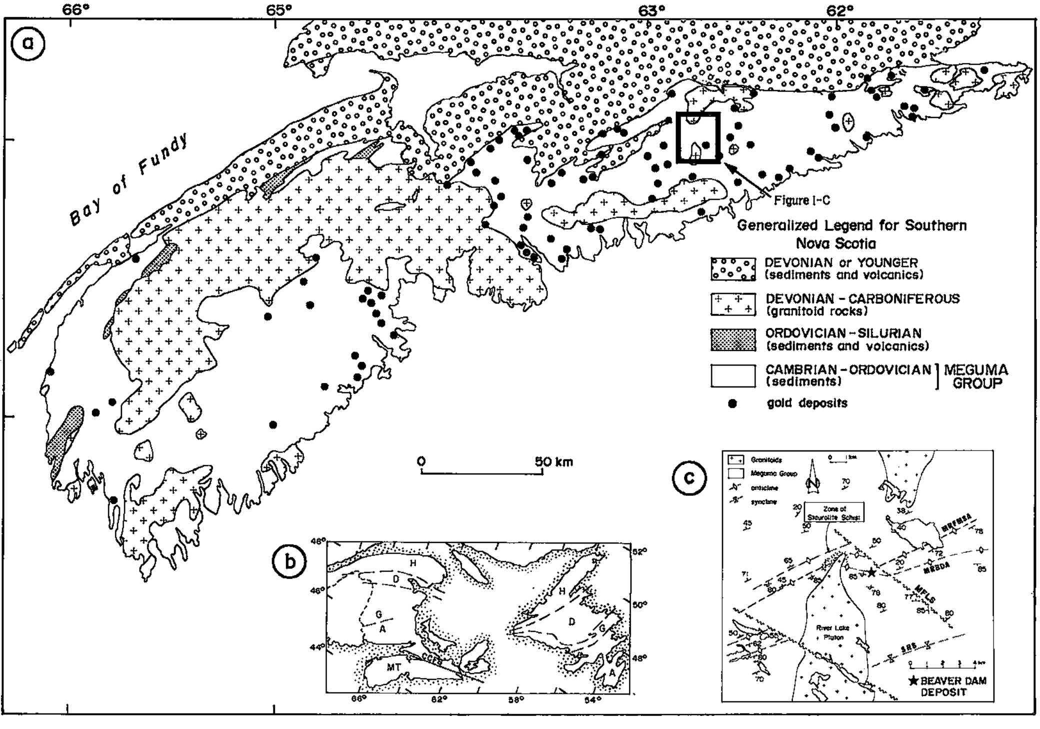

FIG. 1. (a) Regional geological map of southern Nova Scotia, showing the location of gold districts within the Meguma Group metasedimentary rocks and the location of the Beaver Dam area. (b) The location of the Meguma Terrane in the Canadian Appalachians (Williams & Hatcher 1983). Abbreviations: A Avalon, G Gander, D Dunnage, H Humber, MT Meguma Terrane. CCFS Cobequid – Chedabucto fault system. (c) Location and local geology of the Beaver Dam area [modified after Faribault (1899) and Thomas (1982)]. Abbreviations: MRFMSA Moose River – Fifteen Mile Stream anticline, MRBDA Moose River – Beaver Dam anticline, SHS Sherbrooke Syncline, MLFS Mud Lake fault system.

GEOLOGICAL SETTING

The study area is located in southern Nova Scotia, within the Meguma Terrane of the Canadian Appalachians (Fig. 1a; Williams & Hatcher 1983). The area is underlain by three main lithotectonic units (Fig. 1b), namely Lower Paleozoic metasedimentary and volcanic rocks, large volumes of peraluminous and lesser metaluminous granitic rocks of Late Devonian age, and Late Paleozoic – Mesozoic sedimentary and volcanic rocks. The Cambro-Ordovician Meguma Group, host rocks to the deposit, consists of the lower, sandstone-dominated Goldenville Formation (5500 m) and overlying, shale-dominated Halifax Formation ($\leq$4500 m). These rocks were deformed into open, upright folds and metamorphosed to greenschist to upper amphibolite facies during the Acadian Orogeny of *ca.* 400 ± 10 Ma age (Reynolds & Muecke 1978, Muecke *et al.* 1988, Keppie & Dallmeyer 1987). More localized deformation of the Meguma Terrane continued along fault zones [*e.g.*, Cobequid–Chedabucto Fault System; Fig. 1 (Mawer & White 1987, Keppie 1982)], and this has been dated (Rb–Sr, ^{40}Ar/^{39}Ar) at *ca.* 370 Ma in the eastern Meguma Terrane (Keppie & Dallmeyer 1987) and 250–330 Ma in the western Meguma Terrane (*e.g.*, Kontak & Cormier 1991). The Meguma Terrane was intruded by large volumes of metaluminous to peraluminous granitic magma (*e.g.*, the South Mountain Batholith; MacDonald *et al.* 1992) and volumetrically minor amounts of mafic magma (Giles & Chatterjee 1986) at *ca.* 370 Ma (Reynolds *et al.* 1981, 1987, Kempster *et al.* 1989, Kontak *et al.* 1990b).

The Beaver Dam deposit (Fig. 1c) is hosted by psammitic lithologies of the Goldenville Formation, which crop out on the southern, overturned limb of the Moose River – Beaver Dam Anticline. The northern contact of the 371 ± 2 Ma (^{40}Ar/^{39}Ar; Kontak *et al.* 1990c) River Lake pluton, a two-mica monzogranite, crops out about 2 km west of the deposit area. Approximately 4 km due south of the deposit area, slate of the Halifax Formation crops out in the core of the Sherbrooke Syncline. Late, northwest-trending faults crosscut the area, offsetting both the River Lake pluton and the deposit area itself in its easternmost extention (Mud Lake fault system in Fig. 1c).

GEOLOGY OF THE BEAVER DAM DEPOSIT

The Beaver Dam deposit area is underlain by psammitic and pelitic rocks that show sedimentary and structural features typical of turbiditic sediments. The most obvious feature is the graded nature of the massive sandstone units, which fine upward to thin beds of graphitic shale; locally, well-preserved primary sedimentary structures are observed. Three main stratigraphic packages are recognized; in order of oldest to youngest, these are the Crouse, Papke and Austen zones (Fig. 2). Variable amounts of calcareous beds ($\leq$5 cm) occur throughout the stratigraphic sequence.

The sequence is overturned to the south and strikes 110°/70–75°N. A well-developed, penetrative fabric (S_1) parallels bedding (S_0) and locally is transposed by a second penetrative fabric (S_2). The S_2 fabric is best observed in closures of minor folds (see below), where it is axial planar to such folds; S_1 is transposed into the plane of S_2 (see Kontak *et al.* 1990c).

The entire stratigraphic sequence is cut by quartz veins that are either concordant (Figs. 2, 3a) or discordant with respect to S_0 (Fig. 2). Most of the bedding-concordant veins vary from 0.5 cm to 1 m thickness, but

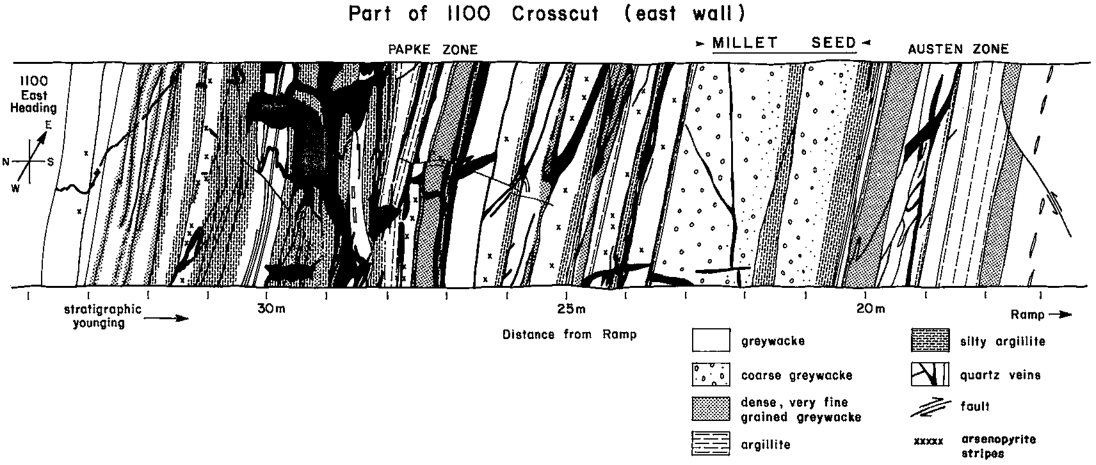

FIG. 2. Geological map of underground workings (east wall 1100 crosscut) of the Beaver Dam gold deposit, illustrating the nature of veining (*e.g.*, condordant and discordant).

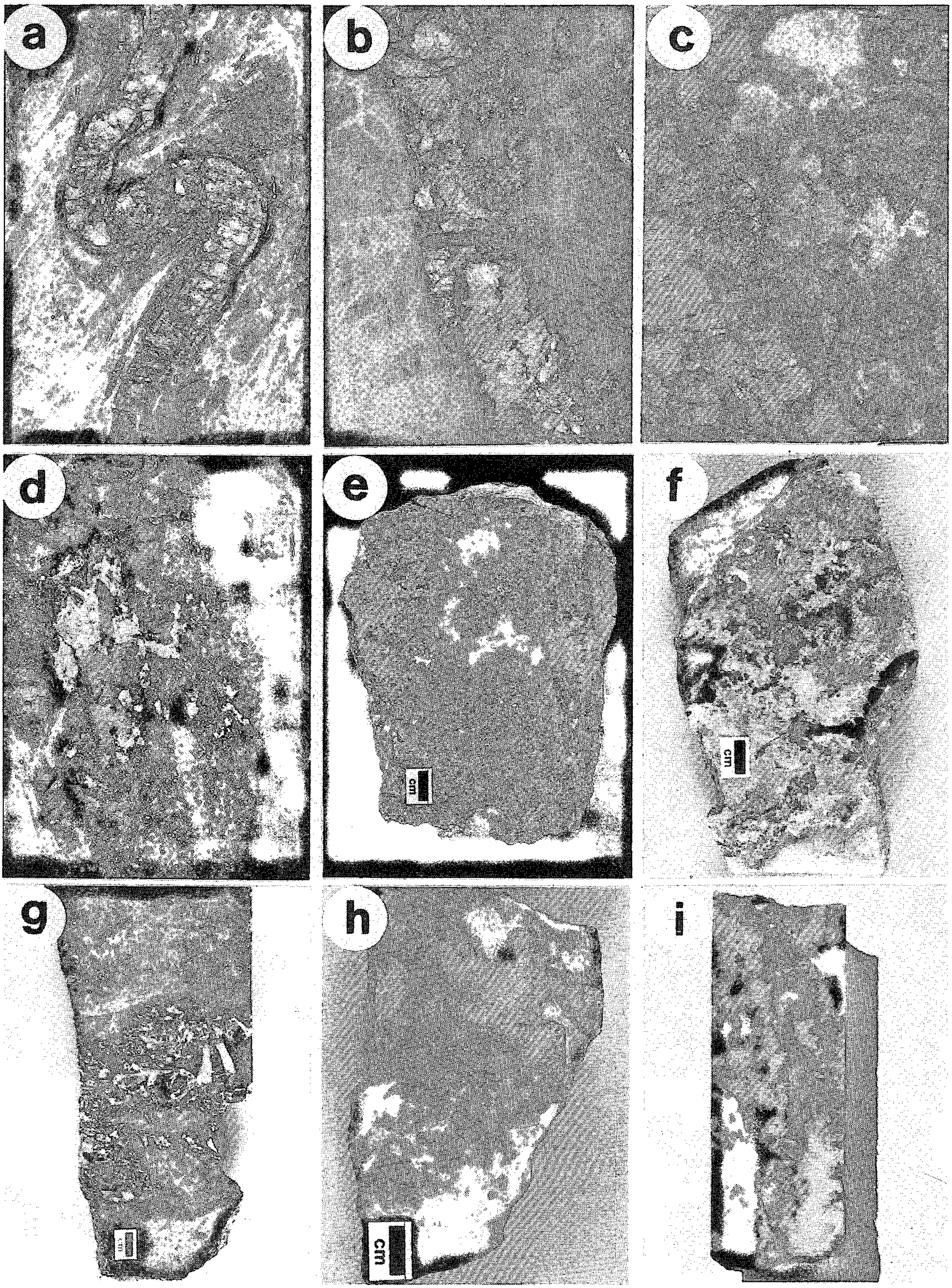
a
b
c
d
e
cm
f
cm
g
cm
h
cm
i

veins of 2–3 m thickness occur. Locally, these veins exhibit crack–seal or ribbon texture; the degree of vein deformation is highly variable. In contrast, the discordant veins (to 1–2 m thickness), including the *ac* veins (to 10–15 cm thickness) of Henderson & Henderson (1986), cross-cut the concordant veins, are massive, and generally show little evidence of the intense deformation recorded in the concordant veins (Figs. 3b, c, d). Although crack–seal textures are not abundant, they are nevertheless present in the discordant veins (*cf.* Mawer 1985, 1987).

The wallrocks within the deposit area, but away from the quartz veins, contain the assemblage Qtz – Bt – Chl – Ms – Ab – Cal – Ilm – Tur (abbreviations used throughout are those of Kretz 1983); in addition, graphite is present in pelitic units, and amphibole and garnet may be seen in carbonate-rich beds (calc-silicate). This assemblage is typical of the biotite zone of the greenschist facies, which dominates this part of the Meguma Terrane (Douma 1988). However, west of the deposit (<1 km), we have observed the appearance of andalusite, garnet, cordierite and staurolite in pelitic units in drill core, and immediately north of the River Lake intrusion there is a zone of staurolite schist and abundant float containing coarse andalusite (to 20–30 cm) in a log-jam texture. Present in the wallrocks adjacent to the veins (*i.e.*, within few cm) are cm-size clots of Qtz + Bt ± Ilm ± sulfides ± Cal ± Chl ± Ms with aspect ratios (length:width) of 1:1 to 25:1. These clots are informally referred to as oikocrysts and are tentatively interpreted to represent retrograded porphyroblasts of andalusite(?). These clots have been noted at all the gold deposit districts in the eastern Meguma Terrane (Smith & Kontak 1986).

The age of the vein-forming event has been estimated at *ca.* 374 Ma based on ^{40}Ar/^{39}Ar dating of hydrothermal amphibole, biotite and muscovite by Kontak *et al.* (1990c; 1993) and petrofabric studies of the vein and wallrock material. This age is similar to ^{40}Ar/^{39}Ar ages for other Meguma gold depoits in the eastern Meguma Terrane (Kontak *et al.* 1990c, 1992).

VEIN MORPHOLOGY, MINERALOGY AND PARAGENETIC RELATIONSHIPS

Vein morphology

Veins at Beaver Dam are invariably quartz-rich (*i.e.*, >>90%), but they vary greatly with respect to dimensions, geometry and mineralogy (Figs. 3, 4). The veins are very similar in terms of morphology and geometry to those of other metaturbidite-hosted vein packages (*e.g.*, Cox *et al.* 1991, Forde 1991). The vein textures may be broadly grouped into the following types (see Table 1 for summary): (1) quartz-only veins that contain trace amounts of sulfides or laminated carbonate (Fig. 3a); (2) quartz veins with the characteristic crack–seal or ribbon texture (*e.g.*, Mawer 1985, 1987), in which variable amounts of wallrock septae are incorporated into the veins (see below), (3) "pegmatoid" veins in which quartz locally gives way to coarse-grained, silicate-rich (>50–60%) mineral clots (Figs. 3d, g, h, i), and (4) massive, whitish quartz generally referred to as bull quartz or fissure veins, which may contain vugs infilled by a euhedral assemblage of Qtz ± Cal ± Chl ± Ab ± Ms ± Py (Figs. 3b, c). Locally, alteration of pre-existing vein minerals (stage I; see below) has occurred, and the alteration minerals generally include Ms + Cal + Ab or Cal + Chl. These veins also may contain variable amounts of wallrock material and locally have the crack–seal or ribbon textures developed.

Bedding-concordant veins characterized by quartz ± suldifes ± carbonate and crack–seal or ribbon texture account for the greatest proportion of the veins. However, we emphasize that the features of a vein may change along strike. For example, bedding-concordant veins may have features 1, 2 and 3 (see Table 1) within the same 20–30 m strike length. The nature of the quartz in these vein types is highly variable and reflects different degrees of dynamic recrystallization or annealing. Where there is abundant recrystallization, the quartz is cloudy to dark, but where deformation is minimal, the

FIG. 3. Photos of vein assemblages at the Beaver Dam deposit. (a) Typical bedding-concordant, quartz ± sulfide vein in fine-grained metaturbiditic sediments (looking east). Most of the material in the vein other than quartz is pyrite. Vein is *ca.* 15 cm thick. (b) Discordant quartz vein cutting psammitic beds containing disseminated arsenopyrite aligned parallel to S_0/S_1 (lower left of photo). The dark patches in the vein are chlorite-rich clots ± carbonate – albite. Vein is *ca.* 25–30 cm side. (c) Closeup of a chlorite – carbonate ± sulfide ± scheelite clot in discordant quartz vein. Width of photo is *ca.* 25–30 cm. (d) Discordant, "pegmatoid"-type vein containing coarse plagioclase-carbonate and finer-grained sulfides – garnet – scheelite – tourmaline – biotite. Vein is *ca.* 30 cm wide. (e) Slabbed sample of intensely altered "pegmatoid" vein replaced predominantly by fine-grained muscovite – carbonate – albite. Dark patches in middle are chlorite-rich infill, and on the right is a late quartz – carbonate – albite vein. (f) Stage-I quartz–plagioclase assemblage overprinted by chlorite – albite – carbonate – muscovite of stage II. Note the lack of a sharp vein–wallrock contact at the top of photo. (g) Calc-silicate vein consisting of amphibole – plagioclase – biotite – carbonate. (h) Monomineralic plagioclase vein. In this sample, plagioclase has an emerald green color. (i) Quartz – plagioclase – biotite assemblage of stage I in discordant(?) vein from drill core. Note the intimate intergrowth of the silicates. Core sample is 4 cm wide.

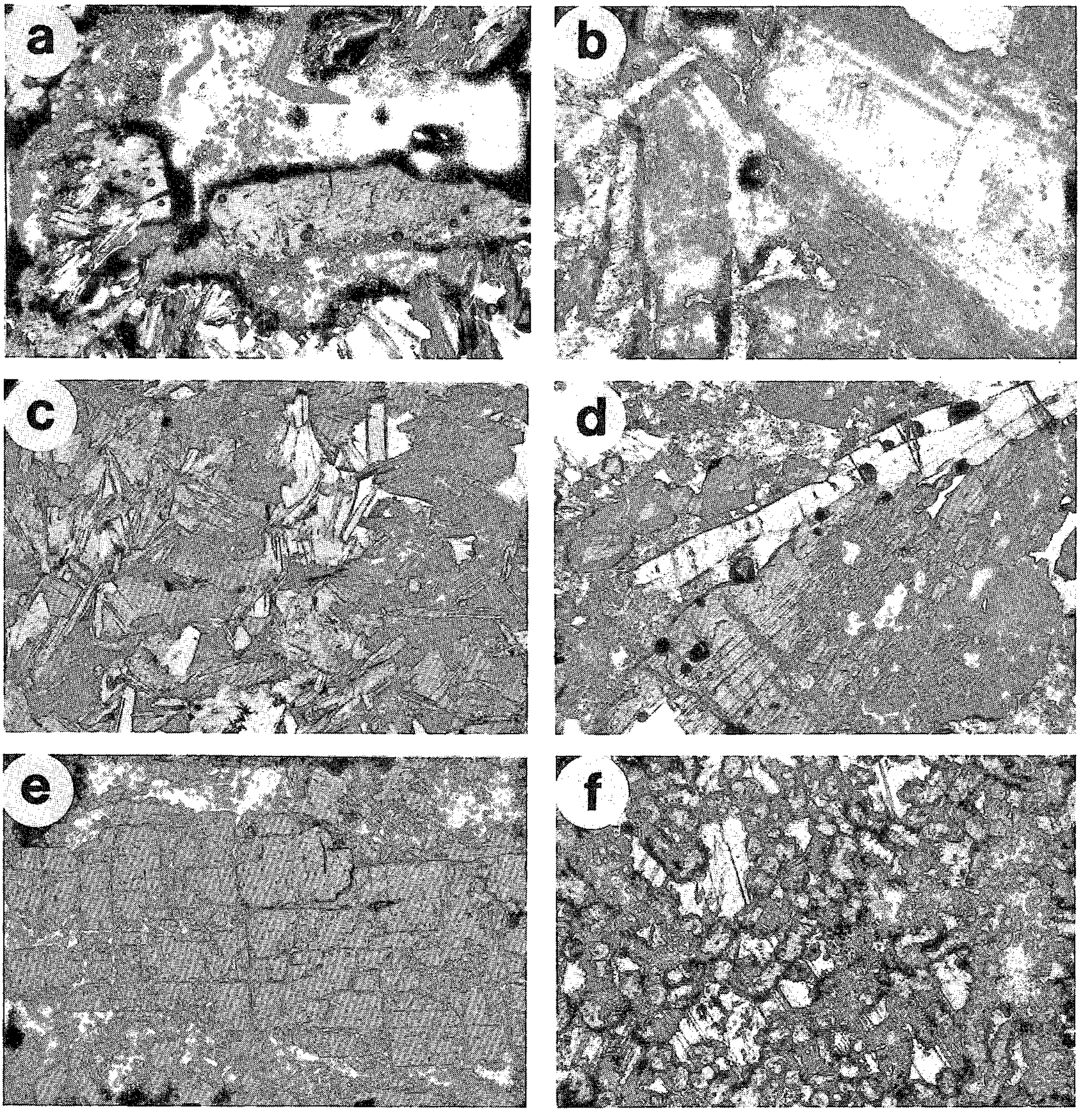

FIG. 4. Photomicrographs of vein assemblages (silicates only) at the Beaver Dam deposit. In all photos, the width is *ca.* 1 mm across. (a) Euhedral grains of plagioclase strongly zoned on their margins (*i.e.*, An_{60-30}), with interiors replaced with coarse rosettes of muscovite that are mantled by areas of albitic alteration. The center of the photo shows a fine-grained intergrowth of albite – carbonate – chlorite – muscovite infilling that may have been open space. (b) Coarse grains of unaltered plagioclase showing normal zonation, from a massive plagioclase-rich vein sample similar to that in Figure 3b. (c) Sample of pristine clot of intimately intergrown biotite (80%) and tourmaline (20%). (d) Coarse needles of euhedral tourmaline arranged in rosette pattern cross-cutting plagioclase that is partially altered to albite + muscovite. Note the color zonation in the tourmaline. (e) Coarse grains of euhedral apatite surrounded by chlorite + muscovite + albite + carbonate assemblage that has partially replaced calcic plagioclase. (f) Intergrowth of chlorite and carbonate representing a primary assemblage in a late-stage quartz vein. Note the worm-like texture to the chlorite and the dark rims (brownish color) bordering the grains.

quartz may be translucent, and coarse euhedra are preserved (*i.e.*, to 10–20 cm in discordant veins).

With respect to veins containing the crack–seal or ribbon texture, a composite history of formation is suggested. The crack–seal-textured quartz accounts for only a few per cent of the vein, the remainder being composed of white, crystalline quartz, and the lateral continuity of the thin septae is rarely more than a few cm

TABLE 1. SUMMARY OF VEIN FEATURES AND MINERALOGY, BEAVER DAM DEPOSIT

VEIN TYPE	VEIN MORPHOLOGY, FEATURES	MINERALOGY
bedding concordant veins; generally $\leq$10 cm but up to 1 m	parallel to sub-parallel to S_o; crack-seal or ribbon texture common; variably deformed (folded, boudinaged); silicate clots present near vein margins	Qtz dominant with sulfides, carbonate (laminated), silicates (Bt-Pl-Tur±Ap±Grt ±Hbl±Ilm±EP); overprint alteration (Ms +Chl+Cal+Ab+Ant/Rt)
discordant veins (including angulars, bull, spurs)	massive veins up to 2-3 m; crack-seal or ribbon texture rare; cross-cut bedding concordant veins; coarse Qtz crystals common; vuggy textures present and infilled with stage II mineralogy; generally undeformed	Qtz dominant with clots of Chl-Cal ±Ms±Ab±Py±Tur±Bi-Tesulfides;stage I mineralogy rare (Bt-Pl-Tur-Ap-Grt-Ilm)
ac veins	perpendicular to S_o and fold axial plane; $\leq$5-10 cm thickness; mostly undeformed	Qtz dominant with rare silicates (stage I and II), sulfides

Abbreviations after Kretz (1983)

(*cf.* Mawer 1987). Detailed examination of these specific textures from a macro- to a microscale (Fig. 5) indicate that there is a progression from unaltered material (similar in all respects to the immediate wallrock) to variably silicified or altered material. Where silicification is most intensely developed, thin, parallel laminae are observed (Fig. 5) that consist of the residual material (micas, graphite, oxides in different proportions). Whereas some of the laminated texture in the veins is most possibly due to sequential opening and closing of veins resulting from hydrofracturing and mineral precipitation (*i.e.*, micas) in the classic model of Ramsay (1980), the vast majority of the crack–seal-textured quartz is herein considered to have formed as a result of variable digestion and replacement of wallrock material. In many cases, the vestiges of beds can still be traced within the quartz veins (Fig. 5a), and wallrock material still rooted in the wall of the vein also is observed (Figs. 5b, c). These features are considered as further support for a replacive origin for the crack–seal-textured quartz. A similar replacive origin for crack–seal quartz has been suggested by Forde (1991) for the breccia veins in the slate-belt-hosted gold deposits of Australia.

In summary, therefore, we emphasize that the bulk of the veins comprise white, massive crystalline quartz considered to postdate the crack–seal type of quartz since the latter is enveloped by this quartz. Within the veins, variable amounts of silicates, carbonates and sulfides also occur, in addition to quartz; these were deposited in two stages (see below). Thus, the veins are composite in nature, with at least two distinct periods of vein formation, as represented by the different types of quartz.

Mineralogy and paragenesis

The paragenetic sequence observed at the Beaver Dam deposit is based on examination of drill core, underground mapping, cutting of several hundred rock slabs and petrographic study of thin and polished sections. The paragenesis is summarized in Figure 6, whereas some of the features are illustrated in Figures 3 and 4. We emphasize that the entire sequence is not represented by a single sample, but has been established by systematically recording mutual relationships among mineral phases and incorporating whole-rock geochemistry. This latter point was important in determining, for example, the presence and extent of the Bi – Te – Ag – W association (Smith & Kontak 1988). The paragenetic sequence consists of two hypogene stages (I and II); however, there are deviations from this generalized trend with respect to muscovite, tourmaline, sulfides and probably gold, which appear in part to transcend this simple two-fold subdivision. The sulfide mineralogy is discussed separately below. In terms of the vein types and their mineralogy, as summarized in Table 1, the following general statement applies. Bedding-concordant veins contain stage-I mineralogy, with an overprint or alteration of stage-II mineralogy. In contrast, the discordant veins are dominated by stage-II mineralogy (stage I rarely present), and the *ac* veins rarely have stage-I or -II mineralogy.

Stage-I mineralogy

In addition to quartz, stage-I mineralogy is dominated by the assemblage Pl – Bt ± Tur with, in order of relative importance, accessory ilmenite, sulfides, apatite, garnet, hornblende and epidote (Figs. 3h, 3i, 4a–e). In one instance, a single grain of K-feldspar was detected using the electron microprobe, but its relationship to other minerals and extent remain unknown. The plagioclase is Ca-rich and of emerald-green to dark green color, with lesser reddish orange plagioclase present. In many cases, stage-I consists of exceptionally pristine, euhedral minerals, commonly coarse grained (*i.e.*, to 1–3 cm), and

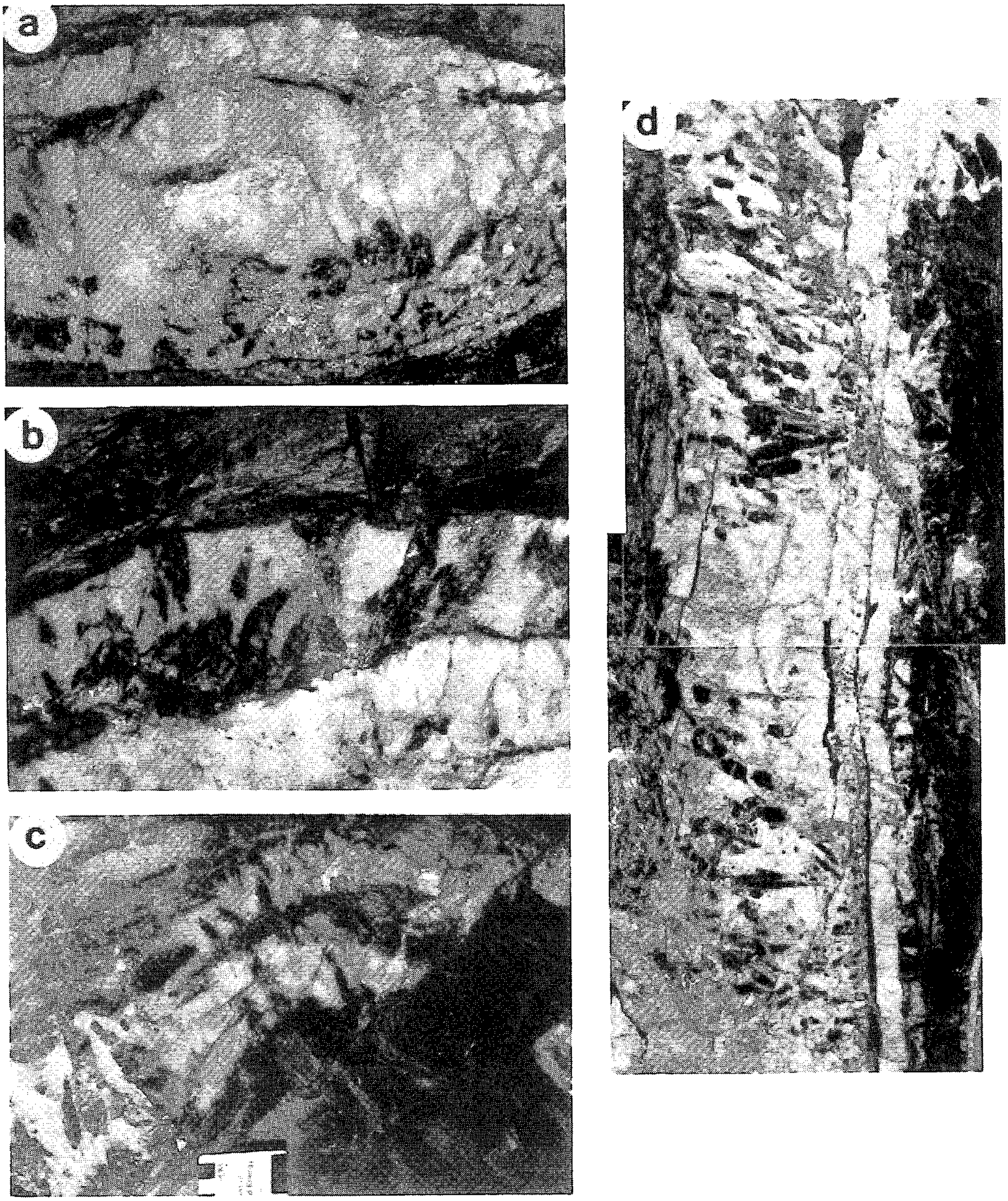

plagioclase may be strongly zoned, with both normal and oscillatory zoning observed in thin section (Figs. 4a, b). In addition, coarse-grained monomineralic clots occur such that plagioclase, biotite or tourmaline may represent >60–90 % of some hand specimens (Fig. 3h). In some rare cases, apatite may be present to 5 modal %. Similarly, amphibole can be abundant in calc-silicate veins (Fig. 3g). Biotite, garnet, tourmaline and ilmenite are present in both the veins and adjacent wallrock, where they overprint a penetrative fabric (S_2). Both biotite and tourmaline may occur as the dominant mineral phase in these alteration envelopes, indicating

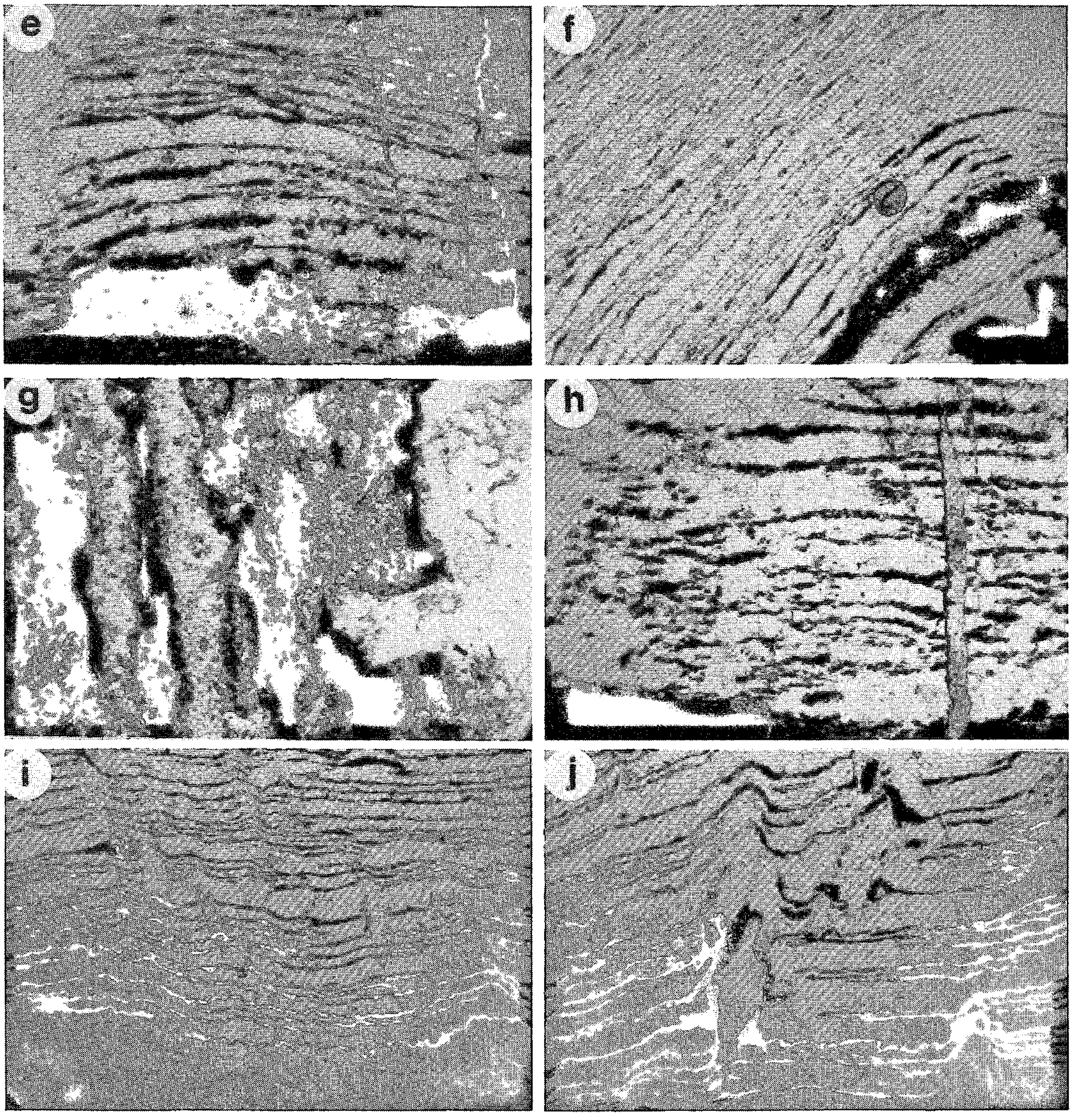

FIG. 5. Photos (underground and thin sections) illustrating the nature of ribbon-textured and crack–seal quartz in veins at the Beaver Dam deposit. (a) Bedding-concordant vein with wallrock fragments entrained within the vein. Note the pyramidal terminations of some fragments and faint crack–seal texture in others (lower right). Vein is *ca.* 0.5 m thick. (b) Closeup of a massive fissure vein with fragments of wallrock near the margin rooted in some cases in the wallrock. Width of photo *ca.* 1 m. (c) Fissure vein containing abundant fragments of wallrock that are in many cases rooted in the adjacent wallrock (*e.g.*, center of photo). Note scale in cm. (d) Bedding-concordant vein with abundant inclusions of wallrock and well-developed ribbon texture. Note that the long axes of the inclusions are oriented perpendicular to the vein–wallrock contact, but that within the fragments S_0/S_1 remain parallel to that in the wallrock. Vein is *ca.* 0.7 m wide. (e, f, g, h, i, j) Thin sections illustrating the nature of the crack–seal texture. Note that in e, f, g and h, the laminae have variable proportions of the wallrock mineral assemblage. In i and j, advanced stages of the crack–seal texture are illustrated with the superimposition of stylolitic textures reflecting the dynamic environment in which these veins formed. Note that the individual laminae are not that continuous and have a very limited lateral extent. Width of photos in e, f, g and h is *ca.* 2.7 mm, and *ca.* 0.7 mm. in i and j.

local metasomatism. Muscovite does appear to occur in equilibrium with some stage-I assemblages and is, therefore, interpreted to represent a transitional phase between stages I and II.

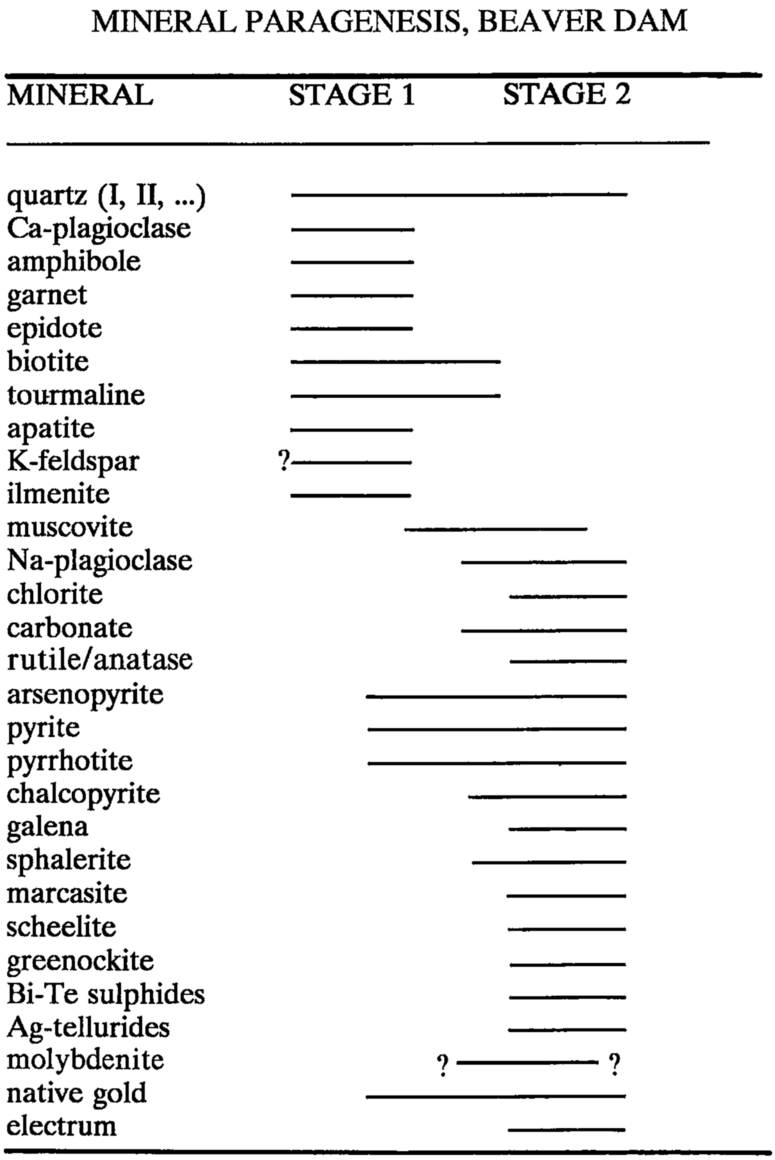

FIG. 6. Paragenetic scheme for veins at the Beaver Dam gold deposit. Details of stages I and II dicussed in the text.

Stage-II mineralogy

Stage-II minerals may occur as either alteration products of stage-I minerals (Figs. 3e, f), as is commonly the case in bedding-concordant veins, or as primary phases in discordant-type veins (Figs. 3b, c, 4f) where stage-I minerals are generally absent. In the first instance, the following alteration or replacements occur: (i) Ca-rich plagioclase is replaced by the assemblage Ab + Cal + Ms ± Chl (Fig. 4a); (ii) biotite is variably chloritized, with the remnant biotite containing abundant oriented inclusions of rutile; and (iii) ilmenite is replaced by anatase and, more rarely, titanite. In these alteration assemblages, muscovite is commonly of rosette texture, and chlorite has a vermicular texture. Where stage-II minerals occur as a primary assemblage, Chl + Cal + Py ± Ab ± Ms is the most common association. Rare tourmaline and ilmenite may also occur. Assemblages of stage-II minerals generally occur as massive clots or open-space infillings. Because of the general absence of intense deformational features, these delicate textures are preserved. For example, albite euhedra (<1 cm) may overgrow a substrate of monomineralic chlorite coating quartz euhedra that project from a base of massive, recrystallized quartz. These albite euhedra may in turn be coated with fine-grained pyrite euhedra. With this second type of stage-II assemblage is commonly associated scheelite and Bi–Te–Ag mineralization.

Sulfides, tellurides and gold mineralogy

The sulfide phases, in order of decreasing abundance, are arsenopyrite, pyrrhotite, pyrite, chalcopyrite, galena, sphalerite, marcasite and löllingite; rare molybdenite occurs as films coating vein–wallrock contacts and is late in the paragenesis, although poorly constrained. Trace amounts of Bi–Te sulfides, a Bi–Te alloy and greenockite also occur (Smith & Kontak 1988). Arsenopyrite occurs as coarse (<0.5–1.0 cm) euhedra either in massive, bedding-concordant veins, along vein-wallrock contacts, disseminated in the wallrock or in narrow (1–2 cm) Qtz – Apy ± Py ± Po veins that roughly parallel S_0. This latter type of occurrence is characteristic of the Papke Zone at the deposit (Fig. 2). Arsenopyrite commonly contains minor amounts of Fe-sulfide inclusions. In contrast, pyrrhotite (<1 cm) is anhedral, and occurs mostly as isolated grains in bedding-concordant veins. Chalcopyrite commonly occurs along its margin or within cross-cutting fractures. Whereas arsenopyrite and pyrrhotite overlap stage-I and -II assemblages, pyrite occurs predominantly in stage II as euhedra intergrown with chlorite and carbonate; trace pyrite occurs with arsenopyrite of stage I. Marcasite is an alteration product of pyrite and, more rarely, pyrrhotite, and in both cases results from constant-volume replacement. Galena occurs in close association with pyrrhotite of stage II and has as inclusions the Bi–Te sulfides. All the main sulfide phases generally have a narrow rim of Chl ± Cal at least partially enveloping the grains and locally developed along internal fractures.

Gold occurs as μm- to mm-size grains, with its habit variable, from flakes, wires to rare crystalline forms. The most common occurrence (*i.e.*, >70%) of gold is as isolated grains in bedding-concordant veins near wallrock contacts or if within the interior of the vein proximal to a wallrock inclusion. Where free gold has been observed in close association with wallrock material, it is common for Chl + Cal + Ms alteration to be present; however, we are unable to say how unique this alteration of the wallrock is in terms of gold mineralization. Gold is also found in the following associations: (1) in arsenopyrite and pyrrhotite (10–15%) as fine-grained (1–5 μm) disseminations, fracture-controlled veinlets and along grain boundaries, (2) in grain contact with galena and chalcopyrite; the association with galena may also include the presence of a Bi–Te sulfide and a Ag–Te alloy, (3) in fractures cutting plagioclase altered to Ab + Ms + Cal, (4) along fractures or cleavage in both fresh and chloritized biotite, and (5) in wallrock. One of the most common features of the gold is that several size fractions occur together, most commonly with a coarse central grain that is then surrounded by a corona of finer grains. Finally, although most gold occurs in bedding-concordant veins, a minor amount occurs in discordant-type veins.

It is difficult to constrain the paragenetic position of gold given that it occurs in a variety of sites, most commonly and volumetrically important as free gold in quartz of bedding-concordant veins. However, based on the mutual relationship with other mineral phases, gold is considered to have been deposited synchronously with stage-II minerals. This is not to say that remobilization of earlier gold has not occurred.

MINERAL CHEMISTRY

Analytical techniques

High-quality mineral separates and mineral phases in polished thin section were analyzed using wet-chemical facilities (the Technical University of Nova Scotia,

TABLE 2. REPRESENTATIVE COMPOSITIONS OF AMPHIBOLE

Sample	87-61A		85-10	
Point	1	3	10	39
SiO_2 (wt.%)	42.63	43.64	43.57	42.69
TiO_2	0.19	0.30	0.08	0.40
Al_2O_3	15.88	13.96	15.10	14.49
Cr_2O_3	0.04	0.03	0.05	0.00
FeO	14.47	15.53	14.34	18.52
MnO	0.66	0.76	0.67	0.40
MgO	9.92	9.82	9.60	6.33
CaO	12.35	12.27	12.20	11.68
Na_2O	1.26	1.12	1.18	1.05
K_2O	0.48	0.41	0.44	0.20
Σ	97.55	97.84	97.23	95.80
NUMBER OF CATIONS BASED ON 23 OXYGEN				
Si	6.350	6.467	6.770	6.523
^{iv}Al	1.650	1.533	1.230	1.477
^{vi}Al	1.067	0.905	0.872	1.133
Ti	0.021	0.033	0.018	0.046
Cr	0.005	0.004	0.007	0.000
Fe	1.803	1.925	1.703	2.367
Mn	0.084	0.095	0.084	0.052
Mg	2.146	2.169	2.396	1.441
Ca	1.921	1.948	1.922	1.912
Na	0.355	0.322	0.256	0.311
K	0.089	0.078	0.056	0.039

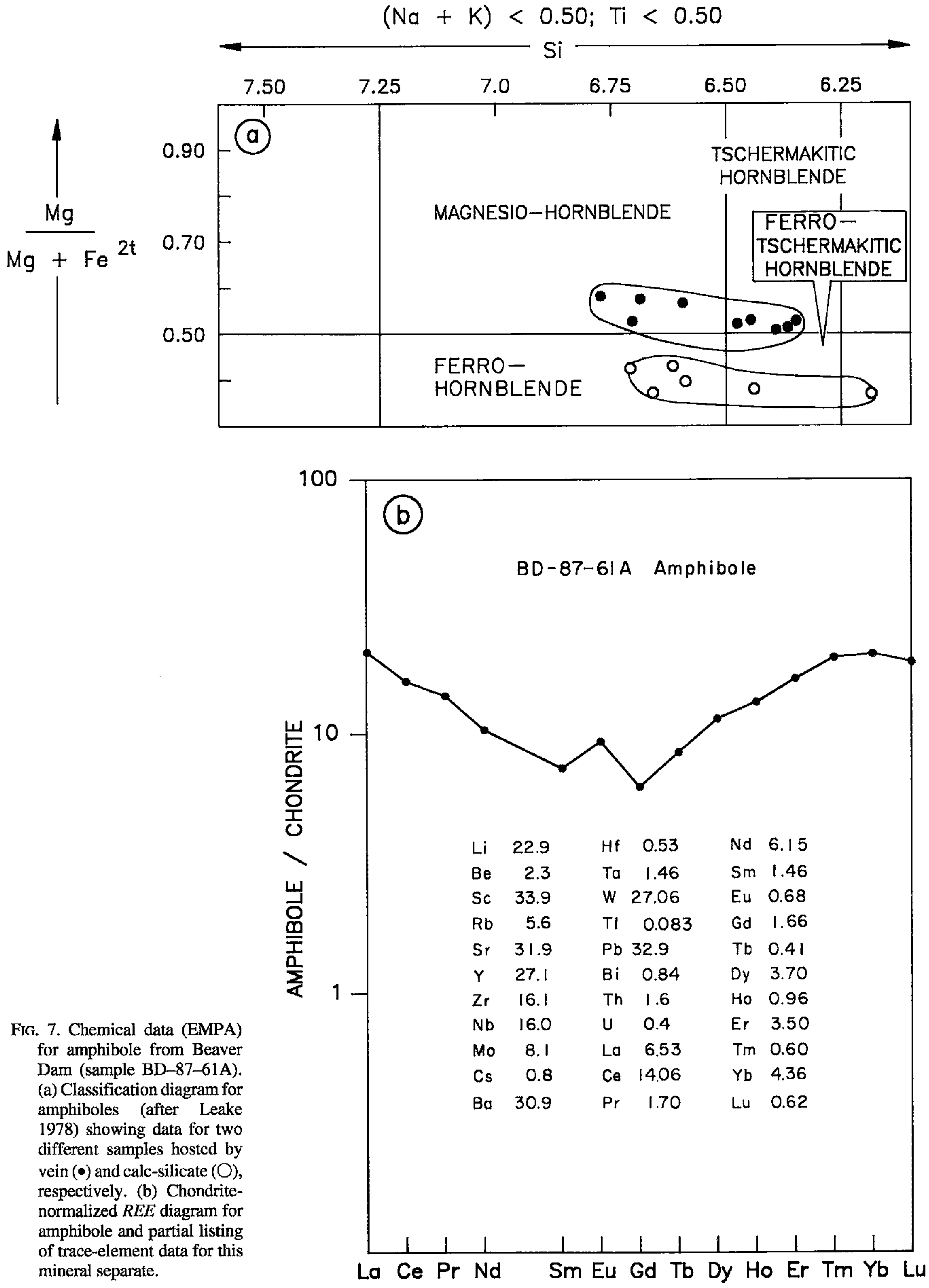

Li	22.9	Hf	0.53	Nd	6.15
Be	2.3	Ta	1.46	Sm	1.46
Sc	33.9	W	27.06	Eu	0.68
Rb	5.6	Tl	0.083	Gd	1.66
Sr	31.9	Pb	32.9	Tb	0.41
Y	27.1	Bi	0.84	Dy	3.70
Zr	16.1	Th	1.6	Ho	0.96
Nb	16.0	U	0.4	Er	3.50
Mo	8.1	La	6.53	Tm	0.60
Cs	0.8	Ce	14.06	Yb	4.36
Ba	30.9	Pr	1.70	Lu	0.62

FIG. 7. Chemical data (EMPA) for amphibole from Beaver Dam (sample BD–87–61A). (a) Classification diagram for amphiboles (after Leake 1978) showing data for two different samples hosted by vein (•) and calc-silicate (○), respectively. (b) Chondrite-normalized *REE* diagram for amphibole and partial listing of trace-element data for this mineral separate.

Halifax), a JEOL 733 electron microprobe (Dalhousie University, Halifax) and ICP–MS (Memorial University, St. John's). Mineral separates of plagioclase, muscovite, biotite, chlorite and amphibole (–40 to +80 mesh, but –80 to +120 for amphibole) were prepared using conventional magnetic and heavy-liquid techniques and supplemented with hand picking. For calcite separates, samples of concentrate were pulverized and sieved to –35/+60 mesh and hand picked under a binocular microscope; these concentrates may contain $\leq$ 2–3% quartz impurities.

Major- (Chl, Pl, Cal) and trace-element chemistry (Chl) of mineral separates was established using wet-chemical techniques as follows [see Chatterjee *et al.* (1983) for complete details]: fusion and calorimetry for Si, acid leach and atomic absorption spectroscopy (AAS) for Mn, Co, Cr, Cu, Ni, Pb, V and Zn, acid leach and calorimetry for P, fusion and AAS for Ti, Al, ΣFe, Mn, Mg, Ca, Na and K, and titration for ferrous iron. Electron-microprobe analyses (EMPA) were obtained using the wavelength-dispersion technique on a JEOL 733 Superprobe with natural mineral specimens as standards. Operating conditions were: 15 kV accelerating voltage, 10 nA sample current, and 1–3 μm beam size. Data were processed using the Tracor Northern ZAF matrix-correction program. Abundances of trace elements, including the *REE*, for mineral separates (Bt, Ms, Chl, Pl, Cal) were obtained using an ICP–MS with the procedures as outlined by Jenner *et al.* (1990). This procedure involves digesting 0.1 g of sample in a Teflon® bomb using HF and HNO_3 (HCl for carbonates) and, after evaporation, taking up in 2–3 mL of 8N HNO_3, transferring to a 125-mL bottle and diluting with water to 90 g. The instrumentation, data acquisition and processing, plus details of precision and accuracy are given in Jenner *et al.* (1990) and Longerich *et al.* (1990).

Amphibole

The major-element chemistry of two amphibole-bearing samples (Table 2) has been determined (EMPA), one from a vein (BD–87–61A) and one in wallrock marginal to a vein (BD–85–10), and data are plotted in the Si *versus* $Mg/(Mg+Fe^{2+})$ classification diagram of Leake (1978) in Figure 7a. Compositionally, the amphibole is ferro- to magnesio-hornblende or tschermakitic hornblende; there is no compositional difference in core *versus* rim for individual samples, and

TABLE 3. REPRESENTATIVE COMPOSITIONS OF PLAGIOCLASE

Sample	140C	140R	143C	143R	10	169C	169R	164.2C	164.2R
SiO_2 (wt.%)	60.97	66.56	56.93	56.61	68.88	58.25	59.96	68.43	68.86
Al_2O_3	25.13	20.69	27.54	26.89	19.76	25.95	24.48	19.58	19.12
FeO	0.11	0.15	0.10	0.17	0.00	0.06	0.05	0.07	0.01
CaO	6.00	1.27	8.72	9.26	0.29	8.61	6.82	0.13	0.18
Na_2O	8.04	10.16	6.55	6.36	11.35	7.14	7.93	11.54	11.65
K_2O	0.12	0.11	0.14	0.13	0.11	0.10	0.12	0.04	0.00
Σ	100.37	98.94	99.98	99.42	100.39	100.11	99.36	99.79	99.82
NUMBER OF CATIONS BASED ON 8 OXYGEN									
Si	2.696	2.938	2.550	2.554	3.000	2.608	2.690	2.993	3.009
Al	1.309	1.076	1.454	1.430	1.000	1.370	1.294	1.009	0.985
Fe	0.004	0.005	0.009	0.006	0.000	0.005	0.004	0.005	0.000
Ca	0.284	0.060	0.418	0.447	0.013	0.413	0.327	0.006	0.008
Na	0.688	0.868	0.568	0.556	0.965	0.620	0.689	0.978	0.987
K	0.006	0.005	0.007	0.007	0.005	0.005	0.006	0.002	0.000
END MEMBER IN MOLE %									
An	29.0	6.4	42.0	44.2	1.3	39.7	31.9	0.6	0.8
Ab	70.3	93.0	57.2	55.0	98.1	59.7	67.4	99.3	99.2
Or	0.7	0.6	0.8	0.8	0.5	0.6	0.7	0.1	0.0

Abbreviations: C = core analysis; R = rim analysis

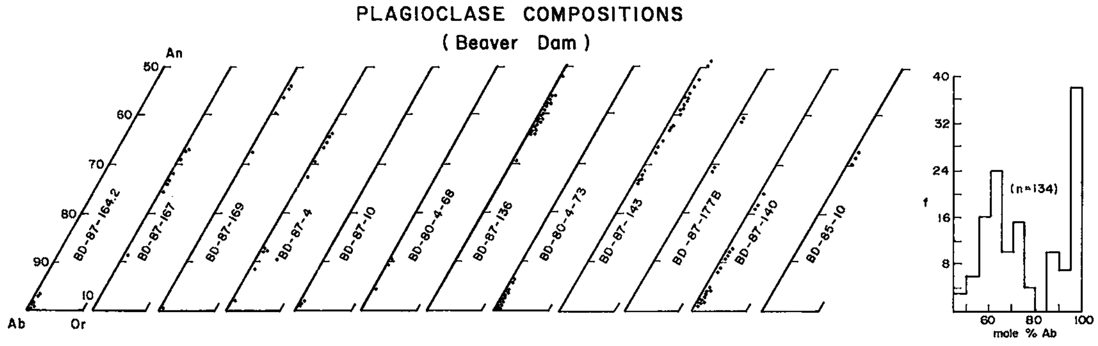

FIG. 8. Chemical data (EMPA) for plagioclase from different vein samples at Beaver Dam plotted in An–Ab–Or diagram, with the total data-set summarized in the histogram. Note that none of the feldspar samples contain >1 mole % Or, but for purposes of plotting all the data, some seem to be relatively more Or-rich.

there is a slight chemical difference between the two sample localities. Trace-element data (ICP–MS) for a single amphibole, including *REE* (Fig. 7a), indicate contents (ppm) of Y (27), Zr (16), Pb (32) and W (27); it is possible that the elevated contents of these elements reflect submicroscopic inclusions of the appropriate phases. The chondrite-normalized pattern for this amphibole (Fig. 7b) has an overall concave shape that is similar to that of igneous amphiboles (Hanson 1980), with a positive Eu anomaly [$(Eu/Eu^*)_N$ = 1.34] and $(La/Lu)_N$ value of 1.

Plagioclase

Core and rim compositions of plagioclase in 12 samples (Table 3) indicate two broad groupings: An_{0-15} and An_{20-60} (Fig. 8). Spot checks were made for Sr and Ba, but both elements were found to be below the detection limit. No single sample shows the complete range of compositional variation. In fact, the intrasample variation is generally only 10–25 mole % An or less, especially in the samples dominated by albite. In a few samples, there is a clear gap in the compositions observed; for example, in one sample, the compositional ranges are An_{27-36} and An_{2-13}, whereas in another, the gap is between An_{32-46} and An_0.

The compositional profiles for four plagioclase grains examined in detail are shown in Figure 9. The two complete rim-to-rim profiles show broadly similar patterns, with an An-rich core (to An_{40-45}) and an An-poor rim. In one profile (BD–87–171.2), there is a suggestion of reverse zonation in the core. The two remaining profiles, for core-to-rim traverses, show a normal-type profile, with an An-rich core (to An_{64-66}), and a drop in a continuous and systematic fashion to An_{22-24} at the rims. In both of these latter profiles, the rim is in contact with calcite.

Trace-element data for nine plagioclase separates (ICP–MS) are presented in Table 4. Bulk analyses (AAS) of these separates indicate compostions (our

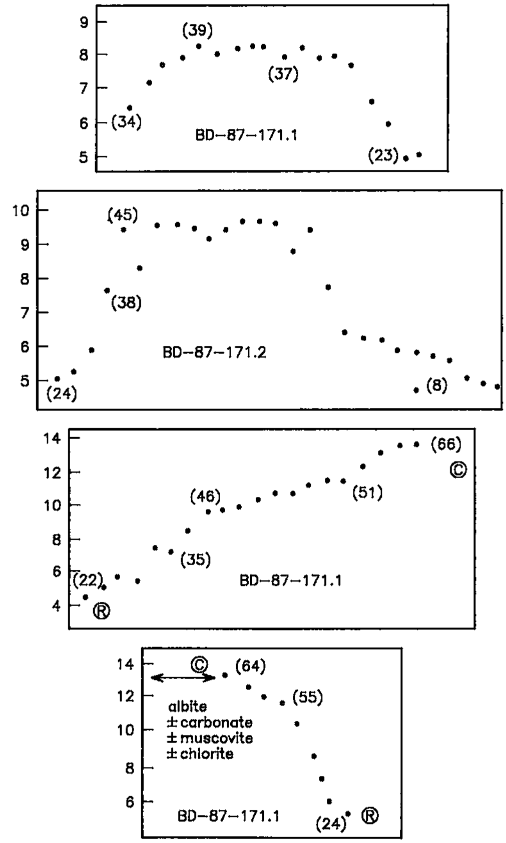

FIG. 9. Plagioclase grains in sample BD–87–171 from Beaver Dam illustrating chemical zonation (measured as wt.% CaO) as determined from EMPA. The numbers in the chemical profiles refer to mole % An, and the data points represent increments of *ca.* 10 μm across the grain. Abbreviations C and R refer to core and rim, respectively.

TABLE 4. TRACE ELEMENT DATA FOR PLAGIOCLASE

Sample	90-A	167	41B	1080-7B	41C	1080-6B	177D	170B	CX-86-6
Li (ppm)	16.5	54.2	42.9	7.7	22.7	27.8	20.5	5.2	4.1
Rb	75.1	100.9	73.5	78.8	48.4	19.3	103.5	28.3	23.5
Sr	648	605	410	450	575	494	431	538	104
Y	3.1	1.4	13.2	1.5	2.6	1.0	13.7	4.5	0.49
Zr	3.8	0.7	9.1	1.9	2.2	2.4	5.8	3.0	5.53
Cs	7.3	11.7	9.4	2.9	7.7	4.5	13.4	3.4	1.0
Ba	98.7	284	230	149	81	107	495	132	48.4
Hf	0.1	ND	0.4	0.1	0.3	0.1	0.4	ND	ND
Pb	69.8	197	227	98.1	92.8	215	237	64.6	41.9
Bi	0.4	0.1	0.1	0.2	0.3	0.1	3.9	0.3	0.37
Th	0.1	0.04	0.4	0.08	0.1	0.06	0.2	0.2	0.73
U	0.09	0.03	0.2	0.02	0.04	0.04	0.07	0.04	ND
La	4.11	0.36	4.82	0.60	1.78	0.29	7.00	0.42	0.16
Ce	8.65	0.73	12.01	1.04	4.26	0.62	13.60	0.85	0.13
Pr	1.07	0.09	1.43	0.12	0.57	0.07	1.74	0.12	0.09
Nd	4.38	0.36	5.65	0.46	2.55	0.30	7.31	0.58	0.089
Sm	1.15	0.17	1.65	0.10	0.65	0.12	2.01	0.30	0.062
Eu	0.82	0.35	0.86	0.44	0.64	0.39	0.75	0.36	ND
Gd	1.12	0.35	2.20	0.28	0.69	0.24	2.54	0.73	0.16
Tb	0.18	0.04	0.40	0.03	0.10	0.03	0.44	0.14	0.04
Dy	0.99	0.28	2.47	0.25	0.62	0.23	2.91	0.89	0.20
Ho	0.13	0.05	0.50	0.05	0.10	0.04	0.56	0.18	0.004
Er	0.28	0.14	1.53	0.14	0.28	0.11	1.49	0.51	0.014
Tm	0.03	0.02	0.23	0.01	0.03	0.01	0.18	0.06	0.016
Yb	0.14	0.13	1.74	0.13	0.18	0.09	0.94	0.44	ND
Lu	0.02	0.01	0.25	0.01	0.01	0.01	0.10	0.06	ND

ND = not detected

unpubl. data) of An_{5-27}, with <0.1 wt.% P_2O_5, up to 1–1.5 wt.% combined MgO and Fe_2O_3, and up to 2 wt.% K_2O in rare cases. The presence of Fe, Mg and K are attributed to fine-grained products of alteration (Chl, Ms) in the plagioclase; thus, the trace-element data must be considered with these limitations in mind. Concentrations (mean ± 1σ, ppm) of Li (24.6 ± 15.6), Cs (7.5 ± 3.5) and Rb (65.9 ± 29.2) are positively correlated, along with Ba, which is of higher concentration (197 ± 130), whereas Sr (518 ± 81) shows no correlation with the aforementioned elements. The contents of Pb (150 ± 70) are not attributed to microinclusions of galena because of the low Bi values (see below). The Pb contents are of interest given the characteristic green color of the plagioclase and the general association of elevated Pb contents with amazonitic feldspars (*e.g.*, Stevenson & Martin 1986). The Zr abundance (3.7 ± 2.6) indicates that whereas microinclusions of zircon may be present, they are not abundant.

Chondrite-normalized *REE* patterns for the plagioclase separates (Fig. 10) show a large overall range, reflecting the variation in Σ*REE* of 3.0 to 41.5 ppm (avg. = 15.9 ± 14.6). There is no relationship among the Σ*REE*, amount of fractionation, bulk composition and any of the trace elements (Fig. 10). Despite the large absolute spread in Σ*REE* abundance, the shape of the profiles remains fairly constant, except for the *HREE* in samples BD–87–167 and 1080–6B; whereas there is little change in Eu_N values, the degree of the Eu anomaly changes considerably (Eu/Eu* from 1 to 8.1). Presumably this latter feature indicates that $f(O_2)$ was sufficiently low to stabilize Eu^{2+} over Eu^{3+} (Drake 1975). Moderately flat chondritic patterns are exhibited for all but two of the feldspar samples, with these latter samples having

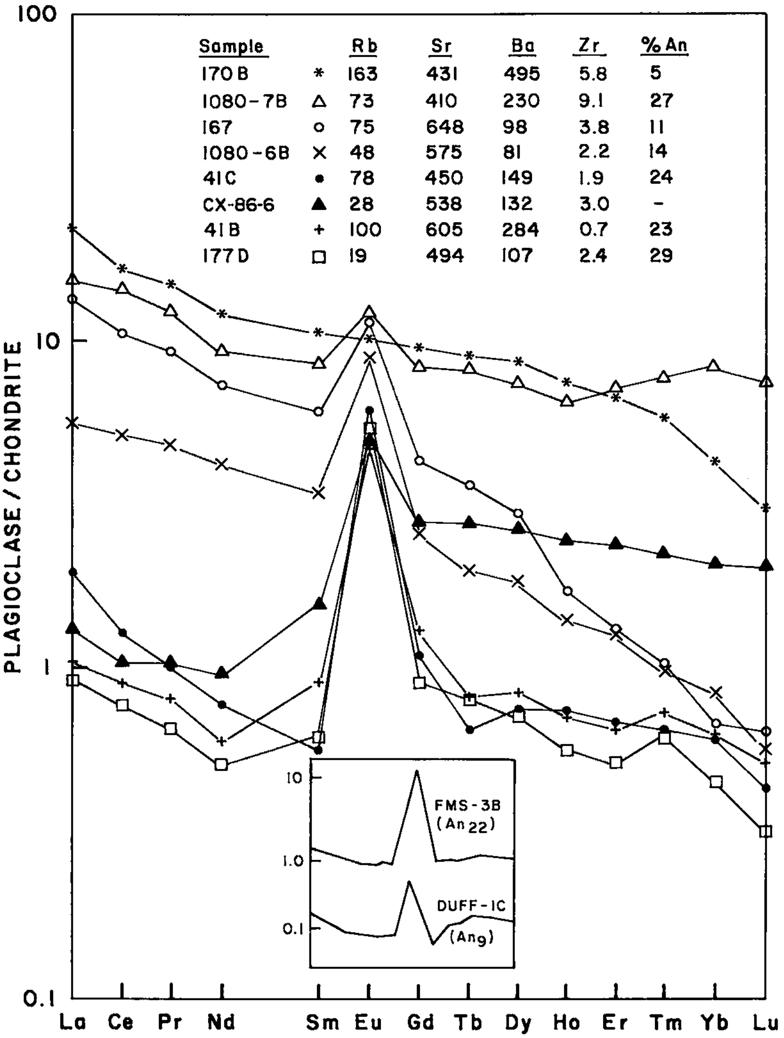

Sample		Rb	Sr	Ba	Zr	%An
170B	*	163	431	495	5.8	5
1080-7B	△	73	410	230	9.1	27
167	○	75	648	98	3.8	11
1080-6B	×	48	575	81	2.2	14
41C	●	78	450	149	1.9	24
CX-86-6	▲	28	538	132	3.0	-
41B	+	100	605	284	0.7	23
177D	□	19	494	107	2.4	29

FIG. 10. Chondrite-normalized *REE* diagram for plagioclase separates from Beaver Dam. The trace-element data for the samples are arranged, from top to bottom, according to decreasing abundance of the *REE* to illustrate the apparent lack of correlation between abundance, degree of fractionation and trace-element chemistry. The bulk composition of the plagioclase separates was determined from wet-chemical analyses (AAS, Technical University of Nova Scotia, Halifax) and are reported as mole % An. Note that sample 90–A is not plotted because its chondrite-normalized *REE* patterns falls at <1.0. Inset shows the chondrite-normalized profiles for two plagioclase grains from other gold districts (Fifteen Mile Stream, FMS; Dufferin, DUFF) for purposes of comparison (see text).

strongly fractionated patterns [$(La/Lu)_N$ = 18 to 36], more typical of feldspar in granitic rocks (Hanson 1980).

Comparison of the Beaver Dam with analytical data on two plagioclase samples from other gold districts (our unpubl. data) indicates a comparable enrichment of trace elements. The chondrite-normalized *REE* patterns, shown as an inset in Figure 10, illustrate that despite coming from other deposits, similar patterns are observed, albeit with different absolute abundances. Note again the strong Eu anomalies despite the low absolute abundances.

TABLE 5. REPRESENTATIVE COMPOSITIONS OF GARNET

Sample	152-2			152-1		171-2		171-1	
Point	2	20	25	4	6	27	32	1	4
SiO_2 (wt.%)	37.30	36.88	37.07	37.02	36.95	36.88	37.08	36.78	36.75
TiO_2	0.48	0.29	0.23	0.24	0.30	0.12	0.28	0.33	0.17
Al_2O_3	20.75	20.71	20.87	20.92	20.93	20.85	20.80	20.91	21.25
Cr_2O_3	0.08	0.10	0.08	0.12	0.12	0.05	0.09	0.05	0.08
FeO	12.81	20.26	23.81	20.02	16.91	25.62	16.92	22.28	21.79
MnO	17.19	15.06	12.62	14.66	15.74	11.20	13.28	12.90	13.15
MgO	0.90	1.45	1.73	1.34	1.26	1.78	1.50	1.40	1.69
CaO	9.70	4.72	3.56	5.30	6.83	3.49	9.78	5.22	5.15
Σ	99.21	99.47	99.97	99.60	99.05	100.00	99.71	99.87	100.04
NUMBER OF CATIONS BASED ON 12 OXYGEN									
Si	6.003	5.986	5.992	5.988	5.984	5.973	5.956	5.951	5.926
Al	3.937	3.963	3.977	3.989	3.996	3.981	3.939	3.939	4.040
Ti	0.058	0.035	0.028	0.029	0.057	0.015	0.034	0.040	0.021
Cr	0.010	0.013	0.010	0.015	0.015	0.006	0.011	0.006	0.010
Fe	1.724	2.750	3.219	2.708	2.294	3.470	2.246	3.015	2.939
Mn	2.343	2.071	1.728	2.009	0.304	1.537	1.807	1.768	1.796
Mg	0.216	0.351	0.417	0.323	2.159	0.430	0.359	0.338	0.406
Ca	1.673	0.821	0.617	0.919	1.185	0.606	1.683	0.905	0.890
END MEMBER IN MOLE %									
Alm	28.9	45.9	53.8	45.5	38.6	57.4	36.8	50.0	48.7
Spess	39.3	34.6	28.9	33.7	36.3	25.4	29.6	29.3	29.8
Py	3.6	5.9	7.0	5.4	5.1	7.1	5.9	5.6	6.7
Gross	28.1	13.7	10.3	15.4	19.9	10.0	27.6	15.0	14.8

Vein garnet: 152-1, 2; wallrock garnet: 171-1, 2

Garnet

Garnet (Table 5) has been analyzed in both vein (BD–87–152.1, 152.2, 171.1, 171.2) and wallrock (BD–85–10, BD–87–100.2, 171.3) samples, where it occurs as euhedral grains (the only exception is for BD–85–10, where it occurs as a symplectititic intergrowth with quartz). In Figure 11, plots of the Fe–Mn–Ca end-member components are given, along with compositional profiles for the major cations. Compositionally, the garnet is dominated by spessartine (25–45 mole %), almandine (30–65 mole %) and grossular (10–40 mole %), with pyrope consistently less than or equal to 5–7 mole %, although the range for a single grain is less than this. In sample BD–85–10, garnet coexists with calcic amphibole; hence, the relative increase in grossular component is a function of bulk-rock composition.

Detailed zoning profiles have been obtained for three grains, two of which are in the same sample (BD–87–171), and two additional core-to-rim trends are shown for samples BD–87–100.2 and BD–87–171.3 in the triangular plots. There is generally an enrichment of Mn in the core, although this may be mantled by a narrow zone of more elevated Mn, as in samples BD–87–171.1 and 171.2. The presence of Mn depletion in the rim of these latter samples may reflect re-equilibration and Mn diffusion. The Mn trend is mimicked by Ca, whereas the reverse is shown by Fe. In sample BD–87–152, the garnet profile (core to rim) is substantially different from that illustrated in sample BD–87–171. A simple profile

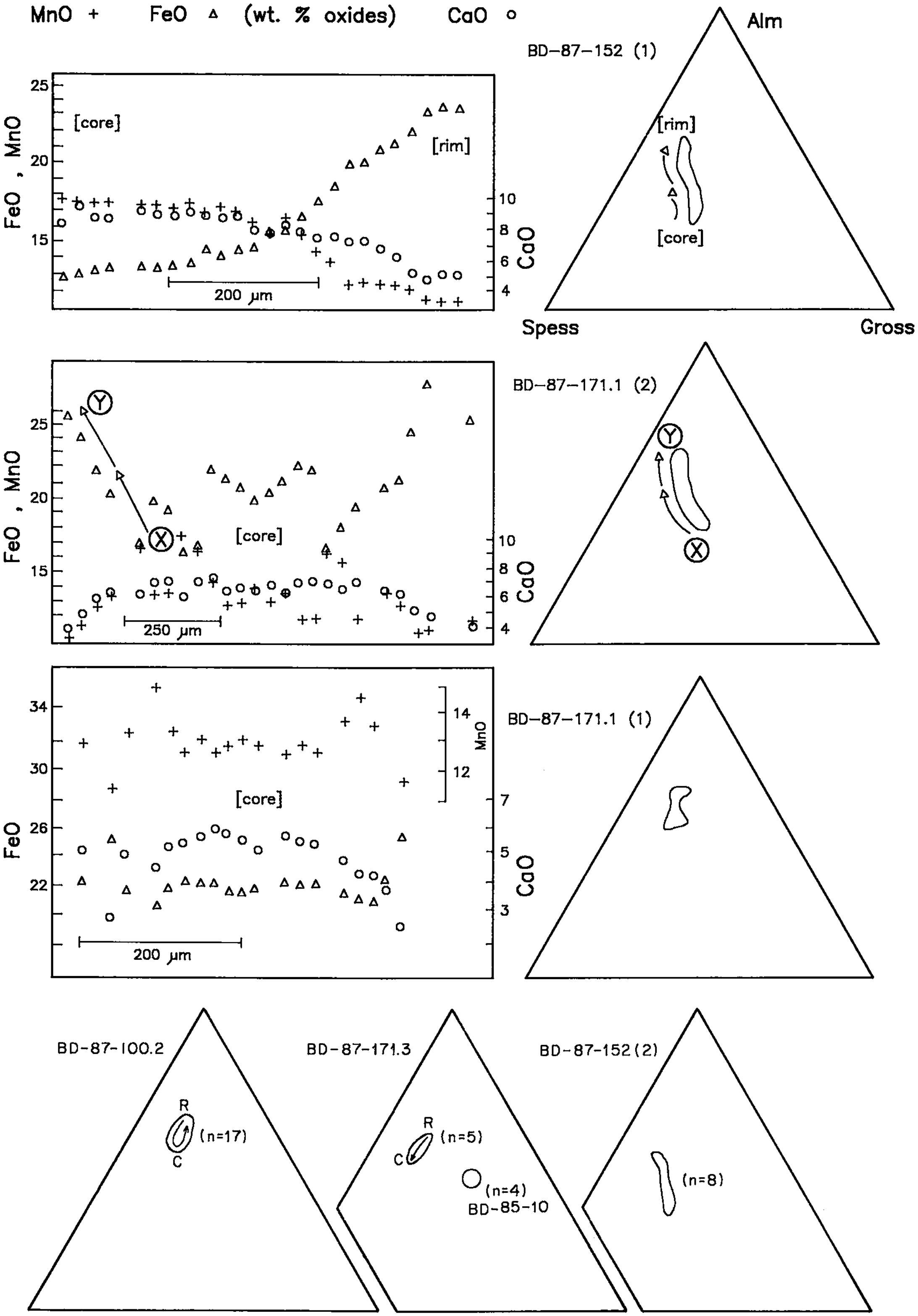
MnO + FeO △ (wt. % oxides) CaO ○
FeO , MnO
CaO
[core]
[rim]
200 μm
25
20
15
10
8
6
4
Alm
Spess
Gross
BD-87-152 (1)
BD-87-171.1 (2)
Y
X
250 μm
BD-87-171.1 (1)
FeO
MnO
34
30
26
22
14
12
7
5
3
BD-87-100.2
R
C
(n=17)
BD-87-171.3
(n=5)
(n=4)
BD-85-10
BD-87-152 (2)
(n=8)

of concentrations is observed in BD–87–152, with a Mn- and Ca-rich core (16–17 wt.% MnO, ~9 wt.% CaO) that gives way to an Fe-rich (24 wt.% FeO) rim. However, the overall compositional range is broadly similar to that in garnet in sample BD–87–171.

Epidote

Epidote (Table 6) has been analyzed in a single specimen (BD–87–171), where it occurs as euhedral grains showing a distinct blue to blue-green color with varying shades suggesting chemical zonation. However, EMPA of several grains, including core and rim compositions, indicate exceptionally uniform chemistry, with constant abundances of Al (28–30 wt.% Al_2O_3), Ca (24–25 wt.% CaO) and Fe (4–7 wt.% FeO). The chemistry conforms to clinozoisite and in fact is almost identical to a clinozoisite composition given in Deer *et al.* (1966) for an epidote vein in amphibolite.

Biotite

Biotite (Table 7) has been analyzed from six vein and seven wallrock samples. Despite the variety of occurrences (*i.e.*, vein *versus* wallrock) and mineral associations, its chemistry is remarkably uniform, with $Fe^{2+}/(Fe^{2+}+Mg) = 0.50 \pm 0.05$ (deviations from this value are discussed below), $0.12 < Ti < 0.27$ apfu, $2.36 < {}^{IV}Al < 2.68$, $18 < FeO < 20$ wt.% and $9 < MgO < 10$ wt.%. The only exceptions to the general average are for samples BD–87–61A and BD–85–10, which contain calc-silicate assemblages. The biotite has a larger range in *mg* values compared to the rest of the data set. The full data-set (n=131) is summarized in Figures 12 and 13,

TABLE 6. REPRESENTATIVE COMPOSITIONS OF EPIDOTE

Point	43	44	47	48	51	52
SiO_2 (wt.%)	37.25	37.56	37.59	37.99	36.67	37.65
TiO_2	0.57	0.37	0.14	0.16	0.19	0.14
Al_2O_3	28.96	29.80	28.28	28.64	28.85	28.80
FeO	5.43	4.42	6.85	5.35	6.05	6.15
MnO	0.39	0.39	0.18	0.55	0.35	0.49
MgO	0.06	0.05	0.06	0.09	0.03	0.05
CaO	24.52	24.70	24.46	24.42	24.56	24.35
Na_2O	0.05	0.05	0.00	0.00	0.00	0.00
Σ	97.75	97.36	97.58	97.21	96.72	97.67
NUMBER OF CATIONS BASED ON 13 OXYGEN						
Si	3.068	3.068	3.107	3.120	3.042	3.09
${}^{iv}Al$	0.000	0.000	0.000	0.000	0.000	0.000
${}^{vi}Al$	2.808	2.873	2.756	2.782	2.821	2.795
Ti	0.039	0.026	0.013	0.013	0.013	0.013
Fe	0.377	0.299	0.468	0.364	0.416	0.429
Mn	0.026	0.026	0.013	0.039	0.026	0.039
Mg	0.013	0.000	0.013	0.013	0.000	0.013
Ca	2.158	2.158	2.158	2.158	2.184	2.145
Na	0.013	0.013	0.000	0.000	0.000	0.000

FIG. 11. Compositional profiles (EMPA) of garnet grains from vein samples at Beaver Dam, illustrating chemical zonation; end-member compositions are indicated in the adjacent Almandine – Spessartine – Grossular plots for the three profiles along with additional compositions of garnet-bearing samples. The arrows in the plots indicate the chemical zonation from rim (R) to core (C).

TABLE 7. REPRESENTATIVE COMPOSITIONS OF BIOTITE

Sample Host	61A V	152 V	152 WR	87-2.1 WR	87-2.1 STR	135 STR	164 V	141 WR
SiO_2 (wt.%)	37.69	36.00	36.64	35.84	35.70	36.18	36.53	35.05
TiO_2	1.36	1.37	1.46	2.22	2.33	1.78	1.96	1.44
Al_2O_3	16.83	19.07	18.40	18.36	18.31	19.15	18.23	19.23
FeO	16.68	18.66	17.14	20.02	18.81	19.96	19.13	19.46
MnO	0.41	0.31	0.30	0.49	0.48	0.20	0.25	0.21
Cr_2O_3	0.04	0.06	0.00	0.08	0.04	0.06	0.04	0.06
MgO	13.09	10.41	11.39	9.75	9.50	9.69	9.75	9.49
CaO	0.01	0.01	0.06	0.11	0.47	0.10	0.04	0.03
Na_2O	0.10	0.17	0.16	0.03	0.51	0.04	0.00	0.10
K_2O	9.15	9.34	8.81	9.57	9.18	9.15	9.84	9.11
Σ	95.35	95.40	94.35	95.28	95.58	96.33	95.78	94.17
NUMBER OF CATIONS BASED ON 22 OXYGEN								
Si	5.641	5.447	5.541	5.456	5.436	5.445	5.529	5.396
^{iv}Al	2.359	2.553	2.459	2.544	2.564	2.555	2.471	2.604
^{vi}Al	0.611	0.848	0.813	0.751	0.723	0.842	0.782	0.885
Ti	0.153	0.154	0.165	0.254	0.267	0.201	0.223	0.165
Fe^{2+}	2.088	2.360	2.167	2.396	2.395	2.512	2.422	2.505
Mn	0.052	0.039	0.037	0.063	0.062	0.025	0.032	0.026
Cr	0.005	0.005	0.000	0.010	0.005	0.005	0.005	0.005
Mg	2.920	2.347	2.567	2.212	2.156	2.173	2.199	2.175
Ca	0.002	0.002	0.011	0.018	0.077	0.016	0.006	0.004
Na	0.029	0.048	0.046	0.009	0.151	0.012	0.000	0.028
K	1.747	1.804	1.700	1.859	1.783	1.757	1.900	1.788

61A biotite is intergrown with Mg-rich hornblende; 152WR biotite occurs as oikocryst in wall rock; 152V biotite is adjacent garnet; 135 biotite is adjacent coarse arsenopyrite; 141WR biotite is flattened porphyroblast.
Abbreviations: V = vein; WR = wall rock; STR - striping

plots of ^{IV}Al and wt.% TiO_2 *versus* $Fe^{2+}/(Fe^{2+}+Mg)$, respectively, and Figure 14, a histogram plot of Ti. The biotite is annitic and shows a positive correlation between ^{IV}Al and *mg* value, with an almost complete overlap for vein- and wallrock-hosted samples. In at least one instance (BD–87–152), however, there is a distinct separation between the two types, with vein-hosted biotite characterized by lower *mg* values, whereas the ^{IV}Al contents are similar. In addition, it is clear that the compositional variation of biotite in individual samples is considerably smaller than that for the whole data-set (Figs. 12, 13). In terms of TiO_2, there is a complete overlap for vein- and wallrock-hosted biotite (Figs. 13, 14).

A detailed examination of potential compositional variation in biotite on a mm- to cm-scale is illustrated in Figure 15 for different morphological occurrences of biotite in four specimens. Samples BD–87–141, 87–135 and 87–2.1 show that biotite in quartz-arsenopyrite bands is compositionally identical to biotite hosted by either psammitic or pelitic lithologies regardless of proximity or abundance of sulfides.

The F and Cl contents of biotite from vein and wallrock are constant at 0.2 ± 0.1 wt.% and <0.05 wt.%, respectively. There is no apparent difference among the samples or among different morphological occurrences in a single sample. The low F content of the biotite, which translates into low F/(F+OH) values, combined

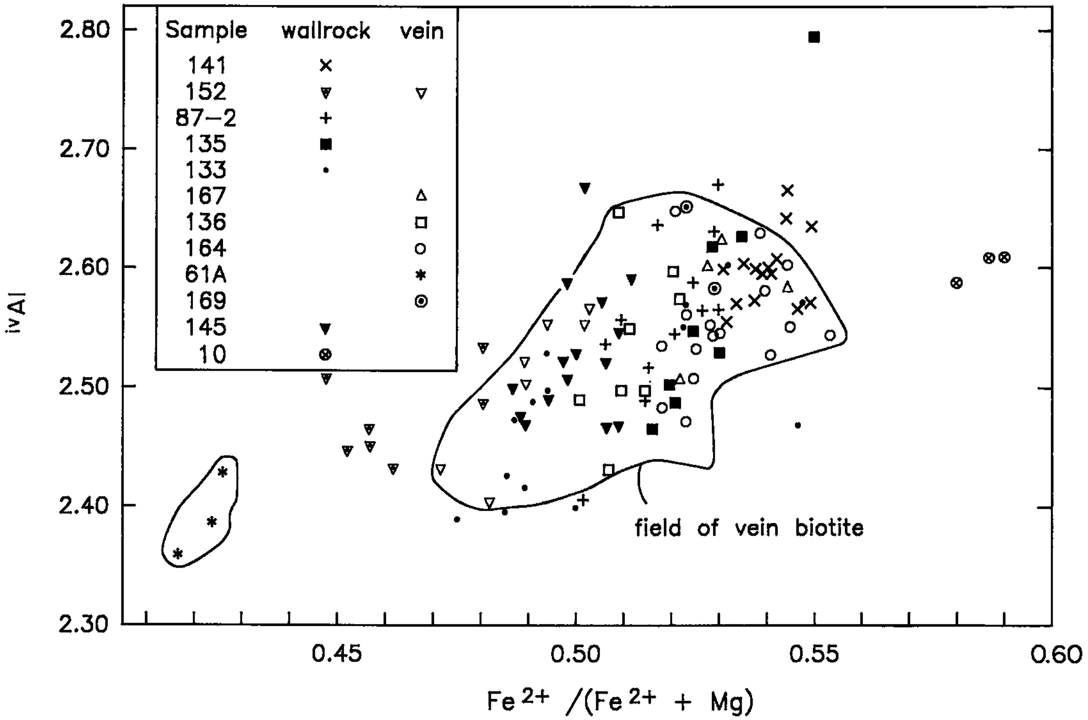

FIG. 12. Chemical data (EMPA) for vein- and wallrock-hosted biotite from Beaver Dam plotted in the ^{IV}Al *versus* Fe^{2+}/(Fe^{2+}+Mg) diagram. Note that the fields for vein and wallrock overlap, except for samples BD–87–10 and 61A (see text).

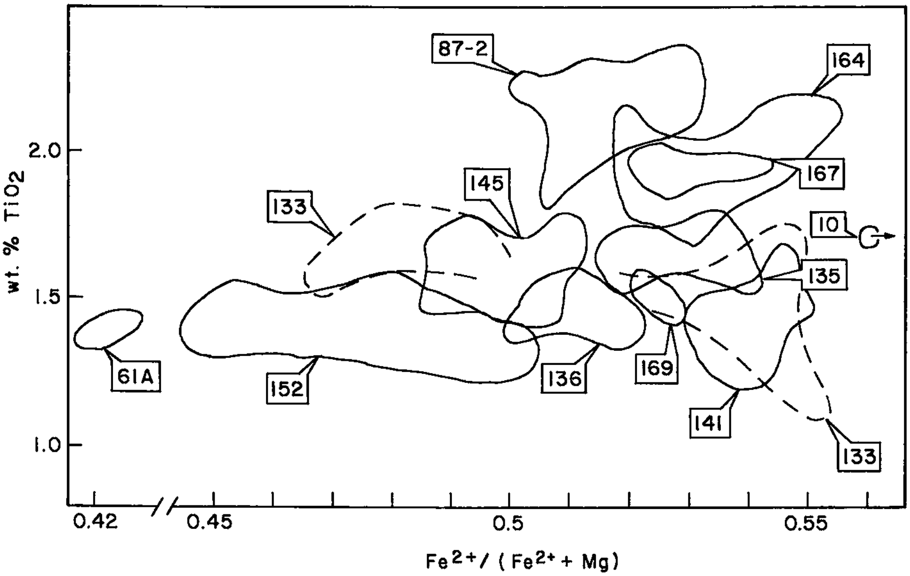

Sample	n
61A	3
87–2	13
164	17
167	5
135	9
133	16
141	15
169	2
136	8
145	15
152	15
10	3
Σ	131

FIG. 13. Chemical data (EMPA) for vein- and wallrock-hosted samples (see Fig. 12 for sample identification) from Beaver Dam plotted in wt.% TiO$_2$ *versus* Fe^{2+}/(Fe^{2+}+Mg) diagram. Numbers (n) refer to individual EMPA results for each sample. For sample BD–87–133, the data group into two clusters separated by a compositional gap as indicated.

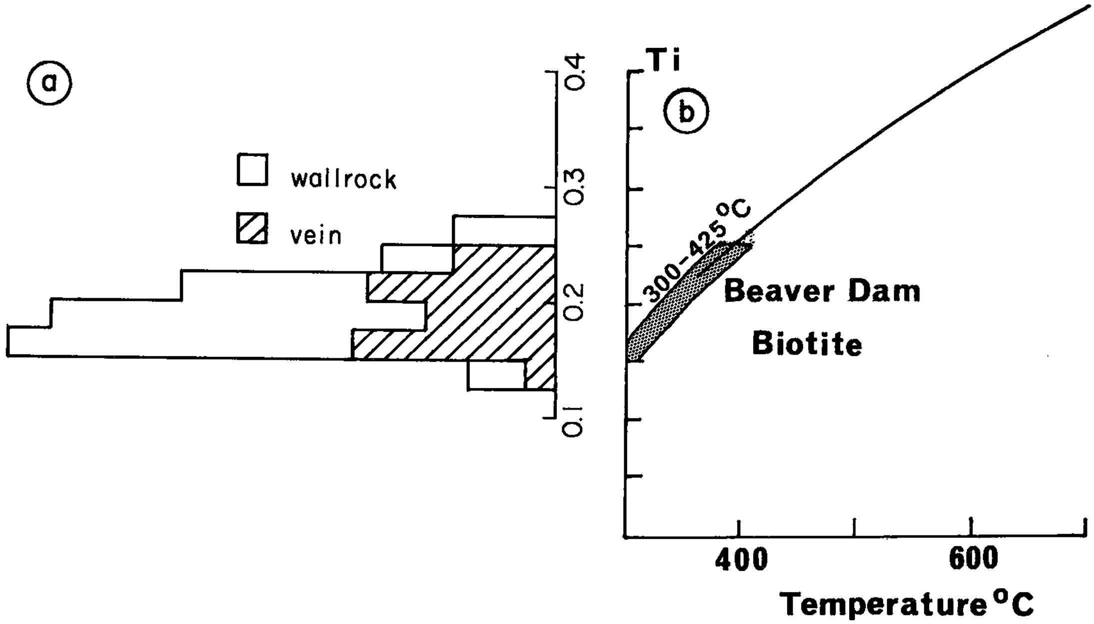

FIG. 14. Chemical data for biotite from Beaver Dam. (a) Histogram of Ti content for biotite (22 oxygen atoms pfu) for vein and wallrock samples. (b) Ti content for biotite (22 oxygen atoms p.f.u.) *versus* temperature (°C), with calibration after LeBel (1979; see text for discussion). The compositional data for the biotite at Beaver Dam indicate a range of 300–425°C.

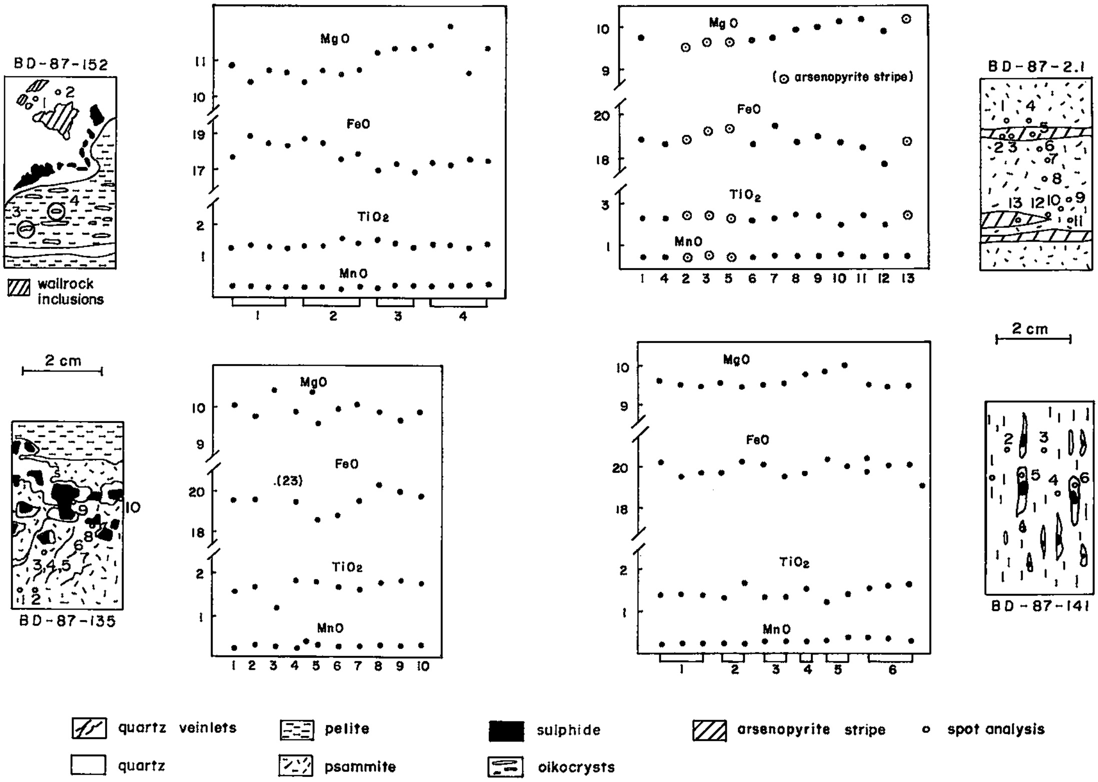

FIG. 15. Sketches of polished sections of vein and wallrock samples from Beaver Dam, with locations of individual spot-analyses of biotite grains indicated by numbers. Results of the analyses are plotted as a function of wt.% MgO, FeO, TiO_2 and MnO. Note that in all the diagrams, there is no clear distinction in the biotite chemistry or a relationship to paragenesis or morphology.

TABLE 8. TRACE ELEMENT DATA FOR MICA SEPARATES

	CX-86	FMS-	90A	293	41A	181	172B	165	9C	103	80-5-1	121A	10	80-1-2	169.2	169.1	87-10	116	171	267	CAR-13	USH-3
Mineral	Bt	Bt	Chl	Chl	Chl	Chl	Chl	Chl	Chl	Chl	Chl	Chl	Chl	Chl	Chl	Chl	Ms	Ms	Ms	Ms	Ms	Ms
Li (ppm)	183	250	235	464	157	137	306	189	256	1.93	85.0	312	352	192	75.3	187	24	81.0	45.7	46.3	59.8	73.1
Rb	563	375	0	60.6	0.3	27.6	15.6	0.6	8	48.5	84.6	1.0	2.3	9.2	0.13	0.32	101.4	428	486	321	381	135
Sr	4.8	24.2	1.53	33.7	8.6	33.1	25.6	4.2	7.5	8.7	177.2	4.5	54.9	28.6	4.2	4.7	57.9	24.9	89	24.8	62.3	10.3
Y	4.7	6.2	17.3	13.4	1.3	50.9	16.5	5.5	14.2	8.3	9.7	9.9	19.5	6.1	3.3	7.5	1.25	2.8	11	9.7	0.6	0.6
Zr	5.0	54.3	2.64	23.3	0.9	21.4	2.9	4.6	1.4	5.6	106.5	3.3	3.4	12.7	3.03	1.8	4.9	49.2	22	2.1	1.0	4.8
Cs	93.4	24.7	ND	3.4	0.62	1.5	0.2	0.1	0.7	3.2	4.4	0.18	0.2	0.9	0.09	0.15	4.6	21.4	10	19.2	22.3	3.2
Ba	1108	1339	1.8	177	4.6	68.6	64.1	5.5	74	207	153	8.5	2.1	39.6	1.7	2.1	195	1211	768	1523	1380	226
Hf	0.2	1.6	ND	1.2	0.03	0.6	0.18	0.23	0.06	0.83	3.5	0.08	0.57	0.45	0.08	0.07	0.06	1.6	0.7	0.32	ND	0.1
Tl	2.9	1.9	ND	0.3	0.01	0.1	0.16	0.02	0.12	0.25	0.33	0.03	0.64	0.05	0.01	0.0	0.95	1.8	1.3	1.4	2.3	1.3
Pb	11.4	110	4.1	19.4	5.8	27.9	28.0	10.1	20	7.5	72.5	64	426	19.9	11.5	9.3	54.0	4.0	6.8	8.7	7.9	12.7
Bi	0.1	1.3	0.3	0.2	0.03	0.9	0.21	0.09	0.06	0.0	ND	1.2	ND	0.37	0.03	0.02	176	0.0	0.1	-	ND	ND
Th	0.2	5.2	0.1	1.7	0.04	1.6	0.26	0.65	0.06	0.23	5.3	0.06	0.11	0.98	0.25	0,3	1.31	4.1	1.0	0.2	ND	ND
U	0.1	0.8	0.1	0.5	0.02	0.9	0.12	0.09	0.58	0.24	1.9	0.2	0.21	0.21	0.19	0.17	0.12	1.3	0.4	0.1	ND	ND
Sc	-	35.4	41.4	-	-	-	-	-	8.9	-	-	15	-	28.1	5.1	16.6	5.5	32.0	12.54	-	6.8	5.8
Nb	-	32.9	0.3	-	-	-	-	-	-	-	-	21	-	1.2	-	1.8	1.9	8.7	7.6	-	7.0	1.1
Ta	-	2.3	ND	-	-	-	-	-	2.6	-	-	1.3	-	0.11	-	-	0.29	0.36	0.6	-	1.9	0.2
W	-	-	-	-	-	-	-	-	71.0	-	-	45.6	-	36.6	124	9.1	-	35.4	137	-	27.7	18.3
La	0.62	15.8	24.70	7.37	0.40	36.96	11.98	13.18	0.81	1.38	17.08	2.49	5.54	5.63	10.1	30.7	0.29	5.95	2.71	9.87	0.32	0.67
Ce	1.33	30.7	50.68	15.26	0.80	58.54	24.20	26.50	3.69	2.91	35.04	6.30	10.34	11.23	24.5	66.5	0.47	13.15	6.00	18.52	0.59	1.32
Pr	0.15	3.76	6.17	2.01	0.10	6.41	2.92	3.21	0.55	0.34	4.01	0.87	1.25	1.27	2.69	7.83	0.12	1.41	0.75	2.03	0.07	0.18
Nd	0.66	13.70	25.40	8.81	0.45	24.80	11.28	12.50	2.62	1.54	15.06	3.69	5.44	4.91	9.78	28.48	0.32	5.16	3.31	7.97	0.30	0.71
Sm	0.23	2.58	6.21	2.32	0.12	4.99	2.58	2.74	0.76	0.47	3.07	3.73	1.57	1.11	2.5	6.53	0.19	0.95	1.22	1.61	0.09	0.18
Eu	Nd	0.62	1.52	0.75	0.09	1.29	0.82	0.65	0.30	0.03	0.65	0.35	0.54	0.38	0.59	1.48	0.15	ND	0.43	0.0	0.00	0.03
Gd	1.15	2.67	7.75	2.64	0.20	6.20	2.84	2.43	1.22	0.52	2.27	1.23	1.86	1.24	2.22	5.46	0.22	0.79	2.04	3.90	0.36	0.17
Tb	0.11	0.30	1.02	0.44	0.03	0.99	0.49	0.34	0.28	0.18	0.38	0.24	0.38	0.22	0.28	0.67	0.03	0.11	0.44	0.31	0.02	0.02
Dy	0.86	1.42	4.56	2.65	0.20	5.94	2.82	1.48	2.37	1.33	2.31	1.71	2.48	1.26	1.14	2.55	0.24	0.64	2.51	2.01	0.13	0.13
Ho	0.17	0.24	0.65	0.51	0.04	1.21	0.55	0.21	0.56	0.32	0.43	0.38	0.51	0.24	0.14	0.31	0.06	0.10	0.45	0.41	0.02	0.02
Er	0.48	0.73	1.18	1.37	0.10	2.93	1.40	0.45	1.87	1.11	1.33	1.23	1.36	0.68	0.23	0.53	0.23	0.34	1.28	1.12	0.08	0.08
Tm	0.07	0.10	0.11	0.20	0.01	0.31	0.17	0.04	0.29	0.16	0.23	0.18	0.14	0.09	0.02	0.03	0.04	0.05	0.20	0.15	0.01	ND
Yb	0.39	0.78	0.47	1.33	0.07	1.63	1.04	0.22	1.88	0.51	1.63	1.14	0.76	0.60	0.11	0.18	0.18	0.40	1.52	1.04	0.07	0.04
Lu	0.04	0.12	0.05	0.19	0.01	0.21	0.15	0.03	0.25	0.14	0.77	0.17	0.09	0.09	0.01	0.01	0.04	0.06	0.26	0.15	0.01	ND

ND - not detected; (-) - not analyzed: Abbreviations: Bt - biotite, Chl - chorite, Ms - muscovite
Samples are from Beaver Dam deposit except FMS (Fifteen Mile Stream), USH (Upper Seal Harbour), CAR (Caribou)

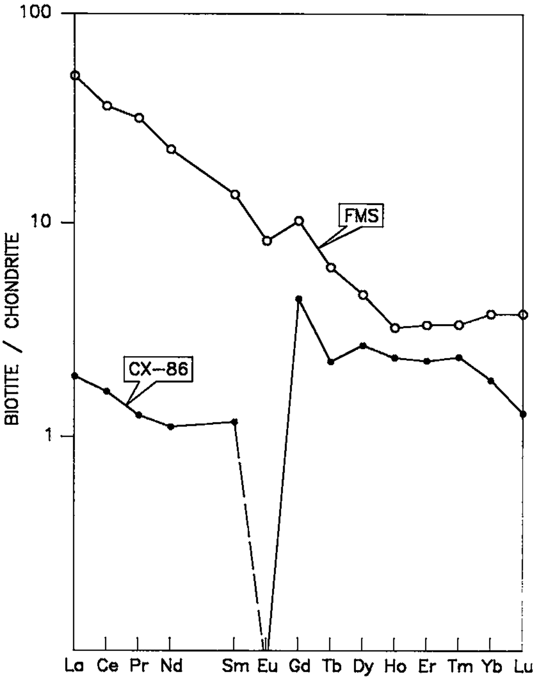

FIG. 16. Chondrite-normalized *REE* plot for biotite separate from Beaver Dam (CX–86) compared to data for vein biotite from the Fifteen Mile Stream (FMS) gold deposit.

with experimental work of Munoz & Ludington (1974), indicates very low F contents of the fluid. These data compare with F and Cl contents of 0.1 to 1.6 wt.% and <0.06 wt.%, respectively, reported by Taner *et al.* (1986) for biotite in Archean lode-gold deposits of Quebec.

A single sample of biotite has been analyzed for trace and *REE* element abundances (Table 8, Fig. 16). This biotite occurs as a fresh, inclusion-free, monomineralic clot in a quartz – biotite – plagioclase vein from drill core. For comparative purposes, a sample of biotite of similar paragenesis from the Fifteen Mile Stream (FMS) gold deposit has been included in Table 8 and Figure 16. The biotite from Beaver Dam contains (in ppm) Li (183), Rb (563), Cs (93) and Ba (1108), with lower abundances of Sr, Y, Zr, Hf, Tl, Th and U; Σ*REE* is equal to 6 ppm. Comparable levels of enrichment and depletion are noted in the FMS biotite. The chondrite-normalized profile for the biotite displays overall depletion, with slight enrichment in the *HREE*, an unfractionated pattern $[(La/Lu)_N=1.5]$ and apparently low Eu/Eu* (*i.e.*, Eu was not detected). In contrast, sample FMS shows considerable *REE* enrichment (Σ*REE* = 73 ppm), a strongly fractionated pattern $[(La/Lu)_N = 13.5]$, comparable to the NASC pattern (Haskin *et al.* 1968, Gromet *et al.* 1984), and a slightly negative Eu anomaly. The levelling off in the *HREE* (Dy to Lu) may be due to microinclusions of zircon (54.3 ppm Zr), which is strongly enriched in *HREE* (Hanson 1980).

Tourmaline

Tourmaline (Table 9) generally consists of equal proportions of schorl and dravite, the Fe- and Mg-rich end members, respectively, with minor elbaite substitution; Mn was not detected, and CaO is consistently less than 1.0 wt.%. The Cr-rich dravite that characterizes Archean lode-gold deposits (King & Kerrich 1989) is absent; in fact, no Cr was detected in the samples examined. This uniform chemistry is recorded despite the occurrence of tourmaline in such widely varying parageneses as wallrock, Qtz – Bt – Pl – Tur veins and Ms–Chl-rich overprinting vein assemblages.

Tourmaline is commonly zoned, with a blue-green (schorl) core and an orange-brown (dravite) rim. Although the color contrast is quite marked in polished section, EMPA traverses across two grains (profiles in Fig. 17) indicate that the chemical discontinuities are not so abrupt. In addition to the minor compositional differences due to Fe and Mg distribution, there is also a slight depletion of Na toward the margin, in one case from *ca.* 2.5 wt.% in the core to 1.8 wt.% in the rim.

In the Al–Fe^{2+}–Mg diagram of Henry & Guidotti (1985), the Beaver Dam data-set overlaps the metasedimentary field in which either Al-saturated phases are present or absent. In addition, we note that the tourmaline data fall within the field in this triangular plot for nongranite mineralized sites in the Meguma Zone (*i.e.*, other Meguma gold deposits), as recently determined by Clarke *et al.* (1989).

TABLE 9. REPRESENTATIVE COMPOSITIONS OF TOURMALINE

Sample	87-4	87-4	136C	136R	136C	136R	73 -
SiO_2 (wt. %)	36.36	36.48	36.97	36.38	35.64	36.07	36.79
TiO_2	0.26	0.54	0.09	0.87	0.70	1.59	0.09
Al_2O_3	34.05	34.89	32.91	32.09	32.83	30.81	33.37
FeO	7.12	6.42	7.95	7.88	5.97	8.34	7.84
MgO	6.05	6.10	6.01	6.42	6.57	6.49	5.79
CaO	0.56	0.77	0.24	0.73	0.96	0.70	0.23
Na_2O	2.00	1.79	2.12	2.17	1.70	2.13	2.12
Σ	86.40	86.99	86.29	86.54	84.37	86.13	86.23
NUMBER OF CATIONS BASED ON 29 OXYGEN							
Si	6.990	6.937	7.137	7.044	6.990	7.044	7.102
^{iv}Al	5.010	5.663	4.862	4.956	5.010	4.956	4.898
^{vi}Al	2.707	2.759	2.630	2.369	2.581	2.138	2.697
Ti	0.038	0.077	0.013	0.117	0.102	0.233	0.013
Fe	1.145	1.021	1.283	1.276	0.979	1.361	1.265
Mg	1.733	1.729	1.729	1.852	1.920	1.888	1.666
Ca	0.116	0.156	0.050	0.151	0.201	0.145	0.047
Na	0.746	0.660	0.793	0.814	0.645	0.806	0.793

87-4 quartz-plagioclase-tourmaline ± muscovite vein; 136 - quartz-plagioclase-biotite-muscovite-tourmaline (tourmaline in vein and pelitic wall rock); 73 - quartz-plagioclase-tourmaline-muscovite-chlorite vein.

Abbreviations: C = core; R = rim.

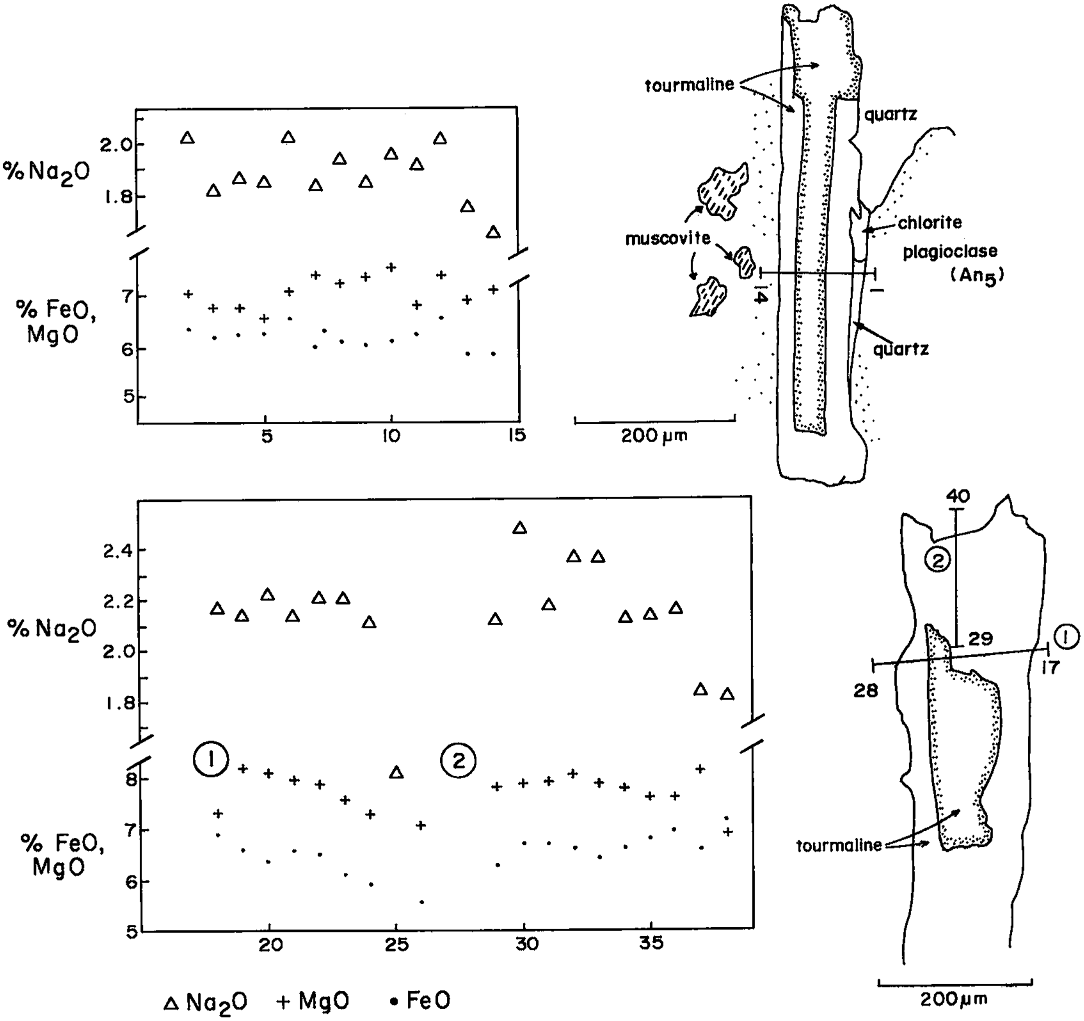

FIG. 17. Sketches of thin sections of vein samples from Beaver Dam showing euhedral tourmaline crystals that are color-zoned, as indicated by the stippled pattern (blue-green core and orange-brown rim). The EMPA traverses and the compositional profiles are indicated in the adjoining plots. Note that the bottom tourmaline grain is surrounded by quartz.

Apatite

Apatite (Table 10) has been analyzed from a single vein (BD–87–10) in which it occurs as coarse (to 1.5 cm) euhedral grains. The apatite is compositionally uniform, with zoning apparently absent; chemically, it conforms to fluorapatite. This composition is very similar to that of apatite from other hydrothermal-vein deposits (Roeder *et al.* 1987) or metasedimentary-host lithologies (Yardley 1985), but contrasts markedly with that of apatite from pegmatites (Jolliff *et al.* 1989) and granites (Kontak 1991, O'Reilly 1988), which generally contains several wt.% MnO. The F contents range from 2.2 to 3.6 wt.%, whereas Cl was just detected in the analysis.

Muscovite

Muscovite (Table 11) has been analyzed in ten different samples encompassing the full range of morphology (*i.e.*, euhedral *versus* anhedral) and paragenesis (*i.e.*, primary *versus* secondary). The muscovite shows considerable variation in chemistry, with limiting abundances (in wt.%) of most elements being quite variable: FeO (<0.10 to 3.6), MgO (<0.10 to 2.8), F (<0.10 to 0.42), TiO_2 (<0.10 to 0.62), and Cr and Mn below the detection limit. This variability is not limited to different samples, but is noted within a single polished section; no systematic change in muscovite chemistry has been detected that can be related to either morphology or paragenesis. In broad terms, muscovite shows a positive correlation between Fe and Mg, although there is not a 1:1 relationship (Fig. 18d). There is a broad correlation between wt.% TiO_2 and the level of the ferromagnesian elements, illustrated in the TiO_2 *versus* MgO plot (Fig. 18b), but again there is no simple exchange. The variation of Si, Al and M^{2+} cations is summarized in Figures 18c and 19a. The following points are noted: (1) there appear to be two distinct trends defined in plots of ^{VI}Al *versus* M^{2+} and ^{VI}Al *versus* Si; (2) in the Al–M^{2+}–Si plot, two trends are apparent, with one corresponding to the celadonitic exchange, and the other to the biotite substitution (Monier & Robert 1986). These two trends or exchanges are identified as 1 and 2 in Figures 18 and 19 and refer to the following substitutions, respectively:

(1) $^{VI}Al,\ ^{IV}Al = {}^{VI}(M^{2+}),\ ^{IV}Si$

(2) $2/3\,^{VI}Al,\ 1/3\,^{VI}\square = {}^{VI}(M^{2+})$

The key point to note here is that whereas both exchanges involve an increase in M^{2+} cations, in reaction (2) Si remains constant. The chemical variation noted above is not correlated with either the texture or occurrence of muscovite.

The volatile chemistry (F, Cl) has been determined in all but three samples. Chlorine was not detected in any appreciable quantity (*i.e.*, <0.10 wt.%), whereas F shows

TABLE 10. REPRESENTATIVE COMPOSITIONS OF APATITE

Point	1	2	3	4	5
SiO_2 (wt.%)	0.00	0.00	0.00	0.00	0.00
FeO	0.17	0.16	0.16	0.15	0.16
MnO	0.14	0.13	0.15	0.10	0.08
CaO	56.80	56.03	56.10	57.10	56.38
Na_2O	0.08	0.06	0.07	0.00	0.09
P_2O_5	42.52	42.25	40.64	42.36	42.00
F	2.47	2.33	3.60	3.42	2.25
Cl	0.00	0.00	0.03	0.00	0.03
	102.18	100.96	100.75	103.13	100.99
F,Cl=O	1.03	0.97	1.51	1.43	0.94
Σ	101.15	99.99	99.24	101.70	100.05
NUMBER OF CATIONS BASED ON 26 OXYGEN					
Si	0.000	0.000	0.000	0.000	0.000
Fe	0.023	0.022	0.022	0.019	0.022
Mn	0.019	0.018	0.021	0.013	0.011
Ca	10.208	10.190	10.271	10.174	10.287
Na	0.012	0.009	0.011	0.000	0.014
P	6.032	6.059	5.875	5.956	6.039
F	1.311	1.224	1.941	1.799	1.207
Cl	0.000	0.000	0.008	0.000	0.008

TABLE 11. REPRESENTATIVE COMPOSITIONS OF MUSCOVITE

Sample	87-100.2	87-169.1		87-4	87-10		86-177B		87-164.2		80-4-69	
Point	25	2	3	1	1	8	3	6	1	4	1	4
SiO_2 (Wt. %)	47.18	46.89	47.87	47.03	47.55	49.44	49.25	47.53	48.15	45.86	48.91	47.49
TiO_2	0.00	0.00	0.00	0.00	0.00	0.02	0.00	0.00	0.48	0.59	0.00	0.36
Al_2O_3	36.69	36.31	38.66	36.63	37.83	33.71	37.34	38.42	32.02	31.96	36.58	36.68
FeO	1.20	3.41	0.29	1.17	0.45	2.73	0.78	0.06	2.60	3.06	0.71	1.10
MnO	0.01	-	-	-	-	-	-	-	-	-	-	-
MgO	0.75	0.01	0.01	0.19	0.11	1.63	0.35	0.00	2.13	2.18	0.76	0.76
CaO	0.00	0.00	0.00	0.00	0.00	0.00	0.00	0.00	0.00	0.00	0.03	0.01
Na_2O	0.33	0.50	0.50	0.70	0.46	0.30	0.41	0.28	0.25	0.31	0.42	0.73
K_2O	10.38	10.63	10.63	11.01	10.72	10.97	9.68	10.67	10.13	10.56	10.59	10.28
Σ	96.54	96.92	97.96	96.73	97.12	98.78	97.80	96.95	95.75	94.48	97.99	96.81
NUMBER OF CATIONS BASED ON 22 OXYGEN												
Si	6.160	6.150	6.136	6.166	6.160	6.378	6.289	6.146	6.393	6.230	6.277	6.195
^{iv}Al	1.840	1.850	1.864	1.834	1.840	1.622	1.711	1.854	1.607	1.770	1.723	1.865
^{vi}Al	3.814	3.765	3.978	3.828	3.938	3.506	3.911	4.003	3.405	3.349	3.811	3.743
Ti	0.000	0.000	0.000	0.000	0.000	0.002	0.000	0.000	0.048	0.060	0.000	0.035
Fe	0.132	0.374	0.031	0.128	0.049	0.295	0.083	0.006	0.289	0.344	0.076	0.120
Mn	0.000	-	-	-	-	-	-	-	-	-	-	-
Mg	0.154	0.045	0.002	0.037	0.021	0.313	0.067	0.000	0.421	0.441	0.145	0.148
Ca	0.000	0.006	0.000	0.000	0.000	0.000	0.000	0.000	0.000	0.000	0.004	0.001
Na	0.088	0.079	0.124	0.178	0.116	0.075	0.102	0.070	0.064	0.082	0.105	0.185
K	1.738	1.627	1.738	1.842	1.772	1.806	1.577	1.760	1.716	1.830	1.734	1.711

(-) not detected

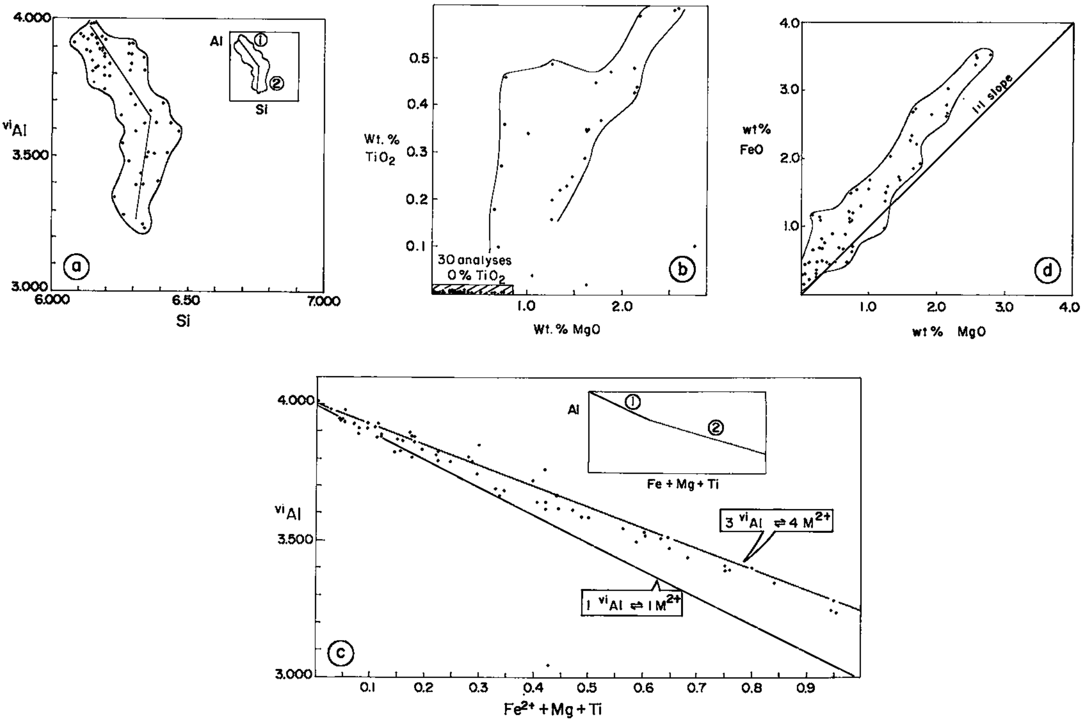

FIG. 18. Chemical data (EMPA) for muscovite from Beaver Dam plotted in a variety of diagrams: (a) ^{VI}Al *versus* Si, (b) wt.% TiO_2 *versus* wt.% MgO, (c) ^{VI}Al *versus* M^{2+} cations, and (d) wt.% FeO *versus* wt.% MgO. The significance of trends 1 and 2 shown in Figures 18a and 18c is discussed in the text.

a bimodal distribution of concentrations, ≤ 0.1 wt.% (*i.e.*, below detection) and 0.3 ± 0.1 wt.% (Fig. 19b). Although this difference between the two populations is small, it is statistically significant (B. McKay, pers. comm., 1992)

Trace-element chemistry (Table 8) has been determined on four muscovite separates representing diverse modes of occurrence at Beaver Dam and an additional two samples of muscovite from other gold districts (Caribou, Upper Seal Harbour). The muscovite from Beaver Dam shows the greatest enrichment (ppm) in Rb (101 to 486) and Ba (195 to 1523). Abundances of other elements are much lower [Li (24–81), Sr (24–89), Cs (4–21), Sc (5–32), others <1–2 ppm)]. Erratic enrichment of some elements (Zr, Pb, Bi, W) suggests contamination due to microinclusions. The two samples of muscovite from other deposits indicate similar elemental abundances.

Chondrite-normalized *REE* profiles for muscovite (Fig. 20) show variable degrees of fractionation and a large overall range in Σ*REE*, with three of the samples having Σ*REE* between 23 and 49 ppm, and the fourth relatively depleted, with only 2.5 ppm. In terms of the degree of fractionation, two samples are strongly fractionated [$(La/Lu)_N$ = 67 and 10.1], whereas the remaining two are unfractionated [$(La/Lu)_N$ = 0.7 and 1.0). The slight enrichment in the *HREE* (Ho to Lu) for two of the samples (BD–87–116 and 171) is attributed to microinclusions of zircon (49 and 22 ppm Zr, respectively). The enrichment in Σ*REE* in three of the four samples is matched by their overall enrichment in Li, Rb, Cs and Ba compared to the fourth sample. Comparison to the chondrite-normalized patterns for the two samples from other gold districts (Fig. 20) indicates patterns similar to the *REE*-depleted muscovite (BD–87–10) from Beaver Dam, with comparable degrees of abundance and fractionation. The notable departure of samples BD–87–116 and BD–87–267 from the otherwise flat *LREE* patterns and $(La/Lu)_N$ values near unity is noted because these samples represent intense phyllic alteration of wallrock adjacent to veins. The similarity of the *REE* patterns to typical shale patterns (McLellan 1989) suggests possible inheritance, a common feature of muscovite from alteration zones (*e.g.*, Ham & Kontak 1988, Alderton *et al.* 1980).

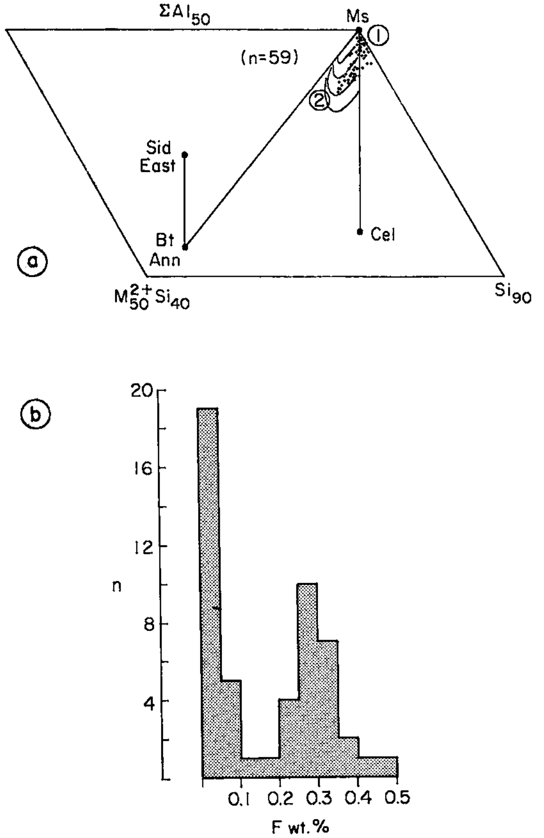

FIG. 19. Chemical data for muscovite from Beaver Dam. (a) ΣAl–Si–M^{2+} plot modified after Monier & Robert (1986) showing the end-member micas (Ms muscovite, Cel celadonite, Bt biotite, Ann annite, East eastonite, Sid siderophyllite) and the different exchange paths (see text for discussion). The diagram is contoured for temperature (°C) with the 600° (top), 500°, 400° and 300°C (bottom) isotherms plotted. (b) Histogram of wt.% F indicating a bimodal distribution of the data.

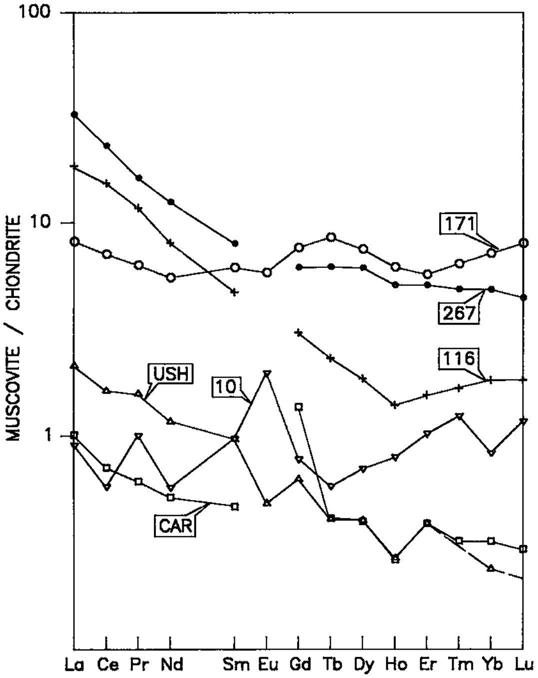

FIG. 20. Chondrite-normalized *REE* plot for muscovite separates from Beaver Dam (BD–87–171, 267, 116, 10) compared to muscovite separates from the Caribou (CAR) and Upper Seal Harbour (USH) deposits.

Chlorite

Chlorite has been analyzed using the electron microprobe (Table 12) and also as mineral separates using wet-chemical techniques (Table 13). Despite the variety of morphological types and occurrences, the chemistry is strikingly uniform and indicates a ripidolite composition (Fig. 21). The low Fe_2O_3 contents (*i.e.*, <4 wt.%) of the chlorite separates indicate that it is unoxidized (Deer *et al.* 1966). The chlorite is depleted in TiO_2 and MnO, but contains elevated abundances of MgO and ΣFe. Consistent but low concentrations of F (0.25 ± 0.1 wt.%) and Cl (<0.05 wt.%) were obtained. The range of chemistry for chlorite replacing biotite (BD–87–164.1, 87–141, 87–177) overlaps the range for chlorite occurring as monomineralic clots, chlorite occurring in quartz–arsenopyrite stripes in pelite (BD–87–133, 87–141), and chlorite replacing plagioclase (BD–87–68).

The mineral separates represent chlorite from clots or vugs with coexisting Cal ± Ab ± Ms ± sulfides; collectively, they show very little range in composition, with a ΣFe/(ΣFe+Mg) of 0.51 ± 0.01. The generally low but erratic abundances of Ti, Ca, K and Na are attributed to trace amounts of impurities such as calcite, muscovite, anatase and plagioclase (compare to EMPA data).

Trace-element abundances have been obtained on mineral separates using AAS (Table 13) and ICP–MS (Table 8) techniques. All of the chlorite samples analyzed represent vug infillings; these generally tend to be monomineralic, but microinclusions of calcite, quartz, muscovite, albite, scheelite and sulfides may occur. The AAS data (n=13) are summarized as follows (mean ± 1σ, ppm): Co (19.3 ± 5.8), Cr (33 ± 22), Cu (12.9 ± 9.8), Ni (31.7 ± 12.6), V (228 ± 64), Zn (519 ± 94) and Pb (28.7 ± 30.5).

The ICP–MS data are partly summarized in Figure 22, binary element plots; in addition the following points are noted: (1) Li is poorly correlated with Rb, Cs and Ba; however, the enrichment of Li, Rb and Cs is not related

TABLE 12. REPRESENTATIVE COMPOSITIONS (EMPA) OF CHLORITE

Sample	141	141	177	80-4-73	164.2	164.1	80-4-68
SiO_2 (wt. %)	24.14	24.31	23.92	25.15	24.52	24.53	24.77
TiO_2	0.10	0.11	0.13	0.08	0.10	0.16	0.10
Al_2O_3	23.55	23.26	21.00	22.51	22.68	22.26	22.83
Cr_2O_3	0.03	0.00	0.05	0.05	0.06	0.04	0.05
FeO	24.89	25.62	26.12	26.37	26.04	26.67	24.68
MnO	0.48	0.43	0.40	0.38	0.58	0.44	0.72
MgO	14.73	14.83	13.64	13.23	14.48	14.14	15.30
CaO	0.04	0.04	0.04	0.03	0.04	0.00	0.09
Na_2O	0.11	0.15	0.00	0.00	0.00	0.00	0.00
K_2O	0.00	0.00	0.00	0.00	0.00	0.00	0.00
Σ	88.08	88.74	85.30	87.96	88.88	88.63	88.89
NUMBER OF CATIONS BASED ON 28 OXYGEN							
Si	5.062	5.079	5.241	5.318	5.152	5.185	5.164
^{iv}Al	2.938	2.921	2.759	2.682	2.848	2.815	2.836
^{vi}Al	2.883	2.807	2.665	2.929	2.769	2.732	2.775
Ti	0.014	0.013	0.021	0.012	0.015	0.025	0.015
Cr	0.005	0.000	0.008	0.008	0.010	0.006	0.007
Fe^{2+}	4.368	4.477	4.786	4.663	4.575	4.714	4.301
Mn	0.084	0.072	0.073	0.067	0.103	0.078	0.131
Mg	4.603	4.617	4.454	4.169	4.534	4.454	4.754
Ca	0.008	0.005	0.008	0.006	0.008	0.000	0.020
Na	0.044	0.058	0.000	0.000	0.000	0.000	0.000
K	0.000	0.000	0.000	0.000	0.000	0.000	0.000

141: chlorite replaces biotite in quartz-arsenopyrite striping; 177: chlorite replaces biotite in silicate-rich pod; 80-4-73: colloform textured chlorite intergrown with muscovite; 164: colloform textured chlorite replacing plagioclase ± muscovite; 80-4-68: late chlorite ± carbonate in vugs in quartz-plagioclase vein

to muscovite contamination given the uniformly low K_2O contents of the chlorite separates (Table 13); (2) Zr is strongly correlated with Th, as are also Hf and U (not shown); (3) Sr and Ba show two possible trends that may indicate different sites for these elements (crystal-chemical control *versus* microinclusions of feldspar); (4) Rb/Sr shows a negative correlation with Li; and (5) the elevated erratic levels of Bi (to 3.4 ppm) and W (to 125 ppm) suggest the presence of Bi phases and scheelite, the former of which occurs as Bi tellurides in the chlorite assemblage (Smith & Kontak 1988). These observations are taken to indicate that Li is decoupled from Cs, Rb and Ba, but that Zr, Hf, U and Th are related to microinclusions (*e.g.*, zircon?). As mentioned above, the concentrations of the transition elements are considered to reflect crystal-chemical controls; the same is suggested for Li, Y, Sc and most of the *REE*.

The *REE* data (Table 8) are plotted against some elemental variables in Figure 22, and in Figure 23, chondrite-normalized profiles are shown. Two features are immediately apparent from the data, namely the large variation in Σ*REE* (3 to 152 ppm) and the variable degree of fractionation with, for example, $(La/Lu)_N$ varying from 0.2 to 313. The poor correlation between Zr (except for two samples) or other trace elements and Σ*REE* mitigates against the relative importance of microinclusions. The best correlation among the *REE* and other elements is between Rb/Sr and *LREE* (Fig. 22), but at present no satisfactory explanation can be offered to account for this.

Chondrite-normalized profiles (Fig. 23) for chlorite show a range in overall normalized abundance ($1 < La_N < 100$), degree of fractionation (above), and highly variable $(Eu/Eu^*)_N$ values. Whereas some of the overall variability in the Σ*REE* and the degree of fractionation may be attributable to microinclusions (see above), the majority of the profiles are similar, with *LREE* enrichment and *HREE* depletion, the exceptions being BD–121A, 9C, 103 and 41A, with the patterns resembling *REE* profiles for clastic sedimentary rocks in general (McLellan 1989), including the Meguma Group (see below). The samples that do not fit this trend generally have unfractionated patterns, with slight enrichment in *HREE* and also lower Σ*REE* abundances.

Carbonate

Carbonate from coarse clots in both concordant and discordant veins as well as carbonate in laminated quartz–carbonate bedding-concordant veins has been analyzed (EMPA and AAS). Triangular plots of the major cations (Ca, Fe, Mg, Mn; Fig. 24) indicate good agreement between the two analytical techniques. Calcite is the dominant carbonate, with minor Fe, Mn and Mg substitution. X-ray analyses of additional samples further support the occurrence of calcite as the only carbonate phase at Beaver Dam.

Selected trace-element data (Sr, Y, Zr, Ba, Pb, Sc, W, *REE*) and chondrite-normalized profiles for 11 samples of carbonate representing all modes of occurrence are presented in Table 14 and Figure 25. Surprisingly, there is a large range for several of the trace elements given the uniform major-element chemistry of the carbonates [*e.g.*, Sr (74 to 3990 ppm) and Y (11 to 206 ppm)]. This is also true of carbonates from other Meguma gold deposits (Kontak *et al.* 1991b). The scatter for Zr, Pb and W may be related to microinclusions of zircon, galena and scheelite, respectively. Large ranges in Sr contents (<100 to >1500 ppm) of hydrothermal carbonates has been noted by others. For example, Möller *et al.* (1984) noted a range of <100 to >1500 ppm in their study of vein carbonates in the Harz Mountains of Germany, whereas Grant & Bliss (1983) reported a range of 100–1000 ppm Sr for calcite in MVT deposits of central Tennessee.

The *REE* data show a large range in terms of absolute abundance (Σ*REE* 25 to 215 ppm), fractionation [$(La/Lu)_N$ 0.09 to 5.9] and $(Eu/Eu^*)_N$ (0.9 to 11.8). The *HREE* enrichment in samples BD–87–1080 and BD–97–9 can be partially attributed to contamination by zircon (112 and 22.5 ppm Zr, respectively), but for sample BD–87–161A such is not the case (<1 ppm Zr). For the remaining samples, the large variation in Σ*REE*, Eu anomaly and $(La/Lu)_N$ seem to be real features of the carbonates. These observations extend to carbonates examined from all the gold districts in the eastern Meguma Zone (Kontak *et al.* 1991b). Of particular note are the data for samples BD–87–100A, 100B and 100.1. The first two samples come from the same sample locality (*i.e.*, vein) and were collected less than 1 m apart,

TABLE 13. MAJOR AND TRACE ELEMENT CHEMISTRY OF CHLORITE SEPARATES

Sample	10	10.1	10.2	41A	49.1	49.2	53	103	121A	165	172B	181	293.4
SiO_2 (wt.%)	23.01	25.89	25.27	24.09	23.72	23.82	25.15	28.86	25.31	25.21	25.25	24.76	25.58
TiO_2	0.06	1.00	0.70	0.10	0.09	0.085	0.20	0.35	0.074	0.097	0.11	0.05	0.64
Al_2O_3	20.97	21.54	20.61	22.55	23.32	22.07	22.74	23.44	22.43	22.42	21.92	23.12	23.27
Fe_2O_3	8.65	2.82	3.47	3.39	1.73	2.62	2.38	1.68	1.56	1.53	2.26	2.16	2.13
FeO	20.08	27.78	22.12	22.61	23.51	23.31	22.45	20.05	23.71	24.21	22.98	23.46	22.18
MnO	0.86	0.44	0.46	0.44	0.44	0.45	0.46	0.37	0.62	0.49	0.44	0.45	0.03
MgO	12.22	13.13	12.77	14.16	14.02	13.91	13.02	12.00	14.26	13.62	14.01	13.62	13.33
CaO	0.01	0.49	0.54	0.50	0.31	0.57	0.56	0.80	0.10	0.57	0.01	0.28	0.03
Na_2O	0.07	0.06	0.10	0.06	0.058	0.076	0.41	0.16	0.04	0.30	0.62	0.09	0.40
K_2O	0.04	0.01	0.01	0.00	0.004	0.007	0.17	1.57	0.029	0.011	0.51	0.14	0.07
P_2O_5	0.02	0.13	0.26	0.01	0.005	0.023	0.023	0.03	0.03	0.015	0.018	0.018	0.02
LOI	11.79	11.24	10.88	11.45	11.31	11.53	11.87	10.36	11.31	11.20	11.72	11.46	11.66
Σ	99.39	99.53	99.63	99.35	98.51	98.47	99.43	99.15	99.47	99.67	99.84	99.60	99.34
NUMBER OF CATIONS BASED ON 28 OXYGEN													
Si	5.001	5.418	5.419	5.070	5.028	5.089	5.288	5.855	5.292	5.275	5.300	5.185	5.322
^{iv}Al	2.999	2.582	2.580	2.930	2.972	2.911	2.711	2.144	2.708	2.725	2.700	2.814	2.678
^{vi}Al	2.337	2.731	2.630	2.666	2.855	2.648	2.924	3.462	2.819	2.806	2.724	2.895	3.028
Ti	0.010	0.157	0.113	0.015	0.014	0.014	0.031	0.050	0.011	0.015	0.017	0.007	0.100
Fe^{3+}	1.415	0.444	0.560	0.537	0.276	0.421	0.376	0.257	0.245	0.240	0.357	0.339	0.333
Fe^{2+}	3.651	3.986	3.967	3.981	4.168	4.165	3.948	3.402	4.145	4.235	4.034	4.109	3.858
Mn	0.157	0.007	0.084	0.078	0.078	0.081	0.081	0.063	0.109	0.086	0.076	0.085	0.005
Mg	3.959	4.094	4.081	4.441	4.429	4.429	4.079	3.628	4.443	4.247	4.383	4.250	4.132
Ca	0.002	0.109	0.123	0.113	0.070	0.131	0.126	0.064	0.637	0.127	0.002	0.062	0.006
Na	0.029	0.024	0.042	0.024	0.024	0.031	0.166	0.062	0.011	0.122	0.252	0.036	0.161
K	0.011	0.002	0.002	0.000	0.001	0.001	0.045	0.406	0.245	0.002	0.136	0.036	0.019
fe	0.561	0.520	0.526	0.504	0.501	0.509	0.515	0.502	0.497	0.513	0.500	0.511	0.504
Co (ppm)	13	23	27	33	21	21	18	15	20	19	17	12	12
Cr	23	30	13	57	28	24	72	18	10	50	77	10	18
Cu	12	5	13	13	7	6	6	22	5	13	9	14	43
Ni	49	54	47	50	30	29	24	25	20	23	22	16	24
Pb	78	10	80	62	4	2	26	2	10	8	74	8	10
V	205	145	141	298	334	333	282	221	163	210	203	172	257
Zn	420	540	473	780	560	560	514	477	510	600	460	390	465

fe = Σ Fe/(Σ Fe + Mg)

whereas the third sample is again from the same vein but from several meters along strike. The three carbonates have remarkably similar chondrite-normalized *REE* patterns and Σ*REE* and demonstrate uniform chemistry on this scale. Thus, although there is a large variation in the *REE* features of the carbonates on a deposit scale, there is apparently uniformity on the scale of a single vein.

Fe–Ti oxides

Although Fe–Ti oxides phases are widespread in the veins, only a limited amount of work has been done on these minerals. The alteration phase observed replacing tourmaline and ilmenite is anatase, whereas the ilmenite occurring as blades has a highly variable composition, with 32 to 45 wt.% FeO and 3.5 to 13.8 wt.% MnO.

Cu, Fe, Cd, Pb, As sulfides, tellurides and Ag–Te alloy

Pyrite has been analyzed (Table 15) from six different sample locations; the compositions obtained are similar. Co, Ni, Cu, Au and Ag were sought, but only in one sample were any of these detected (0.5 wt.% Ni in sample BD–87–78). Pyrrhotite from three different locations was analyzed (Table 15), and similar compositions were obtained. Only trace amounts of Ni (to 0.14 wt.%) were found as impurities in the samples. Chalco-

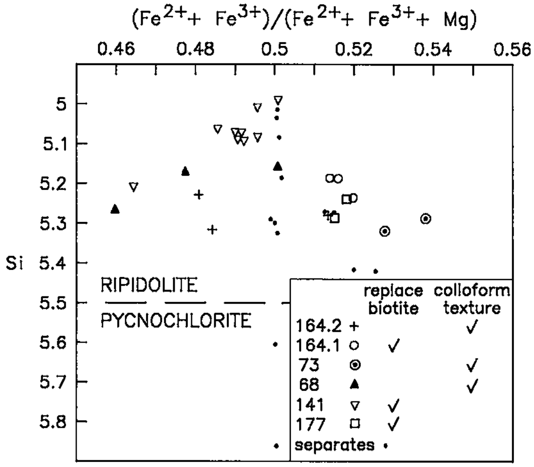

FIG. 21. Chemical data (EMPA and wet chemical) for different morphological types of chlorite from Beaver Dam plotted in the Si *versus* $(Fe^{2+}+Fe^{3+})/(Fe^{2+}+Fe^{3+}+Mg)$ classification diagram of Hey (1954). Note that there is no discernable difference in composition that can be related to mode of occurrence.

pyrite from eight different locations were analyzed (Table 15); compositions were found to be similar in all cases, with no trace amounts of impurities detected.

Arsenopyrite has been analyzed from eleven localities (Table 15), representing vein and wallrock occurrences, and uniform compositions have been obtained. Whereas there is an apparent lack of trace amounts of impurities, generally << 0.1 wt.% Co, Ni, Bi and Sb, there is a strong inverse correlation between S and As; a similar relationship occurs for arsenopyrite from other Meguma gold districts (our unpubl. data). In the Fe–As–S system (Fig. 26), the data points (n=70) converge around 32–34 atomic % As and 33–34 atomic % Fe. This compares well with compositional data for arsenopyrite in other Meguma gold districts (Fig. 26), including data reported by Graves (1976) for fourteen deposit areas, although the data for Cochrane Hill diverge markedly, with a large spread from 32 to 39 atomic % As. The limited compositional range for arsenopyrite from Beaver Dam is consistent with the observed equilibrium assemblage pyrite – pyrrhotite – arsenopyrite, which buffers the arsenopyrite composition (Kretschmar & Scott 1976, Sharp *et al.* 1985).

Galena (Table 15) has been analyzed from samples within the deposit area (*i.e.*, underground workings) and the MEX pit, a large trench located a few hundred m west of the portal area. In Figure 27a, a binary plot of wt.% Ag *versus* wt.% S, there is a clear distinction between galena from these different sites, with the former characterized by elevated Ag (up to 2 wt.%). Compared to galena from two other gold districts (Fig. 27a), this elevated Ag content is anomalous. Galena may also contain up to 4.5 wt.% Bi, although *ca.* 1–3 wt.% is more normal, with Bi showing an inverse correlation with Ag (Fig. 27b) and in the proportion of 2:1 (wt.%) which is typical (Foord & Shawe 1989). Elevated Bi and Ag are not uncommon in galena, and occur in galena from a variety of hydrothermal deposits (Foord & Shawe 1989). Up to 1 wt.% Te occurs in galena; it is strongly associated with Bi. The galena grains characterized by elevated Ag, Bi and Te are paragenetically associated with Bi–Te sulfides, Cd sulfides and Ag–Te complexes.

Bi–Te sulfides occur in association with greenockite and a Ag–Te alloy in discordant veins dominated by stage-II mineralogy. The chemistry of the Bi–Te sulfide phase is very uniform (Table 15) and corresponds to the "tellurbismut" series (Ramdohr 1980), but no specific mineral has been documented for the composition reported here. The homogeneity of the phase in terms of optics and chemistry suggests that it does not represent a mixture. The Ag–Te alloy phase ($Ag_{2.5}Te$; Table 15) is intermediate in terms of its stoichiometry between stutzite (Ag_5Te_3) and hessite (Ag_2Te); the observed optical properties are similarly ambiguous. Associated with the aforementioned phases is greenockite, observed in a single sample and with uniform composition that conforms to normal stoichiometry. A similar association of tellurides with gold in mesothermal quartz veins is described by both Moritz & Crocket (1990) and Tesfaye (1992) for Archean deposits of the Canadian Shield.

Native gold and electrum

Gold has been analyzed from all the different occurrences and paragenetic associations discussed earlier and is of uniform composition (Table 16, Fig. 28), with Ag as the major impurity (*ca.* 5 wt.%), and consistent, but low levels of Cu (0.1–0.3 wt.%). The high purity of the gold is similar to what is found for other Meguma gold deposits (Fig. 28) and is consistent with compositions that characterize mesothermal gold deposits in general and those hosted by metasedimentary rocks in particular (Morrison *et al.* 1991). In addition to high-purity gold, electrum has been noted in a single sample; it is in intimate association with a Bi–Te sulfide phase. The electrum contains between 30 and 48 wt.% Ag, up to 5 wt.% Bi; Cu, present in trace amount in the native gold, is absent.

DISCUSSION

The above presentation involving vein morphology, mineral paragenesis and mineral chemistry for the Beaver Dam deposit provides a data base to address certain aspects of the Beaver Dam and other Meguma gold deposits. Points for consideration include: (1) the nature of the crack–seal or ribbon textures in the bedding-concordant veins, (2) the temperatures attend-

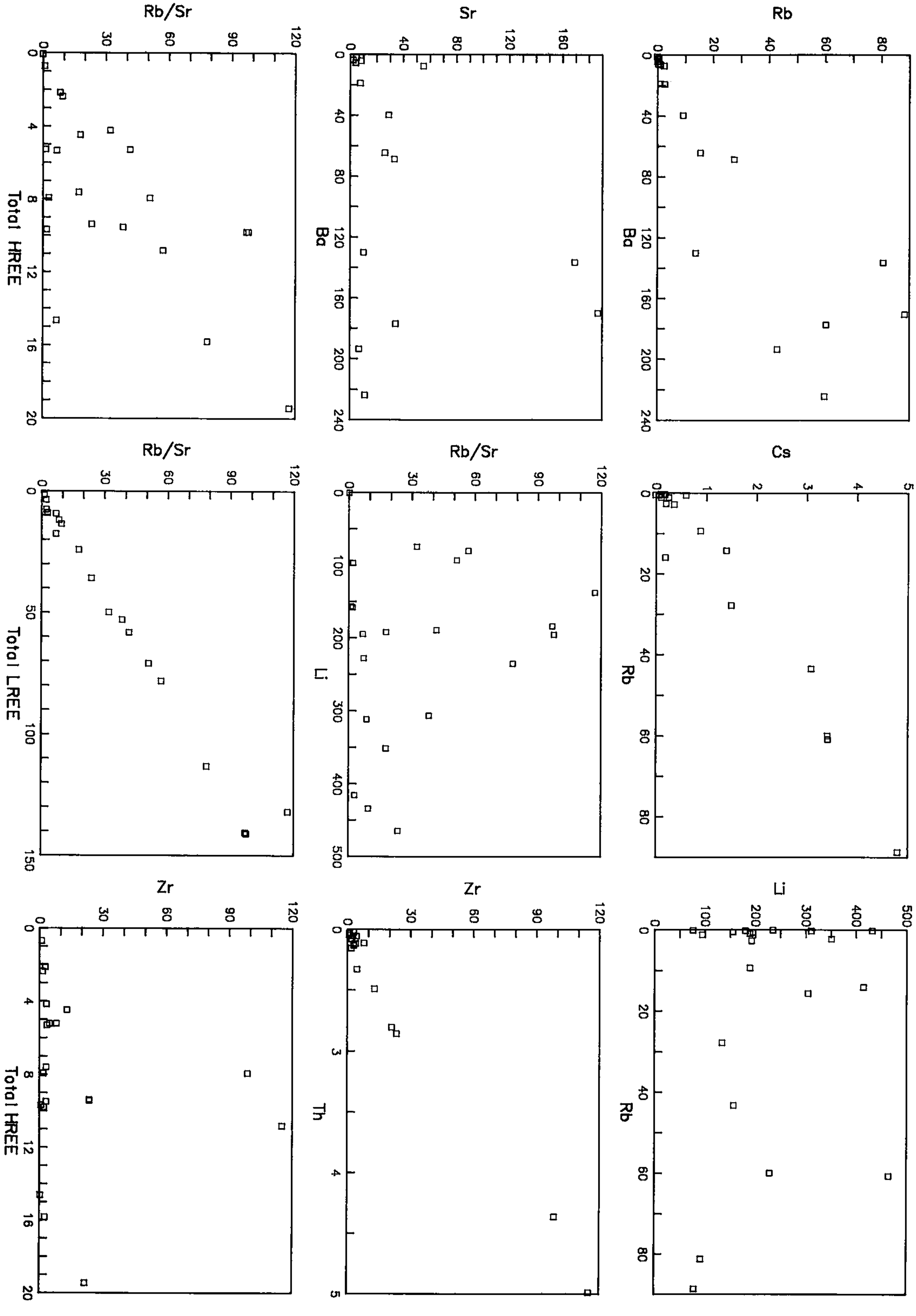
Rb
0
20
40
60
80
Ba
0
40
80
120
160
200
240
Sr
0
40
80
120
160
Ba
0
40
80
120
160
200
240
Rb/Sr
0
30
60
90
120
Total HREE
0
4
8
12
16
20
Cs
0
1
2
3
4
5
Rb
0
20
40
60
80
Rb/Sr
0
30
60
90
120
Li
0
100
200
300
400
500
Rb/Sr
0
30
60
90
120
Total LREE
0
50
100
150
Li
0
100
200
300
400
500
Rb
0
20
40
60
80
Zr
0
30
60
90
120
Th
0
3
4
5
Zr
0
30
60
90
120
Total HREE
0
4
8
12
16
20

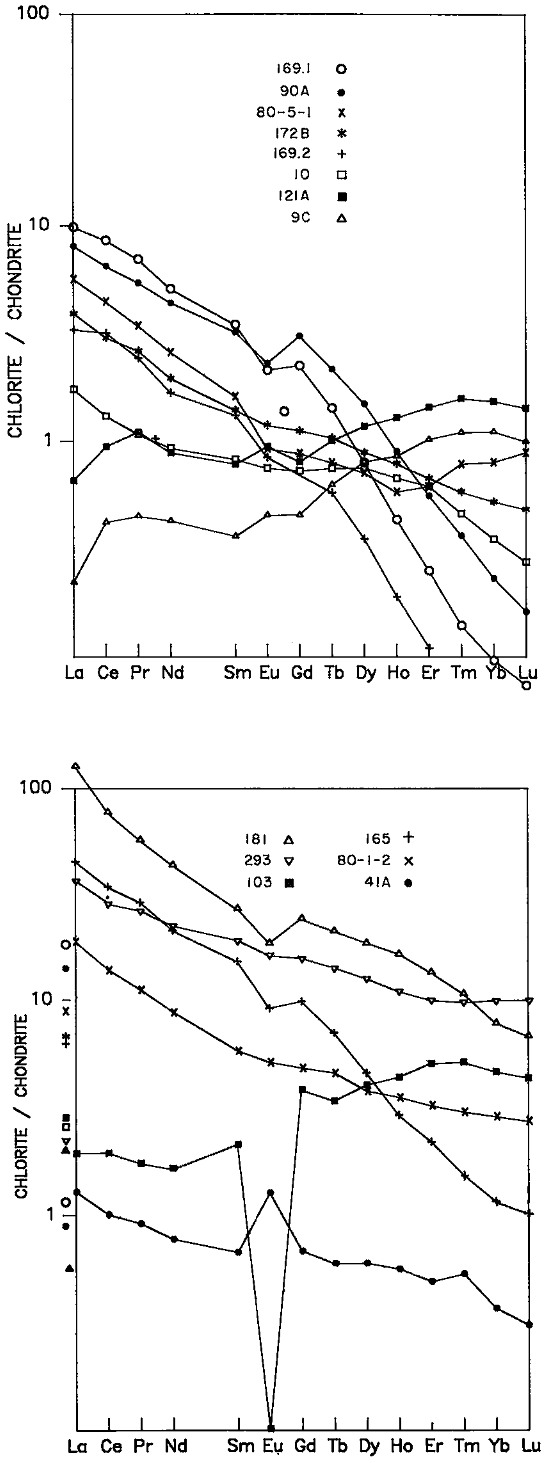

FIG. 23. Chondrite-normalized *REE* plots for chlorite from Beaver Dam.

ing vein formation, (3) the nature of the vein-forming fluid, and (4) the nature of gold mineralization (*e.g.*, paragenesis). These subjects have direct bearing on genetic modeling of Meguma gold deposits; this issue also will be addressed.

Nature of crack–seal or ribbon-textured veins

The crack–seal texture in the quartz veins of the Meguma gold deposits has probably been the most influential single feature of the veins in terms of genetic models proposed for the Meguma gold deposits (*e.g.*, Graves & Zentilli 1982, Henderson *et al.* 1990, Sangster 1990, Mawer 1985, 1986, 1987, Haynes 1986, 1987). The general description of the veins in the older literature indicates that gold was most commonly found in the dark or lustrous, oily quartz veins with a laminated texture (Malcolm 1929). Whereas this is true, more recent observations (*e.g.*, Smith & Kontak 1989, Kontak *et al.* 1990a, Corey 1992, Corey & Mills 1992) indicate that gold is consistently found in the white crystalline rather than the lustrous, oily parts of the veins. The same is true for the Beaver Dam deposit, in which gold is most commonly located in sulfide-bearing, bedding-concordant veins with the crack–seal texture. However, closer inspection indicates that the gold is consistently located in the white crystalline parts of these veins, either near vein margins or wallrock inclusions. This is a feature typical of other metasedimentary-hosted vein gold deposits (*e.g.*, Cox *et al.* 1991, Forde 1991).

The bedding-concordant veins at Beaver Dam are considered to be composite in origin and to have formed in two distinct episodes that overlap in time. The crack–seal or laminated quartz is early and is interpreted to reflect extreme silicification of the adjacent wallrock lithologies. This stage of quartz vein formation is only preserved as fragments in the veins with highly variable degrees of replacement, from incipient to very advanced stages (Fig. 5), with the very thinly laminated crack–seal texture (Figs. 5i, j) representing the advanced stages of this process. During development of the crack–seal textures, P(fluid) is considered to have been less or equal to P(lithostatic), and fluids probably utilized anisotropy such as bedding-parallel cleavage as channelways. The laminated quartz can, however, be traced into areas of massive, white discordant veins (*i.e.*, angular), suggesting that the two are time-equivalents. The second stage of vein formation, at which time massive amounts of the white quartz formed, represents a period during which

FIG. 22. Trace-element data for chlorite from Beaver Dam plotted in a variety of binary diagrams.

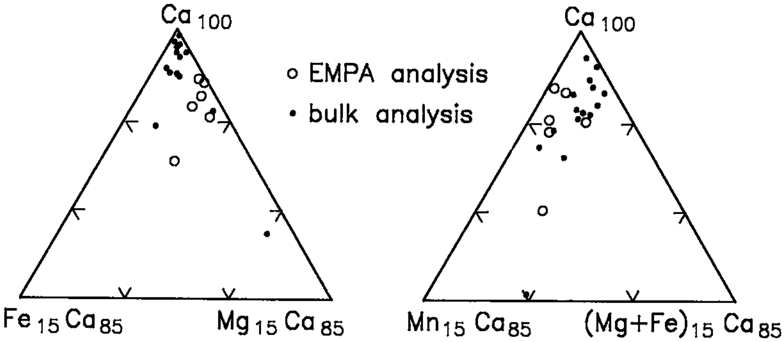

FIG. 24. Chemical data (EMPA and bulk analyses) for carbonate from Beaver Dam plotted in triangular Ca–Fe–Mg and Ca–Mn–(Fe+Mg) diagrams (cationic proportions).

TABLE 14. TRACE ELEMENT DATA FOR CARBONATE SEPARATES, BEAVER DAM

Sample	87-9	87-10	87-1	87-100.1	87-100B	87-100A	87-161A	87-171	87-177C	87-179	87-1080
Li (ppm)	0.65	0.33	0.42	3	0.85	0.27	0.63	2.04	0.38	0.46	1.16
Be	ND	ND	0.79	0.24	0.95	0.55	-	-	1.21	0.48	ND
Sc	6.63	0.42	12.07	5.4	9.73	10.1	-	-	3.21	10	7.22
Rb	1.14	0.30	0.42	1.5	0.40	0.52	0.16	0.15	0.99	0.09	0.17
Sr	87.56	74.7	3990	1793	3129	3157	60.45	82	127.3	718	135
Y	63.61	82.8	206	77.7	158.5	178.6	122.1	118.7	11.1	32	99.7
Zr	22.58	0.46	0.77	1.06	1.81	0.80	0.40	1.2	0.43	0.52	112.5
Nb	1.41	0.22	0.10	0.11	3.32	0.08	-	-	0.74	0.45	4.79
Mo	0.38	0.41	0.58	0.69	0.76	0.33	-	-	0.04	0.16	0.41
Cs	0.03	0.01	0.03	0.13	0.05	0.04	0.08	0.17	0.06	0.03	0.02
Ba	2.93	2.81	5.62	5.87	3.04	3.21	1.83	2.5	4.84	1.68	3.51
Hf	0.30	ND	0.10	0.05	0.10	0	0.03	0.25	0.03	0.04	1.48
Ta	0.18	0.02	0.04	ND	2	0.04	-	-	0.36	0.71	0.50
W	-	24.4	22.8	13.74	5.89	0.49	-	-	4.97	2.755	-
Tl	ND	ND	ND	ND	ND	ND	0.09	0.09	ND	ND	0.06
Pb	12.01	5.09	21.5	10.39	16.89	15.3	2.17	3.99	2.54	4.66	19.08
Bi	0.09	0.05	0.04	0.05	0.04	0.01	0.03	0.10	0.02	0.07	0.13
Th	0.07	0.01	0.19	0.23	0.28	0.25	0.02	0.29	0.05	0.11	0.27
U	0.06	0.12	0.05	0.05	0.04	0.04	0.07	0.07	0.02	0.01	0.09
La	19.25	19.35	6.15	6.62	10.73	10.23	27.58	5.63	4.06	21.73	7.01
Ce	33.73	25.11	12.74	12.27	20.04	19.17	54.77	12.25	8.12	40.7	11.64
Pr	4.57	3.02	1.89	1.61	2.80	2.72	6.22	1.91	1.02	4.83	1.44
Nd	8.4	13.3	10.61	7.66	12.62	13.24	23.81	10.49	3.54	17.56	5.49
Sm	3.98	3.27	7.9	4.41	7.19	7.55	5.94	7.17	0.97	3.74	1.40
Eu	1.71	1.67	27.28	22.32	43.96	44.4	1.929	7.57	0.43	3.68	0.76
Gd	5.69	5.62	21.1	9.12	18.14	19.99	7.37	13.81	1.36	4.73	2.14
Tb	0.95	1.11	5.89	2.26	4.89	5.22	1.60	3.66	0.28	0.78	0.519
Dy	7.56	8.10	41.04	14.57	33.11	34.93	12.64	24.34	2.03	4.4	6.54
Ho	2.26	1.91	8.47	2.72	6.04	6.53	4.05	4.72	0.43	0.93	3.26
Er	9.99	5.20	24.9	7.52	16.57	17.78	19.95	13.78	1.3	2.80	20
Tm	1.98	0.60	3.53	1.06	2.18	2.38	4.28	2.23	0.18	0.39	4.62
Yb	17.13	3.42	21.67	6.24	12.82	14.02	38.73	18.06	1.39	2.67	44.38
Lu	2.67	0.48	2.24	0.59	0.18	1.33	6.36	2.95	0.20	0.39	8.39

ND = not detected; (-) not analyzed.

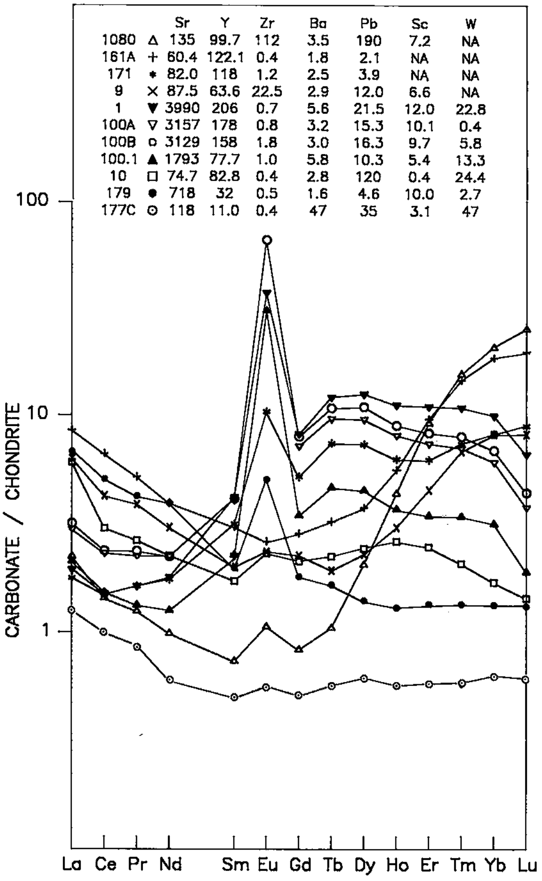

		Sr	Y	Zr	Ba	Pb	Sc	W
1080	△	135	99.7	112	3.5	190	7.2	NA
161A	+	60.4	122.1	0.4	1.8	2.1	NA	NA
171	*	82.0	118	1.2	2.5	3.9	NA	NA
9	×	87.5	63.6	22.5	2.9	12.0	6.6	NA
1	▼	3990	206	0.7	5.6	21.5	12.0	22.8
100A	▽	3157	178	0.8	3.2	15.3	10.1	0.4
100B	○	3129	158	1.8	3.0	16.3	9.7	5.8
100.1	▲	1793	77.7	1.0	5.8	10.3	5.4	13.3
10	□	74.7	82.8	0.4	2.8	120	0.4	24.4
179	●	718	32	0.5	1.6	4.6	10.0	2.7
177C	⊙	118	11.0	0.4	47	35	3.1	47

FIG. 25. Chondrite-normalized *REE* plot for carbonate separates from Beaver Dam with selected trace-element data (ICP–MS) included to illustrate the apparent lack of correlation among Σ*REE*, degree of fractionation and trace-element chemistry.

the P(fluid) exceeded P(lithostatic) (*i.e.*, hydraulic fracturing in sense of Sibson *et al.* 1988), when most veining occurred. The occurrence of coarse euhedral quartz crystals (*i.e.*, to 10–15 cm in length) and vuggy textures, particularly in the discordant veins, indicates open-space infilling of structures. The presence of fragments of the laminated quartz vein material within a mass of white crystals of quartz suggests brecciation of the earlier vein material, possibly due a sudden increase in P(fluid). This sudden surge in P(fluid) is akin to the fault-valve model of Sibson *et al.* (1988). In this context, it is worth noting the presence of the Mud Lake Fault system at the eastern end of the deposit. Although the timing of movement along this fault is poorly constrained, the increase in gold grades toward the fault (J. Campbell, pers. comm., 1991) does suggest that it was active during vein formation.

In summary, the veins at Beaver Dam are interpreted to reflect an early replacement-dominant stage of vein formation during which time laminated-type veins of quartz formed. This process may possibly be linked to the formation of silicate-rich clots, given the local dissolution of wallrock that must have occurred. The second stage of quartz vein formation, which is volumetrically the most important, represents a sudden increase in P(fluid) (related to seismic activity at shallower depth?) and gave rise to veins with features that indicate infilling of dilatant structures.

Temperature of vein formation

The presence of amphibole of suitable composition and coexisting plagioclase permit application of the amphibole–plagioclase geothermometry, based on the NaSi ⇋ CaAl exchange (Spear 1980). In this case, the more recent calibration of Blundy & Holland (1990) has been used; temperatures of 550–715°C are calculated, with the mean close to 675°C (± 75°C), using data for sample BD–87–61A.

The plagioclase compositions can be interpreted in terms of temperature of formation by application of the phase diagram constructed by Moody *et al.* (1985; their Fig. 3) based on experimental growth of plagioclase in the system Na_2O – CaO – Al_2O_3 – H_2O (± FeO, Fe_2O_3, MgO, TiO_2). The presence of strongly zoned Ca-rich plagioclase with subsequent albitization and growth of new albite suggest initial temperatures in excess of 525°C for stage I, with later stages of plagioclase growth (*i.e.*, sodic compositions) occurring below 375°C (stage II). One can also use the experimental data of Lagache (1984) to infer temperatures by combining the plagioclase compositions (stage I) and the composition of the vein-forming fluid as measured by leachate analyses (Kontak *et al.* 1988) [Ca/(Ca+Na) = 0.29 ± 0.11, n=18]. The temperature of plagioclase formation would have approximated 500°C using the 2 kbar experimental data, but the large range in fluid chemistry makes this a crude estimate only.

The exchange of Fe and Mg between coexisting garnet and biotite is primarily a function of temperature (*e.g.*, Ferry & Spear 1978). The chemical data for a vein sample containing hydrothermal garnet and biotite of the stage-I paragenesis have been used to calculate formation temperatures (at a P of 2 kbars) using a variety of presently available geothermometers for this mineral pair (Thompson 1976, Ferry & Spear 1978, Hodges & Spear 1982, Pigage & Greenwood 1982). In these calculations, it is assumed that the rims of the garnet equilibrated chemically with the biotite which, in this sample, is of uniform composition. Geothermometric calculations indicate a temperature range from 450 to 475°C, except for the Pigage & Greenwood (1982) calibration (520 to 545°C). This latter geothermometry is based on the Ferry & Spear (1978) calibration, but

TABLE 15. REPRESENTATIVE COMPOSITIONS OF SULFIDE PHASES

Sample	Cu	Fe	S	Ni	Ag	As	Pb	Bi	Te	Σ
Pyrite										
87-62A	-	47.48	53.93	0.00	-	-	-	-	-	101.41
87-62A	-	47.53	54.12	0.00	-	-	-	-	-	101.65
87-62A	-	46.78	52.53	0.00	-	-	-	-	-	99.31
1018	-	47.23	52.78	0.00	-	-	-	-	-	100.01
1003B	-	46.98	53.13	0.00	-	-	-	-	-	100.25
78	-	46.29	52.96	0.56	-	-	-	-	-	99.80
MEX	-	47.02	52.24	-	-	-	-	-	-	99.26
MEX	-	46.88	52.38	0.19	-	-	-	-	-	98.33
Pyrrhotite										
120.1	-	59.79	39.97	0.10	-	-	-	-	-	99.86
120.1	-	60.25	38.99	0.14	-	-	-	-	-	99.37
1010A	-	59.15	40.60	-	-	-	-	-	-	98.75
Chalcopyrite										
62A	33.84	30.05	35.09	-	-	-	-	-	-	98.97
120.1	34.71	30.36	34.99	-	-	-	-	-	-	100.04
1018	33.99	29.99	35.83	-	-	-	-	-	-	99.81
78	34.95	30.42	35.08	0.02	-	-	-	-	-	100.46
Arsenopyrite										
8	-	34.32	19.99	-	-	45.52	-	-	-	99.81
120.1	-	33.89	19.46	-	-	46.54	-	-	-	99.90
78	-	33.71	18.85	-	-	46.65	-	-	-	99.20
MEX(P/K)	-	34.52	20.38	-	-	45.15	-	-	-	100.05
Galena										
MEX(P/L)	-	-	13.36	-	0.27	-	87.06	-	-	100.69
MEX(P/I)	-	-	13.32	-	0.32	-	85.50	-	-	99.14
MEX(P/I)	-	-	13.06	-	0.16	-	85.56	-	-	98.78
MEX(P/H)	-	-	13.23	-	0.29	-	86.20	-	-	99.72
MEX(P/F)	-	-	13.25	-	0.34	-	86.07	-	-	99.64
8	-	-	13.96	-	1.86	-	81.51	1.18	-	98.51
62A	-	-	13.19	-	1.17	-	80.29	4.65	0.99	100.24
62A	-	-	13.33	-	1.26	-	82.88	2.58	0.27	100.32
62A	-	-	13.53	-	1.22	-	82.39	2.37	0.14	99.65
Bi-Te Sulfide										
62A	0.00	0.00	2.84	-	0.13	-	-	70.26	21.02	94.26
62A	0.18	0.00	2.71	-	0.07	-	-	71.19	20.84	95.49
1010A	0.08	0.01	2.80	-	0.11	-	-	71.26	21.52	95.78
Alloy Ag-Te										
62A	0.00	0.00	0.12	-	63.52	-	-	0.00	35.69	99.33

takes into account the nonideal mixing of Ca in garnet, about 10 mole % Grs in this case (Fig. 11). Hodges & Spear (1982) noted that Mn appears to mix ideally with Mg and Fe in the garnet structure and therefore should have minimal effect on the calibration of the geothermometer. Of interest, therefore, is the geothermobarometric study of the Meguma Group of eastern Nova Scotia by Raeside *et al.* (1988), who found that temperatures derived from

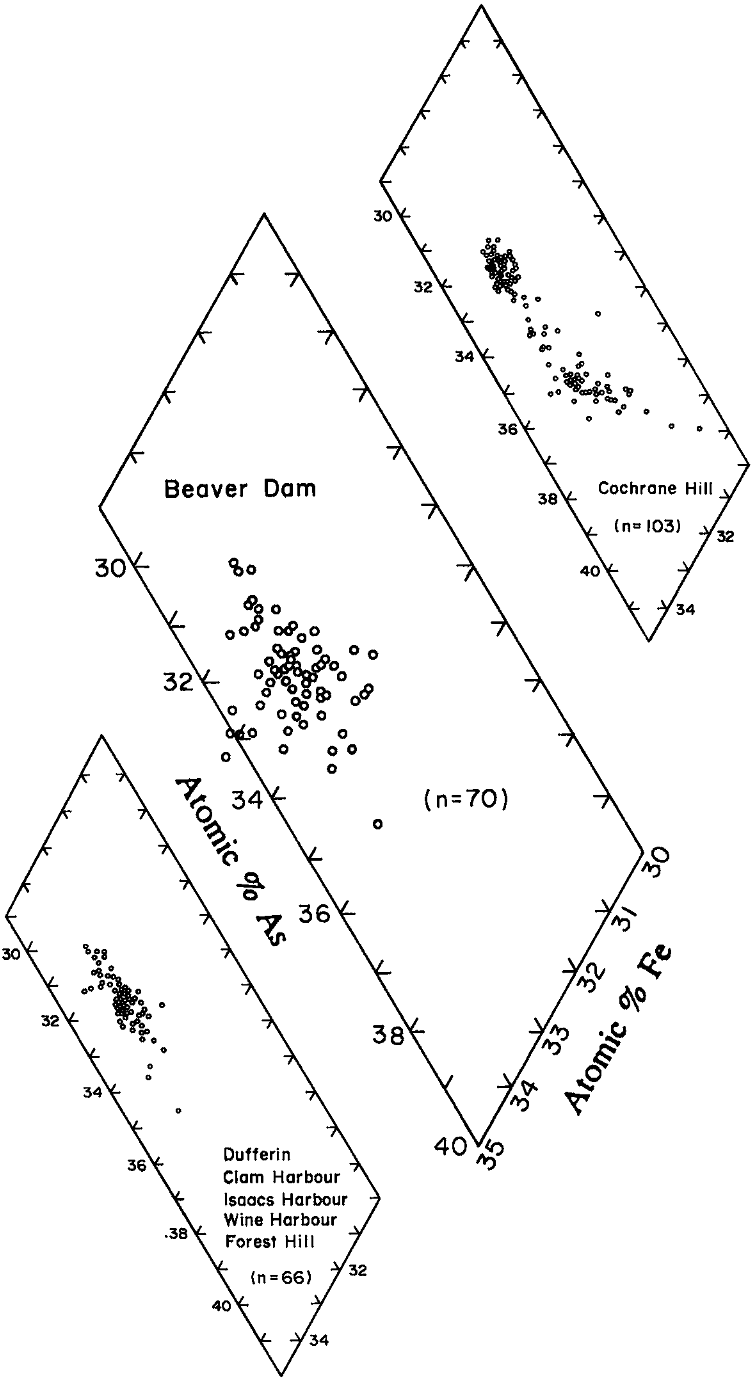

FIG. 26. Fe–As–S plot for arsenopyrite from Beaver Dam compared to data for other Meguma gold deposits (unpubl. data of the authors).

the garnet–biotite geothermometer (Thompson 1976, Ferry & Spear 1978, Hodges & Spear 1982) agree with the temperatures inferred from the mineral assemblages. The garnet grains analyzed by these authors are chemically similar to those from Beaver Dam. For the sample of interest here, a minimum temperature of 450 to 475°C

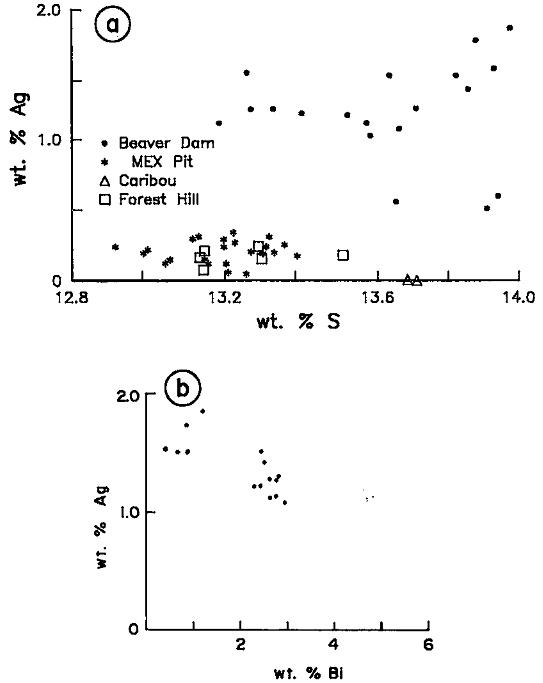

FIG. 27. Binary plots for galena from Beaver Dam and other Meguma gold deposits (note that the MEX Pit is part of the Beaver Dam deposit): (a) wt.% Ag *versus* wt.% S; (b) wt.% Ag *versus* wt.% Bi.

is inferred, whereas 500°C would be an average of all the geothermometric calibrations used and may be more realistic.

LeBel (1979) calibrated a geothermometer based on the concentration of Ti in biotite by combining experimental data with independent geothermometry for the Cerro Verde – Santa Rosa porphyry copper district in Peru. Taner *et al.* (1986) applied this geothermometer in their study of vein biotite from Archean lode-gold deposits in Quebec and inferred temperatures of *ca.* 300–500°C for biotite crystallization. Application of this geothermometer to the Beaver Dam data (Fig. 14b) indicates limiting temperatures of 300–425°C for both vein and wallrock biotite. The data fall on the lower end of the calibration curve; thus, extrapolation to lower temperatures is done with a degree of caution.

Monier & Robert (1986) examined experimentally muscovite solid-solution in the system $K_2O - MgO - FeO - Al_2O_3 - SiO_2 - H_2O$ at $P(H_2O) = 2$ kbar and contoured the Al–Si–M^{2+} diagram for temperature. Their experimental data indicate that with decreasing temperature, the extent of substitution in biotite increases, whereas at high temperatures, compositions tend toward pure end-member muscovite. Interpretation of the two trends (1 and 2 in Figs. 18 and 19) for Beaver Dam samples of muscovite in the context of the experimental results of Monier & Robert (1986) suggests empirically that equilibration occurred over variable temperatures, perhaps in excess of 500°C for trend 1 and <400–500°C for trend 2 (Fig. 19a). Williams (1991) applied the same geothermometer to auriferous quartz veins in Australia and interpreted the vein muscovite to reflect equilibration over the range 300–500°C.

Kretschmar & Scott (1976) calibrated the temperature dependence of arsenopyrite composition with respect to atomic % As for the association pyrite, pyrrhotite and löllingite. The presence of both pyrite and pyrrhotite in equilibrium with arsenopyrite, in conjunction with the restricted compositional range of arsenopyrite, indicate a temperature range for crystallization of 430 to 510°C; use of the mean composition only indicates a temperature of 480°C.

Cathelineau & Nieva (1985) developed an empirical geothermometer based on the solid-solution chemistry of chlorite by comparing the ^{IV}Al content of chlorite and measured temperatures of deep drill holes in the Los Azufres (Mexico) geothermal field. The temperature calculations reported here have been obtained using the modified equation proposed by Kranidiotis & MacLean (1987) to correct for the increase of ^{IV}Al with

TABLE 16. REPRESENTATIVE COMPOSITIONS OF NATIVE GOLD AND ELECTRUM

Sample	1018	1018	MEX	MEX	MEX	MEX	1003B	1008B	1008B	1008B
Au	76.23	80.38	96.57	95.72	93.66	93.53	93.85	62.42	50.62	61.00
Ag	23.82	19.16	3.42	4.62	6.25	5.36	5.50	37.72	44.26	31.64
Fe	0.23	0.25	0.05	0.05	0.07	0.25	0.08	1.33	0.71	0.71
Cu	0.00	0.10	0.26	0.24	0.10	0.00	0.19	0.00	0.00	0.00
Te	0.00	0.11	0.05	0.00	0.05	0.06	0.00	0.00	0.00	0.00
Bi	0.00	0.00	0.00	0.00	0.00	0.00	0.00	0.00	4.79	5.10
Σ	100.28	100.00	100.35	100.63	100.13	99.20	99.63	101.47	100.39	98.45

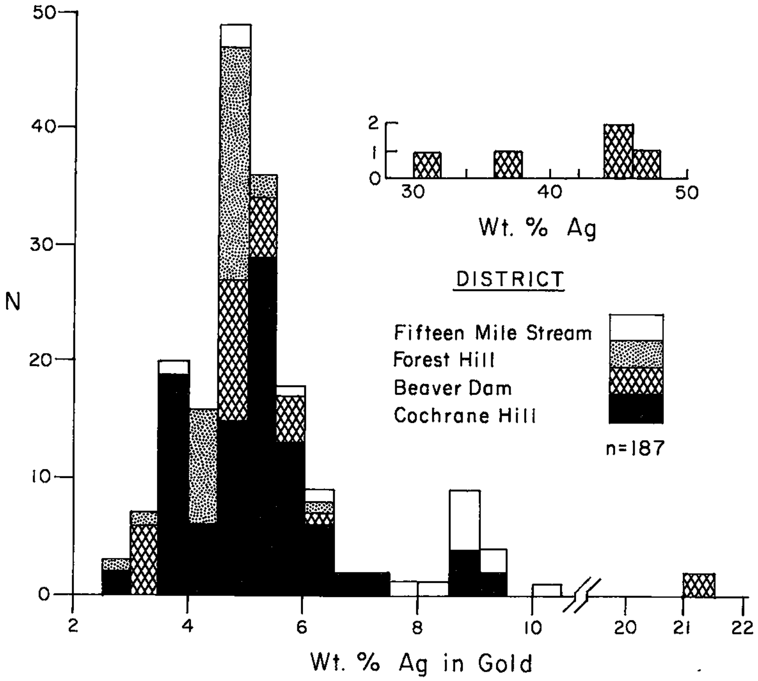

FIG. 28. Histogram illustrating the frequency of wt.% Ag in gold from the Beaver Dam area and other gold deposits. Inset diagram shows the data on electrum grains from Beaver Dam.

Fe/(Fe+Mg). Temperatures of 250–320°C are calculated, with the majority of the data falling in the narrow range 290–310°C. This temperature is slightly less than the 320°C temperature calculated using the chlorite geothermometer of Walshe (1986) based on ^{IV}Si occupancy of chlorite. Jowett (1991) has suggested a further modification of the chlorite geothermometer; use of this version indicates an average temperature of 390°C. The effect of pressure on these geothermometers remains unknown; thus, they are at best probably minimum estimates.

The presence of a Bi–Te sulfide and a Te–Ag alloy coexisting as part of a stage-II assemblage with galena, electrum and Cal–Chl–Ms is constrained to temperatures of ≤350–400°C, based on the work of Afifi *et al.* (1988 and references therein). Application of oxygen isotope geothermometry to plagioclase–amphibole and quartz–chlorite pairs (Kontak *et al.* 1991a) indicates temperatures of 455°C and 300°C, respectively. Also available are homogenization temperatures (T_H) for fluid inclusions in quartz of all vein types (Kontak *et al.* 1988, 1991a); the average T_H is 320°C. These T_H values for the $H_2O - CO_2 -$ NaCl fluids [6 wt.% NaCl, $X(CO_2) = 0.15$] are uncorrected for pressure; the true temperature of entrapment is estimated at 400–450°C for a P of 2 kbars (Brown & Lamb 1989) using isochoric projections (*e.g.*, Bowers & Helgeson 1983).

In Figure 29, the inferred temperatures of vein formation based on the foregoing discussion are summarized, in order of highest to lowest calculated temperatures. Temperatures seem higher for the stage-I assemblages compared to those of stage II, with biotite and muscovite transcending this simple two-fold division. The large variation in the inferred temperatures is interpreted to reflect in part different diffusion-dependent parameters among the minerals examined. For example, the kinetics of diffusion in biotite are such that biotite will continue to re-equilibrate chemically to lower temperatures than amphibole and muscovite (Fortier & Giletti 1991 and references therein). However, the general inference that stage I has higher temperatures of deposition than stage II is consistent with the paragenesis established for the mineral assemblages.

Nature and origin of the vein-forming fluid: implications of major- element chemistry

The presence of zoning profiles in both garnet and plagioclase require (1) disequilibrium during growth between the mineral and fluid, and (2) conditions that can preserve such features. Zoning is a complex phenomenon and may result from several factors, including changes in physicochemical conditions attending mineral growth [*e.g.*, changing $f(O_2)$ will result in garnet

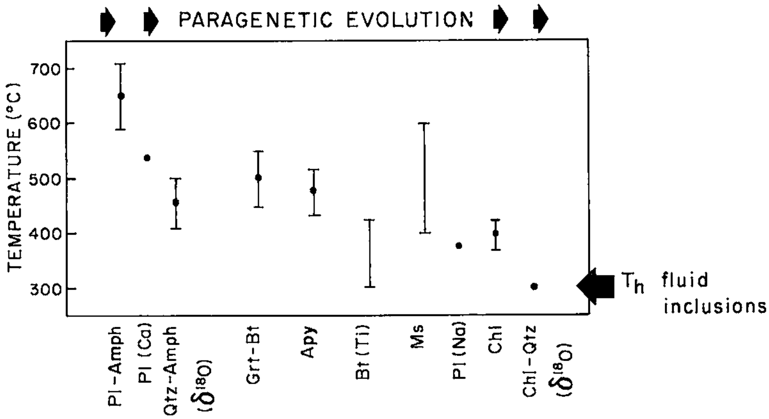

FIG. 29. Summary diagram showing the inferred temperatures of formation for different minerals and assemblages from Beaver Dam deposit, as discussed in the text. Samples have been arranged, from left to right, in order of paragenetic position (see Fig. 6). Thermometers shown are as follows: Pl–Amph: NaSi – CaAl exchange in plagioclase – amphibole (Blundy & Holland 1990); Bt(Ti): biotite thermometer of LeBel (1979); Grt–Bt: garnet – biotite geothermometer (average and range as discussed in the text); Apy: arsenopyrite geothermometer of Kretschmar & Scott (1976); Ms: muscovite thermometer of Monier & Robert (1986); Chl refers to chlorite thermometer [Cathelineau & Nieva (1985), Kranidiotis & MacLean (1987), Walshe (1986), Jowett (1991)]; the oxygen isotope thermometry (Qtz–Amph, Qtz–Chl) is from Kontak *et al.* (1991a); T_H for fluid inclusions (uncorrected for pressure) is from Kontak *et al.* (1988); temperatures for plagioclase compositions are estimated from the work of Moody *et al.* (1985). See text for detailed discussion.

zonation, whereas T fluctuations will affect both garnet and plagioclase]. The important inference here is that the environment of vein formation was clearly dynamic rather than stagnant, and changes on both an intra- and an intergrain scale for the same mineral indicate that local fluctuations occurred in terms of either one or more of the attending physical and chemical conditions.

The presence of zoning profiles also indicates that reheating of the deposit area to temperatures required to induce volume diffusion in garnet and plagioclase did not occur after initial formation of the veins. The temperatures required to promote such diffusion are in the order of $\geq$600° for garnet based on natural occurrences (*e.g.*, Woodsworth 1977), and probably *ca.* 500°C for plagioclase (R.J. Jamieson, pers. comm. 1991) based on observations in regionally metamorphosed rocks. The lack of evidence for heating of the deposit area to high temperatures after vein formation is consistent with ^{40}Ar/^{39}Ar dating of the deposit, in which similar ages (370 Ma) have been obtained for amphibole, muscovite and biotite (Kontak *et al.* 1990b). For example, the large differences in blocking temperatures for these minerals (*i.e.*, about 200°C; McDougall & Harrison 1988) are totally consistent with a single thermal event of short duration for the Beaver Dam area.

The composition of the micas is markedly uniform, given that different mineral assemblages and morphologies have been analyzed. The Fe/(Fe+Mg) values for both chlorite and biotite are uniform at about 0.5, which is similar to the $(Fe^{2+}+Fe^{3+})/(Fe^{2+}+Fe^{3+}+Mg)$ ratio (0.5 ± 0.1) for wallrock lithologies at Beaver Dam (Fig. 30). This uniformity suggests that the Fe/Mg value of the micas has been controlled by the bulk composition of the wallrock. Similarly, the Ca-rich nature of the plagioclase and significant grossular content of the garnet are accounted for by the presence of calc-silicate beds within the local stratigraphy. Thus, there is ample evidence in the form of major-element chemistry of vein minerals to suggest considerable interaction between the local wallrocks and the vein-forming fluids. The very development of the silicate-rich "pegmatoid" veins and the enrichment in silicate minerals at vein–wallrock contacts (*e.g.*, biotite, tourmaline) also suggest local assimilation or exceptional mass-transfer of locally derived material into the veins. We have also suggested above that the occurrence of ribbon-textured veins dominated by graphite + opaque phases + chlorite ± muscovite represents vestiges of variably assimilated wallrock material, the dissolved components of which went in part to form the silicate-rich clots. This model of assimilation, dissolution, transport and precipitation is consistent with patterns of alteration observed in most hydrothermal ore deposits (*e.g.*, Rose & Burt 1979).

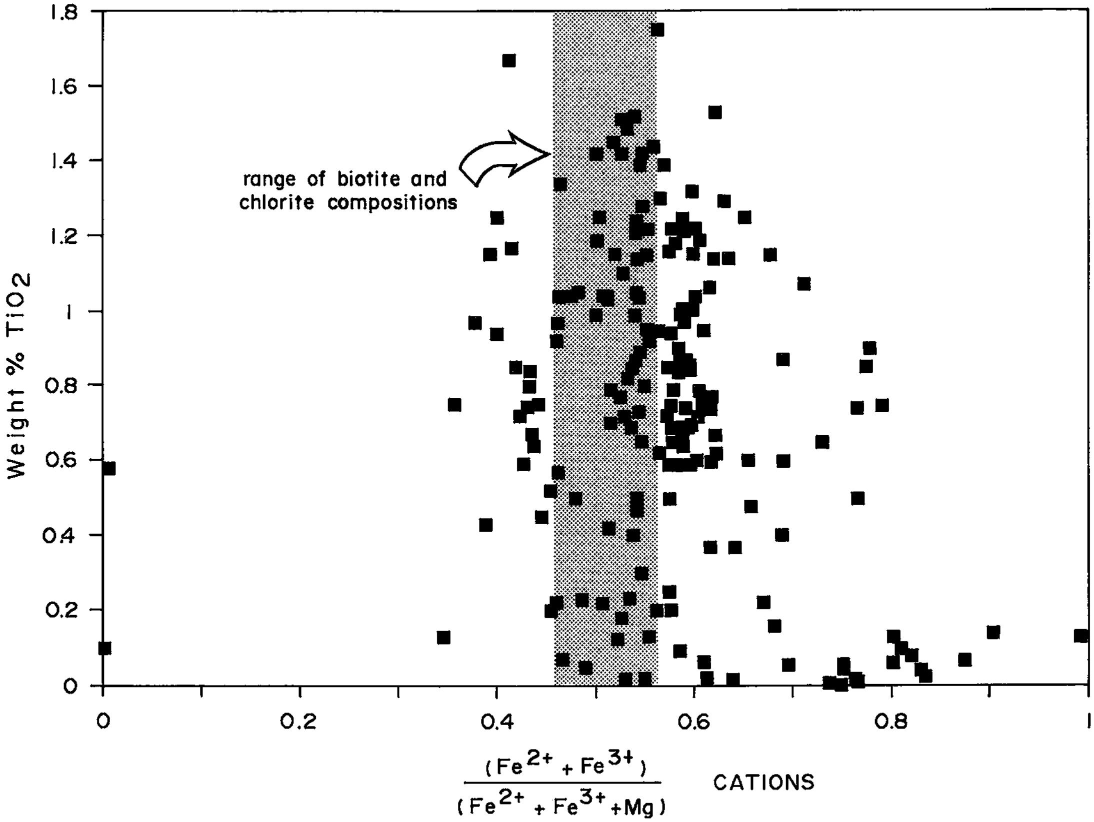

FIG. 30. Plot of wt.% TiO_2 *versus* $(Fe^{2+}+Fe^{3+})/(Fe^{2+}+Fe^{3+}+Mg)$ for vein biotite and chlorite (determined by EMPA; total iron as FeO) and whole-rock samples of wallrock material from Beaver Dam (unpubl. data of the authors).

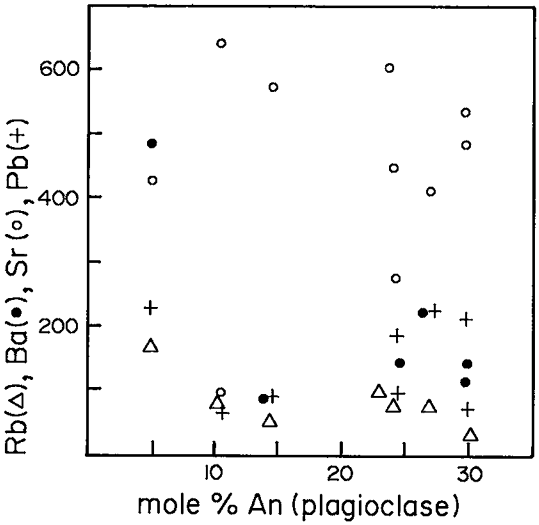

FIG. 31. Binary plot of trace-element data (Rb, Sr, Ba, Pb) data *versus* bulk composition (mole % An) of plagioclase separates.

Nature and origin of the vein-forming fluid: implications of trace-element chemistry

Trace-element chemistry can be an excellent source of petrogenetic information if the factors controlling distribution coefficients are well constrained. Whereas this may be true for igneous rocks (Arth 1976, Hanson 1978, Allègre & Minster 1978), it does not generally apply for hydrothermal minerals except in a few cases (Marchand 1976, Lagache 1984). Instead, crystal-chemical models must be relied upon in order to interpret trace-element abundances in minerals (Morgan & Wandless 1980, Möller *et al.* 1984, Raimbault 1985). However, it is still possible to interpret qualitatively the trace-element data, including those for the *REE*, for individual minerals from specific areas. For example, based on studies of the *REE* distribution in scheelite and tourmaline from Archean gold deposits of the Canadian Shield, Anglin *et al.* (1987) and King *et al.* (1988), respectively, were able to suggest that the vein-forming fluids were either generated from or interacted with variable source-reservoirs.

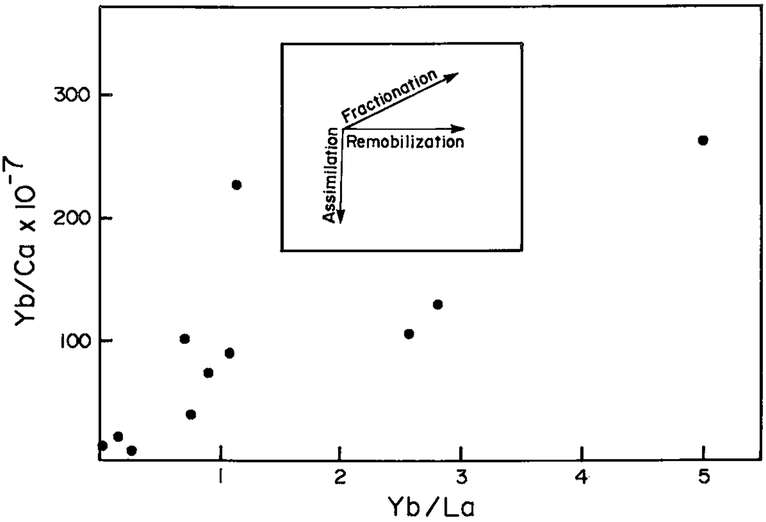

FIG. 32. Plot of Yb/Ca (× 10^{-7}) *versus* Yb/La for calcite from Beaver Dam. The vectors show the effect of fractionation, assimilation and remobilization on the elemental ratios. Diagram is modified from Möller *et al.* (1979).

In the case of biotite and amphibole, only a single analysis of each mineral was carried out, and data are interpreted cautiously. For the biotite, the elevated contents (ppm) of Ba (1108), Rb (563), Li (183) and Cs (93) are notable and are comparable to abundances in biotite from granitic rocks (*e.g.*, Giraud *et al.* 1986). However, the unfractionated chondrite-normalized pattern of the *REE* contrasts with the strongly fractionated (*i.e.*, *LREE*-enriched) patterns for igneous biotite (*e.g.*, Alderton *et al.* 1980, Gromet & Silver 1983, Giraud *et al.* 1986), but is similar to patterns compiled by Grauch (1989) for biotite from amphibolite facies, although these are enriched at 100× chondritic values. The amphibole consistently shows low levels of most trace elements, whereas the Sc enrichment (33 ppm) is expected in this mineral. The *REE* pattern is somewhat similar to that reported by Gromet & Silver (1983) for amphibole from a granodiorite, although the latter has a slightly concave downward pattern and is slightly enriched in Σ*REE*.

Trace-element data for plagioclase cover a broad range, particularly Rb, Sr, Ba and Pb. However, this reflects in part the compositional dependence (*i.e.*, mole% An) of their concentrations (Lagache 1984, Lagache & Dujon 1987, Blundy & Wood 1991). In general, the abundance of these elements should increase systematically toward more albitic compositions. Although there is a suggestion that this may be true for some of the elements, particularly Sr and Pb (Fig. 31), there are obvious complexities that negate this generalization. Since the assumption was made regarding the behavior of Ba and Sr that crystal-chemical controls are dominant over influences of T, P and fluid composition, the results here may indicate that one of these variables is in fact important. If we assume that P and T were relatively constant during precipitation of the calcic plagioclase, then the data suggest that ambient changes in fluid chemistry may have been an important factor in the trace-element chemistry, together with the bulk composition.

The *REE* data for plagioclase are comparable in terms of abundance but are slightly less fractionated, particularly with respect to the *LREE*, compared to both igneous (Gromet & Silver 1983, Giraud *et al.* 1986) and metamorphic (Grauch 1989) plagioclase. However, since two additional data-sets for other gold districts (Fig. 10) show similarly unfractionated patterns, it is possible that this is typical for hydrothermal plagioclase in Meguma gold districts. Although a level of enrichment 10× chondritic values is not unusual for plagioclase hosted by metamorphic rocks (Grauch 1989), the increasing positive Eu anomaly associated with decreasing Σ*REE* is atypical, and arises because the absolute concentration of Eu remains fairly constant (0.57 ± 0.2 ppm).

Muscovite is characterized by elevated, but erratic values of Rb and Ba, although the Rb/Ba ratio is fairly constant at 0.2–0.6. Given that the origin of the muscovite is variable (*i.e.*, it replaces earlier assemblages or is primary), the range in chemistry is to be expected because of inheritance (Alderton *et al.* 1980, Ham & Kontak 1988); the elevated Ba content in one particular case (to 1500 ppm) is suggestive of this. The range in both absolute abundance and degree of fractionation of the *REE* in muscovite also suggests potential inheritance. For example, samples 116 and 267 represent phyllic alteration of psammitic lithologies; their *REE* patterns are somewhat similar to the whole-rock *REE* pattern for these lithologies (Kontak *et al.* 1991a). In contrast, the two samples of muscovite (#10, 171) that have relatively unfractionated patterns occur as coarse vein minerals that did not apparently form as a result of alteration of the immediate wallrock.

The trace-element chemistry of the chlorite is notable because of its variability given the very restricted major-element chemistry [*i.e.*, $\Sigma Fe/(\Sigma Fe+Mg) = 0.5 \pm 0.04$]. As noted above, there is positive covariation among many of the trace elements, including Rb–Ba, Rb–Cs, Li–Cs and Sr–Ba, and an unexplained positive correlation between Rb/Sr and Σ*LREE*. Given the constant composition of the host mineral, a realistic interpretation might be that the fluid chemistry changed during chlorite formation. Three ways this might occur are: (1) fractionation of the vein fluid (static model), (2) enrichment or depletion of the fluid due to interaction with the wallrock or an influx of a recharged fluid (dynamic model), or (3) a combination of the first two mechanisms. In contrast to the aforementioned trace-elements, V and Zn are relatively constant in their abundance (228 ± 64 and 519 ± 94 ppm, respectively), which suggests that they owe their enrichment to a different process.

The *REE* data for chlorite fall into two broad groupings, as noted above, with the strongly fractionated patterns being the norm. These latter patterns are somewhat similar to those of chlorite from altered granites (Arniaud *et al.* 1984, Alderton *et al.* 1980), although in the sample from the Cornish granite there is enrichment in the *HREE* due to the capacity of this mineral to preferentially incorporate these *REE* (Alderton *et al.* 1980). In contrast, the relatively unfractionated patterns resemble chondritic profiles for chlorite from different metamorphic facies given by Grauch (1989), which may have a broad range in abundance (*i.e.*, from 1 to 100 × chondrite). Given that the chlorite samples analyzed formed as vug infillings, have similar bulk chemistry and occupy a similar paragenesis, the differences in *REE* are considered to reflect changing chemistry of the vein-forming fluids.

The trace-element chemistry of calcite is potentially the most informative because of the considerable work has been done in terms of understanding the factors controlling the trace element and *REE* chemistry of this mineral phase (*e.g.*, Graf 1983, 1984, Möller *et al.* 1979, 1984, 1991, Lorens 1981, Lahann & Siebert 1982, Comans & Middelburg 1987, Cantrell & Byrne 1987). Most trace elements are characterized by low abundances in the calcite, and this is in keeping with the very low partition-coefficients for this mineral (*e.g.*, Ba: Pingitore & Eastman 1984). The most relevant work pertaining to this study is that of Graf and Möller *et al.* in their studies of MVT deposits of the central U.S.A. and the Pb–Zn deposits of the Harz Mountains, Germany, respectively. In Figure 32, a plot of Yb/Ca *versus* Yb/La, the data for the calcite samples show a positive covariation. This diagram, first used by Parekh & Möller (1977) and applied to the carbonates of the Harz Mountains (Möller *et al.* 1979), indicates that the variation in calcite chemistry can be attributed to fractionation. This trend shows that the *HREE* are preferentially retained in the fluid due to formation of stronger *REE* carbonate complexes in solution (Dumonceau *et al.* 1978, Cantrell & Byrne 1987), whereas the *LREE* go into the early-formed carbonate. Conversely, remobilization of the *REE* by partial dissolution of carbonate results in preferential enrichment of the solution in *HREE*. In this manner the *REE* data on calcite from Beaver Dam may be interpreted to reflect a combination of fractionation of the vein-forming fluid along with remobilization, which would explain the strong enrichment in the *HREE* in some of the samples. We also note that the samples characterized by *HREE* enrichment also contain elevated Sr contents, a feature which Möller *et al.* (1984) considered indicative of remobilized carbonates. These same samples (*i.e.*, *HREE*-enriched) also are characterized by the highest Eu/Eu^* values, which suggests that during their growth, there was possibly a difference in the $f(O_2)$ of the vein fluid (Drake 1975) relative to the stage at which the earlier(?) calcite precipitated.

Our interpretation of the variation in the *REE* data for the calcite is supported by the experimental data of Graf (1983), which indicate that calcite does not have the capacity to fractionate *REE* and that neither temperature nor salinity caused changes in distribution coefficients. Thus, the changes in *REE* abundance and patterns must reflect changes in fluid chemistry that can be explained in part by fractionation due to mineral precipitation.

The above discussion of trace-element distribution in the major vein-forming constituents in addition to quartz indicates that variability is the norm in most cases. Whereas the variation in Rb, Ba and Sr in plagioclase may be attributed in part to variation in bulk composition (*i.e.*, mole % An), such is not the case for calcite and chlorite. Since the variability is best manifested by the *REE*, the following discussion will focus on that group of elements only. We also re-emphasize that since calcite does not fractionate the *REE*, the variability of the chondrite-normalized patterns for this mineral must reflect changes in the *REE* content of the vein-forming fluid.

Variable *REE* contents of the fluid may be brought about by several mechanisms: (1) discontinuous reactions in the wallrock such that the *REE*-bearing assemblage changes; consequently, there is potential for the fluid in equilibrium with this assemblage to change its *REE* pattern (Alderton *et al.* 1980); (2) unmixing of a CO_2–H_2O–NaCl fluid such that the *REE* are partitioned differently into the immiscible phases (Flynn & Burn-

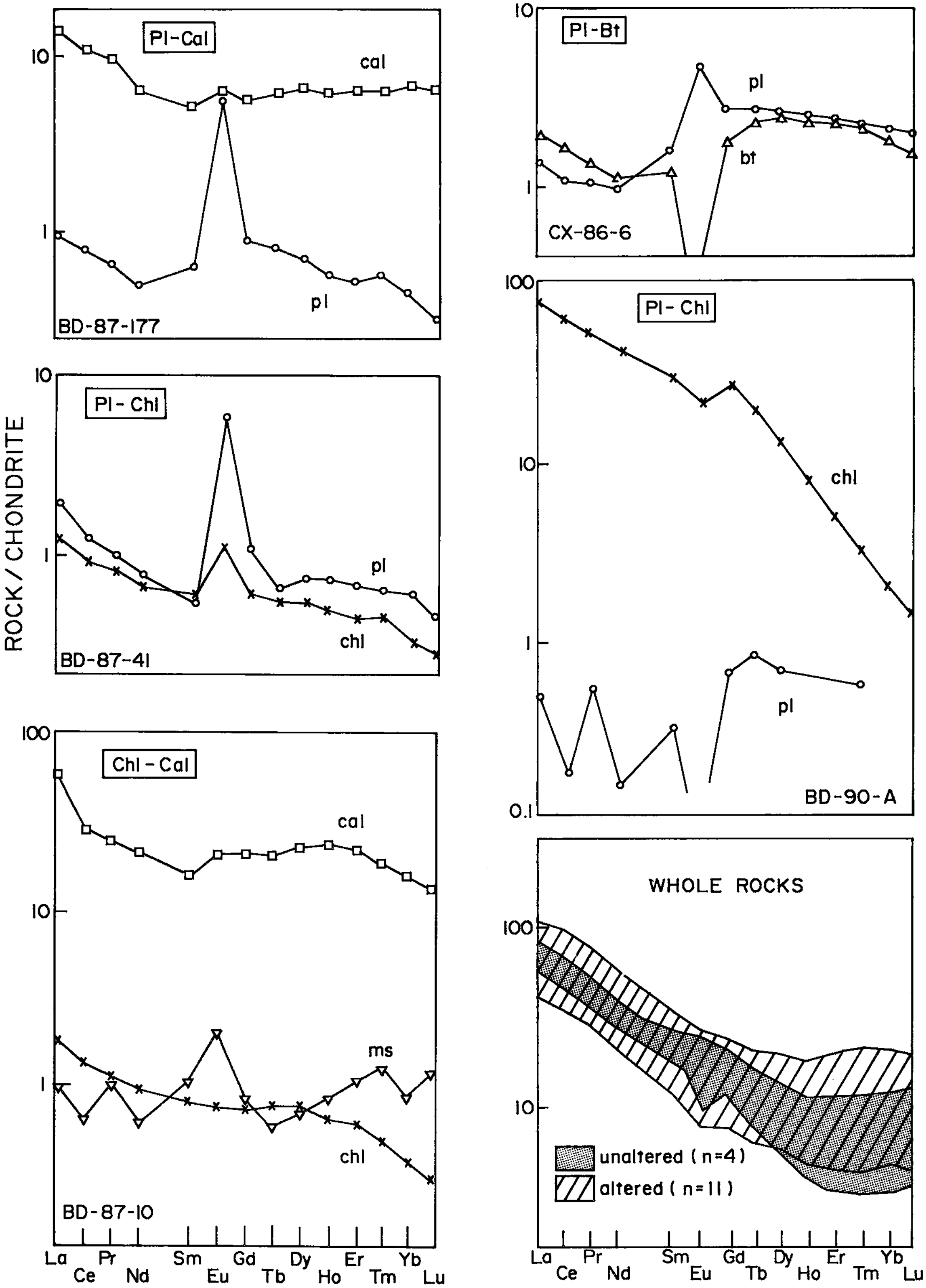
ROCK / CHONDRITE
Pl-Cal
cal
pl
BD-87-177
10
1
Pl-Chl
pl
chl
BD-87-41
10
1
Chl - Cal
cal
ms
chl
BD-87-10
100
10
1
Pl-Bt
pl
bt
CX-86-6
10
1
Pl- Chl
chl
pl
BD-90-A
100
10
1
0.1
WHOLE ROCKS
unaltered (n=4)
altered (n=11)
100
10
La
Ce
Pr
Nd
Sm
Eu
Gd
Tb
Dy
Ho
Er
Tm
Yb
Lu

ham 1978, Dumonceau *et al.* 1978); (3) variable flow-rates of the vein fluids (Möller *et al.* 1991); (4) variable rates of precipitation which, in the case of calcite, are deemed important since adsorption of elements is important in addition to crystal-chemical controls (Lorens 1981, Comans & Middelburg 1987); (5) retrograde alteration and remobilization of vein constituents (Alderton *et al.* 1980, Möller *et al.* 1979, 1984), and (6) variable extent of fluid-wallrock interaction (*e.g.*, Mungall *et al.* 1987). The present data-base for the Beaver Dam deposit indicates that if fluid unmixing did occur, it was minimal (Kontak *et al.* 1988, 1991a) and that the *REE* pattern of the wallrock is similar to the NASC pattern (Kontak *et al.* 1991a). Thus we can eliminate suggestions 2 and 6. In addition, there is no petrographic evidence to support the first possibility. Suggestions 3 and 4 cannot be quantitatively evaluated, but we note that the variation in *REE* abundances is greater than would be expected by such mechanisms (Möller *et al.* 1991). Although variations in fluid flow and rates of precipitation may be contributing factors, they cannot singularly account for the observed ranges. This leaves suggestion 5 (*i.e.*, retrograde alteration) as a possible contributing factor. It is interesting, therefore, to note that the greatest variability in the *REE* data pertains to stage-II minerals, which in part involve replacement of earlier assemblages. If we assume that the model proposed for calcite by Parekh & Möller (1977) is also broadly applicable to chlorite, then we can accommodate the changes observed simply by trace-element fractionation within the vein fluid. Potential variations also may occur because of contributing influences from some of the aforementioned factors.

The *REE* data for the vein minerals are particularly useful in identifying the source reservoir for the fluids if we can eliminate the role of contamination at the present structural level. In order to investigate this possibility, the data for minerals from the same sample have been plotted on chondrite-normalized diagrams in Figure 33. The data indicate that for four of the five cases, similar fractionation of the *REE* occurs and that, in general, there appears to be little fractionation. The sole exception is for sample BD–90–A, in which the chlorite is strongly fractionated. The data indicate that the minerals are in equilibrium with respect to their *REE* chemistry and, furthermore, suggest that the local metasedimentary wallrocks with a pattern typical of shale (Fig. 33) are not the source of the *REE*. The chondrite-normalized patterns for the vein minerals at Beaver Dam are more typical of the flat, unfractionated patterns found in basic rocks. We therefore suggest this as the source reservoir. In this light, it is most significant that in terms of Pb isotope data, Chatterjee & Smith (1991) identified lithologies of the Liscomb Complex, including mafic volcanic rocks, as the source reservoir for the vein-forming fluids.

Implications for the Meguma gold deposits

Collectively, the results of mineral paragenesis and chemistry suggest that for the Beaver Dam deposit area, there was a single hydrothermal event that resulted in the formation of a variety of vein types, dominated by two mineralogically distinct assemblages. Petrographic criteria and mineral chemistry indicate that stage-I and stage-II assemblages represent a continuum and probably reflect the normal progression of a hydrothermal system, which includes thermal and chemical equilibration with the surrounding host-rocks, in this case metaturbidites of the Lower Paleozoic Meguma Group.

The data presented provide some constraints on models for formation of these deposits, assuming that the Beaver Dam deposit is representative of the Meguma deposits. Firstly, the syngenetic exhalative model of Haynes (1986, 1987) is clearly incompatible with the vein mineralogy and textures, as originally discussed by Mawer (1985, 1986). Multiple episodes of vein formation and mineralization, as suggested by Kerswill (1988), also are considered an unlikely scenario given the conclusions of this study, which indicate a single vein-forming event. The suggestion of Sangster (1990, and references therein) and Sangster *et al.* (1988), that the source of vein constituents is the Goldenville Formation is untenable given the *REE* data and lack of inheritance that would be manifested in the chondrite-normalized patterns (*i.e.*, these should have a NASC-type pattern). Similar arguments have been used by Graf (1983, 1984) and Möller *et al.* (1979, 1984) in their studies of base-metal mineralization using *REE* data. Similarly, the possibility that the manganese- and metal-rich strata of the Goldenville – Halifax Transition Zone (Graves & Zentilli 1988) may be an important source of metals (Graves & Zentilli 1988, Sangster 1990, 1992) is considered unlikely given the absence of the expected Mn-rich mineralogy in the veins. In contrast, we would favor derivation of the vein-forming fluids from a source other than the Meguma Group, a model supported by available isotopic data (Sr, Pb; Chatterjee & Smith 1991, Kontak *et al.* 1991b). The fluid was subsequently modified during ascent to this structural level and later interaction with wallrock. This is consistent with the conclusions of other studies directed

FIG. 33. Plot of chondrite-normalized *REE* data for mineral pairs and triplets from vein samples at Beaver Dam (mineral abbreviations after Kretz 1983). The whole-rock data are from Kontak *et al.* (1991a), and *REE* abundances were determined using the analytical technique described in Jenner *et al.* (1990).

at mesothermal lode-gold deposits of Archean to Phanerozoic age (*e.g.*, Goldfarb *et al.* 1988, 1991, Bottrell & Spiro 1988, Kerrich 1987, 1990, Wilson & Golding 1988, Gulson *et al.* 1988, Böhlke & Kistler 1986). The presence of delicate patterns of zoning in many of the silicate minerals mitigates against a pre- or synmetamorphic origin (Graves & Zentilli 1982, Henderson & Henderson 1986, Sangster 1990, 1992) for the veins and instead is more consistent with vein formation during the waning stages of the Acadian Orogeny.

CONCLUSIONS

A detailed study of vein paragenesis and mineral chemistry of the Beaver Dam gold deposit, a typical metaturbidite-hosted mesothermal lode-gold deposit of Late Devonian age, indicates two distinct stages (I and II) for mineralization. Although both stages are dominated by quartz, the associated mineralogy changes from Ca-rich plagioclase + biotite + tourmaline (± amphibole ± garnet ± epidote ± apatite ± ilmenite) to calcite + chlorite + albite, with muscovite being present in both stages; sulfides are associated with both stages, although they are more abundant in stage II. Gold is spatially associated with both stages, but textures (*e.g.*, infilling fractures) suggest a late-stage paragenesis. Mineral chemistry indicates disequilibrium growth of several phases, as revealed by patterns of zoning (plagioclase, garnet), the compositions of several phases (biotite, chlorite, plagioclase) were probably controlled by the bulk composition of the wallrock. Trace element and *REE* data suggest that the chemistry of the vein-forming fluid changed during mineral precipitation and that a local derivation of the fluids is unlikely. Interpretation of the mineral chemistry in terms of geothermometry suggests initial temperatures greater than or equal to 500°C, which dropped to $\leq$300° during the waning stages of vein formation. The data are consistent with a genetic model invoking a late-stage metamorphic origin for the deposit, with the fluids being exotic to the Meguma Group.

Note added in proof: Recent work using the laser-ablation ICP–MS technique (Jackson et al. 1992) has indicated that the *REE* variability documented herein for vein minerals (Chl, Cal, Pl) is characteristic of several other hydrothermal mineral deposits (Kontak & Jackson 1993). A variation in both abundance and fractionation of the *REE* similar to that documented herein has been observed within single grains of carbonate minerals examined on a scale of tens to hundreds of μm, and sampled from an MVT deposit in Nova Scotia and a precious metal deposit of epithermal type in a sedimentary and volcanic terrane of the southwestern United States. These data confirm that the variability observed in concentrations of the *REE*s in the mineral phases from the Beaver Dam deposit are real, and that such trace-element behavior may in fact be typical of hydrothermal systems. Thus, the conclusions inferred above (*i.e.*, that the data reflect variation in the trace-element chemistry of the fluid phase) are strengthened in light of this more recent work.

ACKNOWLEDGEMENTS

Funding for this project was provided by the Canada – Nova Scotia Mineral Development Agreement (1984–1989). Field work at Beaver Dam deposit (1986, 1987) was supported by Seabright Exploration Ltd. The assistance of Ken Adams, Joe Campbell and staff is sincerely acknowledged. The chemical data were acquired with the assistance of C. Coyle (Technical University of Nova Scotia), S. Jackson (Memorial University) and B. McKay (Dalhousie University). Discussions with J. Campbell, K. Adams, R. Kerrich, A.K. Chatterjee, J. Dostal and D. O'Hanley have proved beneficial, but any errors of fact and interpretation remain the responsibility of the authors. Careful and detailed reviews by the referees and the editor resulted in substantical changes that clarified and improved the text. All are sincerely thanked for their considerable efforts. Personnel of the Nova Scotia Department of Natural Resources are acknowledged for their assistance in preparation of the figures and text. This paper is published with permission of the Director of the Mineral Resources Division, Nova Scotia Department of Natural Resources.

REFERENCES

AFIFI, A.M., KELLY, W.C. & ESSENE, E.J. (1988): Phase relations among tellurides, sulfides and oxides. I. Thermochemical data and calculated equilibria. *Econ. Geol.* **83**, 377-394.

ALDERTON, D.H.M., PEARCE, J.A. & POTTS, P.J. (1980): Rare earth element mobility during granite alteration: evidence from southwest England. *Earth Planet. Sci. Lett.* **49**, 149-165.

ALLÈGRE, C.J. & MINSTER, J.F. (1978): Quantitative models of trace element behavior in magmatic processes. *Earth Planet. Sci. Lett.* **38**, 1-25.

ANGLIN, C.D., FRANKLIN, J.M., JONASSON, I.R., BELL, K. & HOFFMAN, E. (1987): Geochemistry of scheelites associated with Archean gold deposits: implications for their direct age determination. *Geol. Surv. Can., Pap.* **87-1A**, 591-596.

ARNIAUD, D., DUPUY, C. & DOSTAL, J. (1984): Geochemistry of Auriat granite (Massif Central, France). *Chem. Geol.* **45**, 263-277.

ARTH, J.G. (1976): Behavior of trace elements during magmatic processes – a summary of theoretical models and their application. *J. Res. U.S. Geol. Surv.* **4**, 41-47.

BATES, J.L.E. (1986): Gold in Nova Scotia. *N.S. Dep. Mines & Energy, Information Ser.* **13**.

BLUNDY, J.D. & HOLLAND, T.J.B. (1990): Calcic amphibole equilibria and a new amphibole–plagioclase geothermometer. *Contrib. Mineral. Petrol.* **104**, 208-224.

______ & WOOD, B.J. (1991): Crystal-chemical controls on the partitioning of Sr and Ba between plagioclase feldspar, silicate melts, and hydrothermal solutions. *Geochim. Cosmochim. Acta* **55**, 193-209.

BÖHLKE, J.K. & KISTLER, R.W. (1986): Rb–Sr, K–Ar and stable isotope evidence for the ages and sourrces of fluid components of gold-bearing quartz veins in the northern Sierra Nevada foothills metamorphic belt, California. *Econ. Geol.* **81**, 296-322.

BOTTRELL, S.H. & SPIRO, B. (1988): A stable isotope study of black shale-hosted gold mineralization in the Dolgellau gold belt, North Wales. *J. Geol. Soc. London* **145**, 941-949.

BOWERS, T.S. & HELGESON, H.C. (1983): Calculation of the thermodynamic and geochemical consequences of nonideal mixing of the system $H_2O–CO_2–NaCl$ on phase relations in geologic systems: equation of state for $H_2O–CO_2–NaCl$ fluids at high pressures and temperatures. *Geochim. Cosmochim. Acta* **47**, 1247-1275.

BOYLE, R.W. (1979): The geochemistry of gold and its deposits (together with a chapter on geochemical prospecting for the element). *Geol. Surv. Can., Bull.* **280**.

______ (1986): Gold deposits in turbidite sequences: their geology, geochemistry and history of the theories and their orgin. *In* Turbidite-Hosted Gold Deposits (J.D. Keppie, R.W. Boyle & S.J. Haynes, eds.). *Geol. Assoc. Can., Spec. Pap.* **32**, 1-13.

BROWN, P.E. & LAMB, W.M. (1989): P–V–T properties of fluids in the system $H_2O \pm CO_2 \pm NaCl$: new graphical presentations and implications for fluid inclusion studies. *Geochim. Cosmochim. Acta* **53**, 1209-1221.

CANTRELL, K.J. & BYRNE, R.H. (1987): Rare earth element complexation by carbonate and oxalate ions. *Geochim. Cosmochim. Acta* **51**, 597-605.

CATHELINEAU, M. & NIEVA, D. (1985): A chlorite solid solution geothermometer. The Los Azufres (Mexico) geothermal system. *Contrib. Mineral. Petrol.* **91**, 235-244.

CHATTERJEE, A.K. & SMITH, P.K. (1991): Potential source rocks for gold in Meguma-hosted auriferous vein deposits, Nova Scotia. *Atlantic Geosci. Soc. Colloquium, Fredericton, New Brunswick, Program Abstr.*

______, STRONG, D.F. & MUECKE, G.K. (1983): A multivariate approach to geochemical distinction between tin-specialized and uranium-specialized granites of southern Nova Scotia. *Can. J. Earth Sci.* **20**, 420-430.

CLARKE, D.B., REARDON, N.C., CHATTERJEE, A.K. & GRÉGOIRE, D.C. (1989): Tourmaline composition as a guide to mineral exploration: a reconnaissance study from Nova Scotia using discriminant function analysis. *Econ. Geol.* **84**, 1921-1935.

COLVINE, A.C., FYON, J.A., HEATHER, K.B., MARMONT, S., SMITH, P.M. & TROOP, D.G. (1988): Archean lode gold deposits in Ontario. *Ont. Geol. Surv., Misc. Pap.* **139**.

COMANS, R.N.J. & MIDDELBURG, J.J. (1987): Sorption of trace metals on calcite: applicability of the surface precipitation model. *Geochim. Cosmochim. Acta* **51**, 2587-2591.

COREY, M.C. (1992): Mineralogical investigations along the Upper Seal Harbour anticline, Goldboro, Nova Scotia. *N.S. Dep. Natural Resources, Open File Rep.* **92-009**.

______ & MILLS, R.F. (1992): Geological and geochemical observations within the Tangier gold deposit. *N.S. Dep. Natural Resources, Open File Rep.* **92-008**.

COX, S.F., WALL, V.J., ETHERIDGE, M.A. & POTTER, T.F. (1991): Deformational and metamorphic processes in the formation of mesothermal vein-hosted gold deposits – examples from the Lachlan Fold Belt in central Victoria, Australia. *Ore Geol. Rev.* **6**, 391-423.

CROCKET, J.H., FUETEN, F., CLIFFORD, P.M., KABIR, A. & HENDERSON, J.R. (1986): Distribution of gold and arsenic in turbidites at Harrigan Cove, Nova Scotia: implications on gold mineralization. *In* Turbidite-Hosted Gold Deposits (J.D. Keppie, R.W. Boyle & S.J. Haynes, eds.). *Geol. Assoc. Can., Spec. Pap.* **32**, 149-159.

DEER, W.A., HOWIE, R.A. & ZUSSMAN, J. (1966): *An Introduction to the Rock-Forming Minerals.* Longman Group Ltd., London.

DOUMA, S.L. (1988): Metamorphism of Meguma Group metasediments – contact aureoles. *In* Mines & Minerals Branch Rep. Activities 1988, Part A (D.R. MacDonald & Y. Brown, eds.). *Nova Scotia Dep. Mines & Energy, Rep.* **88-3**, 97-104.

DRAKE, M.J. (1975): The oxidation state of europium as an indicator or oxygen fugacity. *Geochim. Cosmochim. Acta* **39**, 55-64.

DUMONCEAU, J., BIGOT, S., TREUIL, M., FAUCHERRE, J. & FROMAGE, F. (1978): Détermination des constantes de formation des tétracarbonato-lanthanides (III). *C.R. Acad. Sci. Paris, Sér.* **C 287**, 325-327.

FARIBAULT, E.R. (1899): Upper Musquodoboit Sheet, Nova Scotia. *Geol. Surv. Can., Map* **49**.

FERRY, J.M. & SPEAR, F.S. (1978): Experimental calibration of the partitioning of Fe and Mg between biotite and garnet. *Contrib. Mineral. Petrol.* **66**, 113-117.

FLYNN, R.T. & BURNHAM, C.W. (1978): An experimental determination of rare earth partition coefficients between a chloride containing vapor phase and silicate melts. *Geochim. Cosmochim. Acta* **42**, 685-701.

FOORD, E.E. & SHAWE, D.R. (1989): The Pb – Bi – Ag – Cu – (Hg) chemistry of galena and some associated sulfosalts: a review and some new data from Colorado, California and Pennsylvania. *Can. Mineral.* **27**, 363-382.

FORDE, A. (1991): The late orogenic timing of mineralisation in some slate belt gold deposits, Victoria, Australia. *Mineral. Deposita* **26**, 257-266.

FORTIER, S.M. & GILETTI, B.J. (1991): Volume self-diffusion of oxygen in biotite, muscovite, and phlogopite micas. *Geochim. Cosmochim. Acta* **55**, 1319-1330.

GILES, P.S. & CHATTERJEE, A.K. (1986): Peraluminous granites of the Liscomb Complex. *In* Program and Summaries, Tenth Open House and Review of Activities (J.L. Bates & D.R. MacDonald, eds.). *Nova Scotia Dep. Mines & Energy, Information Ser.* **12**, 83-90.

GIRAUD, A., DUPUY, C. & DOSTAL, J. (1986): Behaviour of trace elements during magmatic processes in the crust: application to acidic volcanic rocks of Tuscany (Italy). *Chem. Geol.* **57**, 269-288.

GOLDFARB, R.J., LEACH, D.L., PICKTHORN, W.J. & PATERSON, C.J. (1988): Origin of lode-gold deposits of the Juneau gold belt, southeastern Alaska. *Geology* **16**, 440-443.

______, NEWBERRY, R.J., PICKTHORN, W.J. & GENT, C.A. (1991): Oxygen, hydrogen, and sulfur isotope studies in the Juneau gold belt, southeastern Alaska: constraints on the origin of the hydrothermal fluids. *Econ. Geol.* **86**, 66-80.

GRAF, J.L., JR. (1983): Rare earth elements in carbonate rocks and minerals from the Viburnum Trend, southeast Missouri. *In* Proc. Int. Conf. on Mississippi Valley Type Lead–Zinc Deposits (W. Pratt, ed.). Univ. of Missouri–Rolla Press, Rolla, Missouri (131-139).

______ (1984): Effects of Mississippi Valley-Type mineralization on REE patterns of carbonate rocks and minerals, Viburnum Trend, southeast Missouri. *J. Geol.* **92**, 307-324.

GRANT, N.K. & BLISS, M.C. (1983): Strontium isotope and rare earth element variations in non-sulphide minerals from the Elmwood – Gordonsville mines, central Tennessee. *In* Proc. Int. Conf. on Mississippi Valley Type Lead–Zinc Deposits (W. Pratt, ed.). Univ. of Missouri–Rolla Press, Rolla, Missouri (206-210).

GRAUCH, R.I. (1989): Rare earth elements in metamorphic rocks. *In* Geochemistry and Mineralogy of Rare Earth Elements (B.R. Lipin & G.A. McKay, eds.). *Rev. Mineral.* **21**, 147-167.

GRAVES, M.C. (1976): *The Formation of Gold-Bearing Quartz Veins in Nova Scotia: Hydraulic Fracturing under Conditions of Greenschist Regional Metamorphism during Early Stages of Deformation.* M.Sc. thesis, Dalhousie Univ., Halifax, Nova Scotia.

______ & ZENTILLI, M. (1982): A review of the geology of gold in Nova Scotia. *In* Geology of Canadian Gold Deposits (R.W. Hodder & W. Petruck, eds.). *Can. Inst. Min. Metall., Spec. Vol.* **24**, 233-242.

______ & ______ (1988): The lithogeochemistry of metal-enriched coticules in the Goldenville–Halifax transition zone of the Meguma Group, Nova Scotia. *Geol. Surv. Can., Pap.* **88-1B**, 251-261.

GROMET, L.P., DYMEK, R.F., HASKIN, L.A. & KOROTEV, R.L. (1984): The "North American shale composite": its compilation, major and trace element characteristics. *Geochim. Cosmochim. Acta* **48**, 2469-2482.

______ & SILVER, L.T. (1983): Rare earth element distributions among minerals in a granodiorite and their petrogenetic implications. *Geochim. Cosmochim. Acta* **47**, 925-939.

GULSON, S.L., ANDREW, A.S., MIZON, K.J., KEAYS, R.R. & STUWE, K. (1988): Source of gold in Ballarat slate belt deposits and potential exploration applications. *In* Bicentennial Gold 88. *Geol. Soc. Aust., Abstr. Ser.* **22**, 331-337.

HAM, L.J. & KONTAK, D.J. (1988): A textural and chemical study of white mica in the South Mountain Batholith, Nova Scotia: primary versus secondary origin. *Maritime Sediments & Atlantic Geol.* **24**, 111-121.

HANSON, G.N. (1978): The application of trace elements to the petrogenesis of igneous rocks of granitic compostion. *Earth Planet. Sci. Lett.* **38**, 26-43.

______ (1980): Rare earth elements in petrogenetic studies of igneous systems. *Ann. Rev. Earth Planet. Sci.* **8**, 371-406.

HASKIN, L.A., HASKIN, M.A., FREY, F.A. & WILDEMAN, T.R. (1968): Relative and absolute terrestrial abundances of the rare earths. *In* Origin and Distribution of the Elements (L.H. Ahrens, ed.). Int. Ser. Monogr. Earth Sci. **30**, Pergamon, Oxford, U.K. (889-912).

HAYNES, S.J. (1986): Geology and chemistry of turbidite-hosted gold deposits, greenschist facies, eastern Nova Scotia, Canada. *In* Turbidite-Hosted Gold Deposits (J.D. Keppie, R.W. Boyle & S.J. Haynes, eds.). *Geol. Assoc. Can., Spec. Pap.* **32**, 161-177.

______ (1987): Classification of quartz veins in turbidite-hosted gold deposits, greenschist facies, eastern Nova Scotia. *Can. Inst. Min. Metall., Bull.* **80**(898), 37-51.

HENDERSON, J.R., HENDERSON, M.N. & WRIGHT, T.O. (1990): Water–sill hypothesis for the origin of certain veins in the Meguma Group, Nova Scotia, Canada. *Geology* **18**, 654-657.

HENDERSON, M.N. & HENDERSON, J.R. (1986): Constraints on the origin of gold in the Meguma Zone, Ecum Secum area, Nova Scotia. *Maritime Sediments & Atlantic Geol.* **22**, 1-13.

HENRY, D.J. & GUIDOTTI, C.V. (1985): Tourmaline as a petrogenetic indicator mineral: an example from the staurolite-grade metapelites of NW Maine. *Am. Mineral.* **70**, 1-15.

HEY, M.H. (1954): A new review for the chlorites. *Mineral. Mag.* **30**, 277-292.

HODGES, K.V. & SPEAR, F.S. (1982): Geothermometry, geobarometry and the Al_2SiO_5 triple point at Mt. Moosilauke, New Hampshire. *Am. Mineral.* **67**, 1118-1134.

_____ & JACKSON, S.J. (1993): Laser ablation microprobe analyses of calcite cements from the Gays River carbonate hosted Zn–Pb deposit, southern Nova Scotia. *Geol. Assoc. Can. – Mineral. Assoc. Can., Program Abstr.* **18**, A53.

JENNER, G.A., LONGERICH, H.P., JACKSON, S.E. & FRYER, B.J. (1990): ICP–MS – a powerful tool for high precision trace element analysis in earth sciences: evidence from analysis of selected USGS reference samples. *Chem. Geol.* **83**, 133-148.

JOLLIFF, B.L., PAPIKE, J.J. & SHEARER, C.K. (1989): Inter- and intra-crystal REE variations in apatite from the Bob Ingersoll pegmatite, Black Hills, South Dakota. *Geochim. Cosmochim. Acta* **53**, 429-441.

JOWETT, E.C. (1991): Fitting iron and magnesium into the hydrothermal chlorite geothermometer. *Geol. Assoc. Can. – Mineral. Assoc. Can., Program Abstr.* **16**, A62.

KEMPSTER, R.M.F., CLARKE, D.B., REYNOLDS, P.H. & CHATTERJEE, A.K. (1989): Late Devonian lamprophyric dykes in the Meguma Zone of Nova Scotia. *Can. J. Earth Sci.* **26**, 611-613.

KEPPIE, J.D. (1976): Structural model for the saddle reef and associated gold veins in the Meguma Group, Nova Scotia. *Can. Inst. Min. Metall., Bull.* **69**(774), 103-116.

_____ (1982): The Minas geofracture. *In* Major Structural Zones and Faults of the Northern Appalachians (P. St-Julien & J. Béland, eds.). *Geol. Assoc. Can., Spec. Pap.* **24**, 263-280.

_____ & DALLMEYER, R.D. (1987): Dating transcurrent terrane accretion: an example from the Meguma and Avalon composite terranes in the northern Appalachians. *Tectonics* **6**, 831-847.

KERRICH, R. (1987): The stable isotope geochemistry of Au–Ag vein deposits in metamorphic rocks. *In* Stable Isotope Geochemistry of Low Temperature Fluids (T.K. Kyser, ed.). *Mineral. Assoc. Can., Short-Course Handbook* **13**, 287-336.

_____ (1990): Carbon-isotope systematics of Archean Au–Ag vein deposits in the Superior Province. *Can. J. Earth Sci.* **27**, 40-56.

KERSWILL, J.A. (1988): Lithogeochemical indicators of gold potential in the eastern Meguma Terrane of Nova Scotia. *In* Mines & Minerals Branch Rep. Activities 1988, Part A (D.R. MacDonald & Y. Brown, eds.). *Nova Scotia Dep. Mines & Energy Rep.* **88-3**, 215-218.

KING, R.W. & KERRICH, R.W. (1989): Chromian dravite associated with ultramafic-rock-hosted Archean lode gold deposits, Timmins-Porcupine district, Ontario. *Can. Mineral.* **27**, 419-426.

_____, _____ & DADDAR, R. (1988): REE distributions in tourmaline: an INAA technique involving pretreatment by B volatilization. *Am. Mineral.* **73**, 424-431.

KONTAK, D.J. (1991): The East Kemptville topaz–muscovite leucogranite, Nova Scotia. II. Mineral chemistry. *Can. Mineral.* **29**, 37-60.

_____, CHATTERJEE, A.K., REYNOLDS, P.H. & TAYLOR, K. (1990b): $^{40}Ar/^{39}Ar$ geochronological study of metamorphic and igneous rocks of the Liscomb Complex, southern Nova Scotia. *In* Mines and Minerals Branch Rep. of Activities 1989, Part B. (D.R. MacDonald, ed.). *Nova Scotia Dep. Mines & Energy, Pap.* **90-1**, 33-40.

_____ & CORMIER, R.F. (1991): Geochronological evidence for multiple tectono-thermal overprinting events in the East Kemptville muscovite-topaz leucogranite, Yarmouth County, Nova Scotia, Canada. *Can. J. Earth Sci.* **28**, 209-224.

_____ JACKSON, S.L., LONGERICH, H.P., DUNNING, G.R. & FRYER, B.J. (1992): The application of laser-ablation microprobe – inductively coupled plasma – mass spectrometry (LAM–ICP–MS) to *in situ* trace-element determinations in minerals. *Can. Mineral.* **30**, 1049-1064.

_____, MACDONALD, D. & SMITH, P.K. (1988): Fluid inclusion study of the Beaver Dam gold deposit, Meguma Terrane, Nova Scotia. *In* Mines & Minerals Branch Rep. of Activities 1988, Part A (D.R. MacDonald & Y. Brown, eds.). *Nova Scotia Dep. Mines & Energy, Rep.* **88-3**, 63-70.

_____ & SMITH, P.K. (1989a): Sulphur isotopic composition of sulphides from the Beaver Dam and other Meguma Group-hosted gold deposits, Nova Scotia: implications for genetic models. *Can. J. Earth Sci.* **26**, 1617-1629.

_____ & _____ (1989b): Preliminary results of a fluid inclusion study of the stockwork zone vein mineralization, Caribou Deposit, Meguma Terrane, Nova Scotia. *In* Mines & Minerals Branch Rep. Activities 1989, Part A (D.R. MacDonald ed.). *Nova Scotia Dep. Mines & Energy, Rep.* **89-3**, 65-70.

_____, _____ & FARRAR, E. (1992): $^{40}Ar/^{39}Ar$ dating of vein muscovite from the West Gore Sb–Au deposit, Meguma Terrane, southern Nova Scotia: evidence for a 370 Ma mineralizing event and recognition of a Late Carboniferous thermal overprinting event. *In* Mines & Minerals Branch, Rep. Activities 1991 (D.R. MacDonald, ed.). *Nova Scotia Dep. Natural Resources, Rep.* **92-1**, 57-63.

_____, _____ & KERRICH, R. (1991a): A mineralogic, isotopic and fluid inclusion study of the Beaver Dam gold deposit, southern Nova Scotia: a metaturbidite-hosted lode gold deposit of 370 Ma age. *Geol. Assoc. Can. – Mineral. Assoc. Can., Program Abstr.* **16**, A67.

_____, _____ & _____ (1991b): Trace element and isotopic (C, O, Sr) chemistry of vein carbonates from Meguma lode gold deposits, Meguma Terrane, Nova Scotia: chemical evidence for source reservoirs. *Geol. Assoc. Can. – Mineral. Assoc. Can., Program Abstr.* **16**, A68.

———, ———, ——— & Williams, P.F. (1990a): Integrated model for Meguma Group lode gold deposits, Nova Scotia, Canada. *Geology* **18**, 238-242.

———, ——— & Reynolds, P.H. (1993): Geology and ^{40}Ar/^{39}Ar geochronology of the Beaver Dam gold deposit, Meguma Terrane, Nova Scotia, Canada: evidence for a 370 Ma age of mineralization. *Econ. Geol.* **88**, 139-170.

———, ———, ——— & Taylor, K. (1990c): Geological and ^{40}Ar/^{39}Ar geochronological constraints on the timing of quartz vein formation in Meguma Group lode-gold deposits, Nova Scotia. *Atlantic Geol.* **26**, 201-227.

Kranidiotis, P. & MacLean, W.H. (1987): Systematics of chlorite alteration at the Phelps Dodge massive sulfide deposit, Matagami, Quebec. *Econ. Geol.* **82**, 1898-1911.

Kretschmar, U. & Scott, S.D. (1976): Phase relations involving arsenopyrite in the system Fe–As–S and their application. *Can. Mineral.* **14**, 364-386.

Kretz, R. (1983): Symbols for rock-forming minerals. *Am. Mineral.* **68**, 277-279.

Lagache, M. (1984): The exchange equilibrium distribution of alkali and alkaline-earth elements between feldspars and hydrothermal solutions. *In* Feldspars and Feldspathoids (W. Brown, ed.). D. Reidel Publ. Co., Dordrecht, Holland (247-279).

——— & Dujon, S.C. (1987): Distribution of strontium between plagioclases and 1 molar aqueous chloride solutions at 600°C, 1.5 kbar and 750°C, 2 kbar. *Bull. Minéral.* **110**, 551-561.

Lahann, R.W. & Siebert, R.M. (1982): A kinetic model for distribution coefficients and application to Mg-calcites. *Geochim. Cosmochim. Acta* **46**, 2229-2237.

Leake, B.E. (1978): Nomenclature of amphiboles. *Can. Mineral.* **16**, 501-520.

Le Bel, L. (1979): Micas magmatiques et hydrothermaux dans l'environnement du porphyre cuprifère de Cerro Verde – Santa Rosa, Pérou. *Bull. Minéral.* **102**, 35-41.

Longerich, H.P., Jenner, G.A., Fryer, B.J. & Jackson, S.E. (1990): Inductively coupled plasma – mass spectrometric analysis of geological samples: a critical evaluation based on case studies. *Chem. Geol.* **83**, 105-118.

Lorens, R.B. (1981): Sr, Cd, Mn and Co distribution coefficients in calcite as a function of calcite precipitation rate. *Geochim. Cosmochim. Acta* **45**, 553-561.

MacDonald, M.A., Horne, R.J., Corey, M.C. & Ham, L.J. (1992): An overview of recent bedrock mapping and follow-up petrological studies of the South Mountain Batholith, southwestern Nova Scotia, Canada. *Atlantic Geol.* **28**, 7-28.

Malcolm, W. (1929): Gold fields of Nova Scotia. *Geol. Surv. Can., Mem.* **156**.

Marchand, L. (1976): *Contribution à l'étude de la distribution des lanthanides dans la fluorine. Étude expérimentale et application au gîte de Maine (Saône-et-Loire, France).* Thèse de doctorat, Univ. d'Orléans, Orléans, France.

Mawer, C.K. (1985): Origin of bedding-concordant auriferous quartz veins, Meguma Terrane, Nova Scotia. *Maritime Sediments & Atlantic Geol.* **21**, 1-9.

——— (1986): The bedding-concordant gold–quartz veins of the Meguma Group, Nova Scotia. *In* Turbidite-Hosted Gold Deposits (J.D. Keppie, R.W. Boyle & S.J. Haynes, eds.). *Geol. Assoc. Can., Spec. Pap.* **32**, 135-148.

——— (1987): Mechanics of formation of gold-bearing quartz veins, Nova Scotia, Canada. *Tectonophys.* **135**, 99-119.

——— & White, J.C. (1987): Sense of displacement on the Cobequid-Chedabucto fault system, Nova Scotia, Canada. *Can. J. Earth Sci.* **24**, 217-223.

McDougall, I. & Harrison, T.M. (1988): *Geochronology and Thermochronology by the ^{40}Ar/^{39}Ar Method.* Oxford Monogr. on Geology and Geophysics **9**, Oxford Univ. Press, New York.

McLellan, S.M. (1989): Rare earth elements in sedimentary rocks: influence of provenance and sedimentary processes. *In* Geochemistry and Mineralogy of Rare Earth Elements (B.R. Lipin & G.A. McKay, eds.). *Rev. Mineral.* **21**, 169-200.

Möller, P., Lüders, V., Schröder, J. & Luck, J. (1991): Element partitioning in calcite as a function of solution flow rate: a study of vein calcites from the Harz Mountains. *Mineral. Deposita* **26**, 175-179.

———, Morteani, G. & Dulski, P. (1984): The origin of the calcites from Pb–Zn veins in the Harz Mountains, Federal Republic of Germany. *Chem. Geol.* **45**, 91-112.

———, ———, Hoefs, J. & Parekh, P.P. (1979). The origin of the ore-bearing solution in the Pb–Zn veins of the western Harz, Germany, as deduced from rare-earth element and isotope distributions in calcite. *Chem. Geol.* **26**, 197-215.

Monier, G. & Robert, J.-L. (1986): Muscovite solid solutions in the system $K_2O - MgO - FeO - Al_2O_3 - SiO_2 - H_2O$: an experimental study at 2 kbar P_{H2O} and comparison with natural Li-free white micas. *Mineral. Mag.* **50**, 257-266.

Moody, J.B., Jenkins, J.E. & Meyer, D. (1985): An experimental investigation of the albitization of plagioclase. *Can. Mineral.* **23**, 583-596.

Morgan, J.W. & Wandless, G.A. (1980): Rare earth element distribution in some hydrothermal minerals: evidence for crystallographic control. *Geochim. Cosmochim. Acta* **44**, 973-980.

Moritz, R.P. & Crocket, J.H. (1990): Mechanics of formation of the gold-bearing quartz–fuchsite vein at the Dome mine, Timmins area, Ontario. *Can. J. Earth Sci.* **27**, 1609-1620.

MORRISON, G.W., ROSE, W.J. & JAIRETH, S. (1991): Geological and geochemical controls on the silver content (fineness) of gold in gold–silver deposits. *Ore Geol. Rev.* **6**, 333-364.

MUECKE, G.K., ELIAS, P. & REYNOLDS, P.H. (1988): Hercynian/Alleghanian overprinting of an Acadian Terrane: $^{40}Ar/^{39}Ar$ studies in the Meguma Zone, Nova Scotia, Canada. *Chem. Geol.* **73**, 153-167.

MUNGALL, J.E., FRAPE, S.K., GIBSON, I.L. & KAMINENI, D.C. (1987): Rare-earth abundances in host granitic rocks and fracture-filling gypsum associated with saline groundwaters from a deep borehole, Atikokan, Ontario. *Can. Mineral.* **25**, 539-543.

MUNOZ, J.L. & LUDINGTON, S.D. (1974): Fluoride–hydroxyl exchange in biotite. *Am. J. Sci.* **274**, 396-413.

O'REILLY, G. (1988): *Geology and Geochemistry of the Sangster Lake and Larrys River Plutons, Guysborough County, Nova Scotia.* M.Sc. thesis, Dalhousie Univ., Halifax, Nova Scotia.

PAREKH, P.P. & MÖLLER, P. (1977): Revelation of the genesis of minerals in paragenesis with fluorites, calcites and phosphates via rare earths fractionation. *In* Nuclear Technique and Mineral Resources. Proc. Int. Symp. on Nuclear Techniques in Exploration, Extraction and Processing of Mineral Resources, Int. Atomic Energy Agency, Vienna (356-369).

PIGAGE, L.C. & GREENWOOD, H.J. (1982): Internally consistent estimates of pressure and temperature: the staurolite problem. *Am. J. Sci.* **282**, 943-969.

PINGITORE, N.E., JR. & EASTMAN, M.P. (1984): The experimental partitioning of Ba^{2+} into calcite. *Chem. Geol.* **45**, 113-120.

RAESIDE, R.P., HILL, J.D. & EDDY, B.G. (1988): Metamorphism of Meguma Group metasedimentary rocks, Whitehead Harbour area, Guysborough County, Nova Scotia. *Maritime Sediments & Atlantic Geol.* **24**, 1-9.

RAIMBAULT, L. (1985): Utilisation des spectres de terres rares des minéraux hydrothermaux (apatite, fluorine, scheelite, wolframite) pour la caractérisation des fluides minéralisateurs et l'identification des magmas sources et des processus évolutifs. *Bull. Minéral.* **108**, 737-744.

RAMDOHR, P. (1980): *The Ore Minerals and their Intergrowths* (2nd ed.). Pergamon Press, London.

RAMSAY, J.G. (1980): The crack–seal mechanism of rock deformation. *Nature* **284**, 135-139.

REYNOLDS, P.H., ELIAS, P., MUECKE, G.K. & GRIST, A.M. (1987): Thermal history of the southwestern Meguma Zone, Nova Scotia from an $^{40}Ar/^{39}Ar$ and fission track dating study of intrusive rocks. *Can. J. Earth Sci.* **24**, 1952-1965.

______ & MUECKE, G.K. (1978): Age studies on slates: applicability of the $^{40}Ar/^{39}Ar$ stepwise outgassing method. *Earth Planet. Sci. Lett.* **40**, 111-118.

______, ZENTILLI, M. & MUECKE, G.K. (1981): K–Ar and $^{40}Ar/^{39}Ar$ geochronology of granitoid rocks from southern Nova Scotia: its bearing on the geological evolution of the Meguma Zone of the Appalachians. *Can. J. Earth Sci.* **18**, 386-394.

ROEDER, P.L., MACARTHUR, D., MA, XIN-PEI, PALMER, G.R. & MARIANO, A.N. (1987): Cathodoluminescence and microprobe study of rare-earth elements in apatite. *Am. Mineral.* **72**, 801-811.

ROSE, A.W. & BURT, D.M. (1979): Hydrothermal alteration. *In* Geochemistry of Hydrothermal Ore Deposits (second edition, H.L. Barnes, ed.). John Wiley & Sons, New York (173-235).

SANGSTER, A.L. (1990): Metallogeny of the Meguma Terrane, Nova Scotia. *In* Mineral Deposit Studies in Nova Scotia **1** (A.L. Sangster, ed.). *Geol. Surv. Can., Pap.* **90-8**, 115-162.

______ (1992): Light stable isotope evidence for a metamorphogenic origin for bedding-parallel, gold-bearing veins in Cambrian flysch, Meguma Group, Nova Scotia. *Explor. Min. Geol.* **1**, 69-79.

______, GRAVES, M.C. & ZENTILLI, M. (1988): Sulphur isotopic variation in Mn–As–Au–Zn–Pb-bearing strata: sedimentation and diagenesis in an anoxic basin in Cambro-Ordovician flysch of the Meguma Group, Nova Scotia, Canada. *Geol. Soc. Am., Abstr. Program* **20**, A301.

SHARP, Z.D., ESSENE, E.J. & KELLY, W.C. (1985): A re-examination of the arsenopyrite geothermometer: pressure considerations and applications to natural assemblages. *Can. Mineral.* **23**, 517-534.

SIBSON, R.H., ROBERT, F. & POULSEN, K.H. (1988): High-angle reverse faults, fluid-pressure cycling, and mesothermal gold-quartz deposits. *Geology* **16**, 551-555.

SMITH, P.K. & KONTAK, D.J. (1986): Meguma gold studies: advances in geological insight as an aid to gold exploration. *In* Tenth Annual Open House and Review of Activities (J.L. Bates & D.R. MacDonald, eds.). *Nova Scotia Dep. Mines & Energy, Information Ser.* **12**, 105-114.

______ & ______ (1988): Bismuth – tellurium – silver – tungsten association at the Beaver Dam gold deposit, eastern Nova Scotia. *In* Mines & Minerals Branch, Rep. Activities, Part A (D.R. MacDonald & Y. Brown, eds.). *Nova Scotia Dep. Mines & Energy, Rep.* **88-3**, 71-81.

______ & ______ (1989): Caribou gold deposit, Nova Scotia: composite ore zone geometry and restrictions on the age of mineralization. *Geol. Assoc. Can. – Mineral. Assoc. Can., Prog. Abstr.* **14**, A2.

SPEAR, F.S. (1980): NaSi $\rightleftharpoons$ CaAl exchange equilibrium between plagioclase and amphibole: an empirical model. *Contrib. Mineral. Petrol.* **72**, 33-41.

STEVENSON, R.K. & MARTIN, R.F. (1986): Implications of the presence of amazonite in the Broken Hill and Geco metamorphosed sulfide deposits. *Can. Mineral.* **24**, 729-745.

TANER, M.F., TRUDEL, P. & PERRAULT, G. (1986): Géochimie de la biotite associée à certains gisements d'or de Val d'Or, Malartic et Chibougamau, Quebec. *Can. Mineral.* **24**, 761-774.

TESFAYE, G. (1992): Ore-microscopic and geochemical studies of gold – tellurides – sulfide mineralization in the Macassa gold mine, Abitibi Belt, Canada. *Mineral. Deposita* **27**, 66-71.

THOMAS, W.C. (1982): *Petrology and Geochemistry of the River Lake Pluton, Halifax County, Nova Scotia.* M.Sc. thesis, Acadia Univ., Wolfville, Nova Scotia.

THOMPSON, A.B. (1976): Mineral reactions in pelitic rocks. II. Calculation of some P–T–X(Fe,Mg) phase relations. *Am. J. Sci.* **276**, 425-454.

WALSHE, J.L. (1986): A six-component chlorite solid-solution model and the conditions of chlorite formation in hydrothermal and geothermal systems. *Econ. Geol.* **81**, 681-703.

WILLIAMS, H. & HATCHER, R.D., JR. (1983): Appalachian suspect terranes. *In* Contributions to the Tectonic and Geophysics of Mountain Chains (R.D. Hatcher, Jr., H. Williams & I. Zietz, eds.). *Geol. Soc. Am., Mem.* **158**, 33-53.

WILLIAMS, P.F. & HY, C. (1990): Origin and deformational and metamorphic history of gold-bearing quartz veins on the eastern shore of Nova Scotia. *In* Mineral Deposit Studies in Nova Scotia (A.L. Sangster, ed.). *Geol. Surv. Can., Pap.* **90-8**, 169-194.

WILLIAMS, P.J. (1991): Geology, alteration and mesothermal Au–Ag mineralization associated with a volcanic-intrusive complex at Mt. Shamrock – Mt. Ophir, S.E. Queensland. *Mineral. Deposita* **26**, 11-17.

WILSON, A.F. & GOLDING, S.D. (1988): Stable isotope constraints on fluid sources for granitoid- and metamorphic-hosted gold-quartz vein deposits in eastern Australia. *In* Bicentennial Gold 88. *Geol. Soc. Aust., Abstr. Ser.* **22**, 495-499.

WOODSWORTH, G.J. (1977): Homogenization of zoned garnets from pelitic schists. *Can. Mineral.* **15**, 230-242.

YANOVER, R.N. (1984): *Laser Decrepitation and Analyses of Fluid Inclusions from the Meguma Complex, Nova Scotia: Nature of the Ore Forming Fluids.* M.Sc. thesis, Florida State Univ., Tallahassee, Florida.

YARDLEY, B.W.D. (1985): Apatite composition and the fugacities of HF and HCl in metamorphic fluids. *Mineral. Mag.* **49**, 77-79.

ZENTILLI, M., WOLFSON, I., SHAW, W. & GRAVES, M.C. (1984): The Goldenville – Halifax transition of the Meguma Group as control for metallic mineralization. *Geol. Soc. Am., Abstr. Programs* **16**, 73.

Received November 1, 1991, revised manuscript accepted October 31, 1992.